[redacted]

Department of Mechanical Engineering
University of New Brunswick
Fredericton, N.B.

CA1
DTC 800
87
T17
c.2

mm
GII
TP8300
E7
T17
c.2

TP8422E

# Tank Thermal Response Analysis: Phase II

## A Study of the Transient Phenomena in a Heated Vessel During Depressurization

Prepared for:
Transport Canada
Transportation Development Centre
Montreal, Quebec H3A 2R3

Prepared by:

Qi Wang & J.E.S. Venart

University of New Brunswick
Department of Mechanical Engineering
P.O. Box 4400
Fredericton, N.B. E3B 5A3

Library and [illegible] Centre / Centre de [illegible] (GSLA)
RECEIVED - REÇU LE
APR 4 1989
Transport Canada / Transports Canada

December 1987

409353

The contents of this report reflect the views of the contractor and not necessarily the official views or policies of the Transportation Development Centre.

Un sommaire en français de ce rapport est inclus après la table des matières.

Transport Canada / Transports Canada
Development / Développement

**REPORT DOCUMENTATION FORM**

| 1. Transport Canada Report No. | 2. TDC Project No. | 3. Recipient's Catalogue No. |
|---|---|---|
| TP 8422E | 4727 | |

| 4. Title and Subtitle | 5. Report Date |
|---|---|
| **TANK THERMAL RESPONSE ANALYSIS: PHASE II**<br>**A Study of the Transient Phenomena in a Heated Vessel during Depressurization** | January 1986 |
| | 6. Performing Organization Report No.<br>UNB-ME-TF |
| 7. Author(s)<br>Qi Wang and J.E.S. Venart | 8. Transport Canada File No.<br>D1465-302-6-6 |
| 9. Performing Organization Name and Address<br>Fire Science Centre<br>University of New Brunwick<br>P.O. Box 4400<br>Fredericton, N.B. E3B 5A3 | 10. DSS File No.<br>11SD.T8200-5-5517 |
| | 11. DSS or Transport Canada Contract No.<br>OSD85-00299 |
| 12. Sponsoring Agency Name and Address<br>Transportation Development Centre (TDC)<br>Guy Favreau Complex<br>200 Dorchester Blvd. West, Suite 601, West Tower<br>Montreal, Quebec H2Z 1X4 | 13. Type of Report and Period Covered |
| | 14. Sponsoring Agency Code<br>Funded under Energy R&D Program |
| 15. Supplementary Notes | 16. TDC Project Officer<br>D.W. Dibble |

17. Abstract


The characteristics of the transient discharge phenomena, including void fraction development, in a partially filled, externally heated horizontal cylinder during depressurization are studied.

Instrumentation has been developed for tests with different liquid fill levels to measure the characteristics of the flashing phenomena, including the pressure, temperature and void fraction in the bulk liquid and the boundary layers adjacent to the heated walls.

An analytical model based on the conservation of mass and energy in the two-phase mixture layer has been made and compared to flux drift model.

It is concluded that the fill of liquid and temperature distribution in the bulk liquid greatly affect the pressure variation and the time of flashing. The developed predictions agree quite well with the obtained experimental data. In the case of low void fraction, the effect of heat flux from the wall cannot be neglected.


| 18. Key Words | 19. Distribution Statement |
|---|---|
| Rail, Tank Car, Thermal, Heat, Energy, Convection, Transfer | Limited number of copies available from the Transportation Development Centre |

| 20. Security Classification (of this report) | 21. Security Classification (of this page) | 22. No. of Pages | 23. Price |
|---|---|---|---|
| Unclassified | Unclassified | | - |

TDC. CDT 79-005
Rev 86

Transports Canada / Transport Canada
Développement / Development

## FORMULE DOCUMENTAIRE DU RAPPORT

| 1. N° du rapport Transports Canada | 2. N° de l'étude — CDT | 3. N° de catalogue du destinataire |
|---|---|---|
| TP 8422E | 4727 | |

| 4. Titre et sous-titre | 5. Date du rapport |
|---|---|
| **TANK THERMAL RESPONSE ANALYSIS: PHASE II**<br>**A Study of the Transient Phenomena in a Heated Vessel during Depressurization** | janvier 1986 |
| | 6. N° du rapport de l'organisme exécutant<br>UNB-ME-TF |
| 7. Auteur(s)<br>Qi Wang et J.E.S. Venart | 8. N° de dossier Transports Canada<br>D1465-302-6-6 |
| 9. Nom et adresse de l'organisme exécutant<br>Fire Science Centre<br>University of New Brunwick<br>C.P. 4400<br>Fredericton, N.B. E3B 5A3 | 10. N° de dossier — ASC<br>11SD.T8200-5-5517 |
| | 11. N° de contrat — ASC ou Transports Canada<br>OSD85-00299 |
| 12. Nom et adresse de l'organisme parrain<br>Centre de développement des transports (CDT)<br>Complexe Guy-Favreau<br>200 ouest, boul. Dorchester, Suite 601, Tour Ouest<br>Montréal, Québec H2Z 1X4 | 13. Genre de rapport et période visée |
| | 14. Code de l'organisme parrain<br>Financé par le programme énergétique |
| 15. Remarques additionnelles | 16. Agent de projet — CDT<br>D.W. Dibble |

17. Résumé


Dans le projet, dont ce rapport rend compte, sont étudiés les phénomènes d'écoulement transitoire et du mouvement ascensionnel des bulles dans un réservoir horizontal partiellement rempli et soumis à une source de chaleur extérieure, au moment de l'ouverture de la soupape le protégeant.

Une instrumentation avait été mise au point pour étudier, à divers niveaux de remplissage, le phénomène de détente en fonction des paramètres de pression, de température et de taux de présence de bulles dans la masse sous-refroidie et les couches pariétales.

Un modèle analytique fondé sur les équations de conservation de la masse et de la quantité d'énergie dans un mélange liquide-vapeur a été élaboré et comparé au modèle figurant le mouvement ascensionnel des bulles sous l'action de la chaleur.

Le rapport montre que le niveau de remplissage et la répartition des températures dans la masse liquide sous-refroidie ont une forte influence sur les variations de pression et sur la durée de la détente. Les prévisions faites concordent bien avec le résultat des expérimentations. Lorsque le taux de présence de bulles est faible, les transferts thermiques pariétaux ne sauraient être tenus pour négligeables.


| 18. Mots-clés | 19. Diffusion |
|---|---|
| Rail, wagon-citerne, flux thermiques, chaleur, énergie, convection, transferts | Le Centre de développement des transports dispose d'un nombre limité d'exemplaires |

| 20. Classification de sécurité (de ce rapport) | 21. Classification de sécurité (de cette page) | 22. Nombre de pages | 23. Prix |
|---|---|---|---|
| non classifié | non classifiée | | - |

CDT/TDC 79-005
Rev 86

Canada

TABLE OF CONTENTS


| | Page |
|---|---|
| Summary | vii |
| Sommaire | ix |
| List of Figures | xi |
| Notation | xiii |
| CHAPTER I INTRODUCTION | 1 |
| 1.1 General | 1 |
| 1.2 Description of the Physical Phenomena. | 2 |
| 1.3 Objectives | 8 |
| CHAPTER II LITERATURE REVIEW | 9 |
| 2.1 Subcooled Boiling | 9 |
| 2.2 Homogeneous Boiling | 13 |
| CHAPTER III PHYSICAL MODELS AND MATHEMATICAL DESCRIPTION | 19 |
| 3.1 Introduction | 19 |
| 3.2 Homogeneous Boiling in a Bulk Liquid During Depressurization | 19 |
| 3.2.1 General | 19 |
| 3.2.2 Analysis of Conservation of Energy and Mass | 21 |
| 3.2.3 Drift Flux Two-Phase Flow Model | 24 |
| CHAPTER IV ANALYTICAL AND NUMERICAL SOLUTIONS | 31 |
| 4.1 Theoretical Solution Analysis | 31 |
| 4.1.1 Overall Average Void Fraction During Depressurization | 31 |
| 4.1.2 Swell Height and Total Vapour Mass Flux | 34 |
| 4.2 Numerical Solution Procedures | 36 |
| 4.2.1 Energy and Mass Analysis in the Bulk Liquid | 36 |
| 4.2.2 Solution of the Drift Flux Model | 39 |

Page

CHAPTER V EXPERIMENTAL APPARATUS, PROCEDURES, AND MEASUREMENTS ..... 43

5.1 Introduction ..... 43
5.2 Test Instruments ..... 44

5.2.1 Apparatus ..... 44
5.2.2 Capacitance Transducers and Electrical Circuits ..... 46

5.3 Experimental Procedures ..... 53
5.4 Measurements and Data Reduction ..... 55

5.4.1 Measurements ..... 55
5.4.2 Data Reduction ..... 59

CHAPTER VI DISCUSSION AND COMPARISONS OF MEASUREMENTS AND MODELS ..... 62

6.1 Experimental Results ..... 62

6.1.1 Pressure ..... 65
6.1.2 Temperature ..... 68
6.1.3 Mass and Swell Height ..... 68
6.1.4 Void Fraction ..... 70

6.2 Comparison of Experiments and Calculations ..... 81

CHAPTER VII CONCLUSIONS AND FUTURE WORK ..... 93

7.1 Conclusions ..... 93
7.2 Future Work ..... 94

REFERENCES ..... 96

Appendix 1: EXAMINATION OF THE EQUATION OF OVERALL AVERAGE VOID FRACTION ..... 102

Appendix 2: ELECTRODE EFFECTS AND IMPEDANCE OF A TWO-PHASE MIXTURE ..... 106

Appendix 3: COMPUTER PROGRAM FOR DATA ACQUISITION ..... 112

Summary

This report presents the experimental results and analysis of a test series designed to evaluate the transient void fraction development in a partially filled, externally heated horizontal cylinder. The work was undertaken by the Fire Science Centre fo the University of New Brunswick as part of a research program concerned with the safe transport of flammable pressure liquefied gases. The research was supported by the Transportation Development Centre (TDC) through DSS file Number 11SD.T8200-5-5517.

Two experiments were performed in an externally heated (80 kWe) R11 filled, 380 mm diameter horizontal cylinder protected with a 9.53 mm diameter preeesure relief valve (PRV) set for 343 kPa; one with a lading of 50% and the other at 75% by volume. The change in liquid level and the flashing phenomena in the vessel were recorded by a time synchronized video system positioned in front of the observation windows of the test vessel. Selected time--dependent temperatures, pressures, as well as mass and bulk fluid plus boundary layer void fraction development were measured. The void fraction measurements utilized rod-ring bulk capacitance and radio frequency (RF) boundary layer probes and the difference in dielectric constant between the vapour and liquid. A high frequency (2.2 MHz) sine wave was applied to either the central rod or one side of the RF probe; the output signal, modulated by the fluid and its time-dependent woid fraction, developed an AC voltage which was filtered and demodulated and rectified in order to

present a D.C. voltage proportional to the magnitude of transducer susceptance. Each of the eight bulk and four boundary layer probes were scanned at a rate of 2500 readings per seond. The average values of each boundary layer probe were deterined from samples of 100 readings per second. These values were used to determine the subcoooled boiling boundary layer development and the bulk flashing behaviour before and after the valve opened, cycled, or continuously vented. Bulk fluid temperature in three locations, mass and swell height (determined from changes in the bulk void fraction gauges) were also measured.

Void fraction development and swell height measurements were compared to models which consider the trnasient behaviour of the boiling boundary layer and the bulk fluid regions. Analytical and numerical solution procedures were developed to consider each region, presuming an initial linear temperature stratification in the liquid. In the region close to the liquid surface, the results of void fraction compare favourably with a model which ignores wall heat flux; however, lower within the bulk, void developmkent is dependent upon the bottom wall heating. The computed transient mass loss compared with these models was greater than that measureed, owing to the cyclic nature of the vlve action; when the valve closed, fluid would be recompressed and condensation occurred; this was not accounted for in the model. The swell hights compare well with those predicted by experimental analysis.

SOMMAIRE

Le présent rapport soumet les résultats et l'analyse d'une série de tests visant à déterminer l'évolution du vide fractionnaire transitoire dans un cylindre horizontal partiellement rempli et chauffé extérieurement. Ce modèle a été élaboré par le Fire Science Center de l'Université du Nouveau-Brunswick dans le cadre d'un programme de recherche sur la sécurité du transport de gaz inflammables liquéfiés sous pression. Les travaux ont été parrainés par le Centre de développement des transports (MAS - dossier 11.SD.T8200-5-5517).

Deux expériences ont été effectuées avec un cylindre horizontal d'un diamètre de 380 mm protégé par une soupape de sûreté de 9,53 mm réglée à 343 kPa; dans les deux expériences, le réservoir était rempli de R11 à 50 % et à 75 % (par volume) respectivement et était chauffé extérieurement (à 80 $kW_e$). La variation du niveau du liquide et la vaporisation instantanée dans le réservoir ont été enregistrées par un système vidéo synchronisé placé devant les fenêtres d'observation du réservoir. La température et la pression, ainsi que le débit massique, la hauteur du liquide et le vide fractionnaire dans la couche limite ont été mesurés en fonction du temps. Le vide fractionnaire a été déterminé en mesurant la constante diélectrique entre la vapeur et le liquide à l'aide d'une sonde de capacité à tige à anneaux; le vide dans la couche limite a été mesuré à l'aide d'une sonde radiofréquence (RF). Une tension sinusoïdale haute fréquence (2,2 MHz) a été appliquée à la tige centrale ou à l'une des bornes de la sonde RF; la tension de sortie alternative de cette dernière, modulée par les variations du niveau du liquide et du vide fractionnaire, a été filtrée, démodulée et redressée pour donner une tension continue proportionnelle à la susceptance du transducteur. Pour chacune des sondes, huit au sein du liquide et quatre dans la couche limite, la fréquence d'échantillonnage était de 2500 lectures par seconde. Pour chacune des sondes dans la couche limite, les valeurs moyennes ont été obtenues à des fréquences d'échantillonnage de 100 lectures par seconde. Ces valeurs ont été utilisées

pour déterminer l'évolution de l'ébullition dans la couche limite sous-refroidie et celle de la vaporisation instantanée avant et après l'ouverture de la soupape, ou durant le fonctionnement cyclique ou l'ouverture continue de cette dernière. La température au sein du liquide, le débit massique et la hauteur de gonflement (déterminée à partir des variations mesurées du vide fractionnaire) ont aussi été mesurés à trois endroits.

Les valeurs mesurées du vide fractionnaire et de la hauteur de gonflement ont été comparées à celles obtenues à l'aide de modèles décrivant le comportement transitoire de la couche limite et du liquide en ébullition. Des calculs analytiques et numériques ont été effectués pour chacune de ces régions en supposant une stratification de température linéaire initiale dans le liquide. Au voisinage de la surface du liquide, les résultats obtenus pour le vide fractionnaire se comparent à ceux obtenus avec un modèle qui néglige les transferts de chaleur dans la paroi; toutefois, plus bas sous la surface, l'évolution du vide fractionnaire dépend de la quantité de chaleur fournie à la paroi inférieure. En raison du comportement cyclique du fonctionnement de la soupape, la perte de masse transitoire calculée à l'aide de ce modèle était supérieure à celle mesurée; lorsque la soupape se ferme, le liquide est recomprimé et il se produit de la condensation, effet dont le modèle ne tient pas compte. Les hauteurs de gonflement calculées concordent avec les valeurs observées.

LIST OF FIGURES


| Figure | | PAGE |
|---|---|---|
| 1. | Physical Model for Subcooled Boiling | 4 |
| 2. | Pressure-Temperature Saturation Curve (R-11) | 6 |
| 3. | Physical Model for Flashing | 7 |
| 4. | Mathematical Model for Conservation of Mass and Energy | 23 |
| 5. | Saturation Region for $t=t_o$ | 30 |
| 6. | Saturation Region for $t+\Delta t$ ($\Delta t > o$) | 30 |
| 7. | Drift Flux Two-Phase Fluid Model | 40 |
| 8. | Experimental Apparatus | 45 |
| 9. | Experimental Instrumentation | 47 |
| 10. | Central Rod-Ring Sensor | 48 |
| 11. | Radio-Frequency Probe | 50 |
| 12. | Experimental Circuit | 52 |
| 13. | Measurement for Depth Effect | 56 |
| 14. | Normalized Results of Depth Effect | 57 |
| 15. | Pressure vs. Time (Experiment 2) | 63 |
| 16. | Pressure vs. Time (Experiment 3) | 64 |
| 17. | Temperature Profile vs. Time (Experiment 2) | 66 |
| 18. | Temperature Profile vs. Time (Experiment 3) | 67 |
| 19. | Pressure, Mass and Swell Height Variations (Experiment 2) | 69 |
| 20. | Pressure, Mass and Swell Height Variations (Experiment 3) | 71 |
| 21. | Mass Variations | 72 |
| 22. | Relative Mass Variations | 73 |

23. Void Fraction Profile with Time (Experiment 2).....74
24. Void Fraction Profile with Time (Experiment 3).....76
25. Comparison of Void Fractions from Experiments 2 and 3.....77
26. Void Probes Response (Experiment 2).....79
27. Void Probes Response (Experiment 3).....80
28(a). Comparison of Numerical Calculations and Experimental Data (Experiment 2).....82
28(b). Comparison of Numerical Calculations and Experimental Data (Experiment 2).....83
28(c). Comparison of Numerical Calculations and Experimental Data (Experiment 2).....84
29. Comparison of Numerical Caluclations and Experimental Data (Experiment 3).....86
30. Comparison of Liquid Masses between Theoretical and Experimental Results (Experiment 2).....89
31. Comparison of Liquid Masses between Theoretical and Experimental Results (Experiment 3).....90
32. Comparison of Swell Heights between Theoretical and Experimental Results (Experiment 2).....91
33. Comparison of Swell Heights between Theoretical and Experimental Results (Experiment 3).....92
A1 Equivalent Circuit for Electrode Effect.....107
A2 Equivalent Circuit for Impedanse of Void Sensor.....108
A3 Equivalent Circuit for Sensor (High Frequency).....111

## NOTATION

| | | |
|---|---|---|
| A | : | Geometric parameter in Eqn. (5-1), m. |
| C | : | Capacitance, farad. |
| Cp | : | Constant pressure specific heat, J/kg K |
| F | : | Friction force exerted on phase g (or ℓ) by viscous action, $kg/m^2s^2$. |
| g | : | Gravitational acceleration, $m/s^2$. |
| G | : | Total mass velocity, $kg/m^2$ s. |
| $h_{fg}$ | : | Latent enthalpy, J/kg. |
| H | : | Heat transfer from neighboring elements of same phase, J/s $m^3$. |
| I | : | Momentum transfer to phase g (or ℓ), $kg/m^2s^2$. |
| J | : | Effect of interactions with other phase occupying the same space, J/s $m^3$. |
| j | : | Entrained fluid flux, $m^3/s$. |
| m(M) | : | Mass, kg. |
| $\dot{m}$ | : | Rate of generation of vapor per unit volume of mixture, $kg/m^2$ s. |
| P | : | Absolute pressure, $N/m^2$. |
| Q | : | Heat flux, $W/m^2$, or Heat transfer to mixture per unit volume, J/s $m^3$. |
| Qex | : | External heat flux, $W/m^2$. |
| r | : | Unit vector in the r-direction. |
| R | : | Tank car radius, m. |

S : Specific entropy, J/kg K, or Cross-sectional area of the vessel, $m^2$.

t : Time, s.

T : Temperature, K.

u : Velocity along the wall or along vertical coordinate, m/s.

v : Velocity along coordinate normal to curved surface or horizontal coordinate, m/s.

V : Volume, $m^3$.

$V_{fg}$ : Saturated specific volume of liquid minus saturated specific volume of vapor, $m^3/kg$.

x : Coordinate along the wall of cylinder or vertical coordinate, m.

y : Coordinate normal to curved surface or horizontal coordinate, m.

GREEK SYMBOLS:

$\alpha$ : Void fraction.

$\delta$ : Boundary layer thickness, m.

$\varepsilon$ : Permittivity, f/m.

$\mu$ : Dynamic viscosity, kg/m s.

$\rho$ : Density, $Kg/m^3$.

$\sigma$ : Surface tension, $N/m^2$.

$\tau$ : Shear stress, $N/m^2$.

$\phi$ : Angle measured from the bottom of the cylinder, rad.

$\omega$ : Angular frequency, rad/s

SUBSCRIPTS:

b : bubble.

g : gas (or vapor).

$\ell$ : liquid.

m($\alpha$) : two-phase mixture or mean value.

s : saturated.

w : wall.

# CHAPTER 1

# INTRODUCTION

## 1.1 GENERAL

Transient two-phase flow phenomena have important effects in heated vessels filled with pressure liquified fluids. The study of these phenomena is necessary to develop analytical predictive techniques for the design and safety assessment of containing systems and safety equipment for such systems. During depressurization, with a pressure relief valve (PRV) for example, the liquid level in such a vessel will differ considerably from the single phase gravitational level, and this will influence the wall heat transfer in both the vapor and liquid spaces of the vessel. The thermohydraulic behavior of a saturated fluid mixture under depressurization is very complex, and directly affects the safety of the heated and pressurized vessel.

Void fraction is one of the essential parameters necessary to describe the flow characteristics of a two-phase fluid. It is, however, also one of the most difficult quantities to measure. This parameter is required for engineering calculations involving fluid acceleration and pressure drop, mean fluid density, heat and mass transfer and hydrodynamic characteristics. It is also important in interfacial area calculations and provides a better understanding of the forces on the internal components of the vessel and the PRV. The design and sizing of

the PRV in pressure vessels depend upon the phase distribution in the bulk fluid. The stability and safety of the vessels are affected largely by the behavior of the fluid inside. An experimental program was therefore designed to determine the magnitude of the void fraction development in an externally heated and partially filled horizontal cylinder containing a pressure liquefied fluid. Analysis of the phenomena was also conducted and the results verified by means of the measurement program.

## 1.2 DESCRIPTION OF THE PHYSICAL PHENOMENA

When a pressurized vessel containing a flashing liquid is exposed to fire or is heated by an external heat source, the fluid inside is heated by conduction across the vessel wall and by convection. The temperature of the fluid in the vessel rises with time with phase change (boiling) occurring as a result of the different heat transfer processes taking place.

When the walls of the vessel are suddenly exposed to uniform heating, heat is transferred from the heated surface to the neighboring fluid layers initially by conduction. The density of a fluid decreases as its temperature increases. This causes the layers to rise between the heated surface and the bulk of the liquid. This upward flow to the free liquid surface creates a free-convection flow which transports heat away from the wall and with time forms a stratified surface layer which itself increases in depth with time. The temperature boundary layer

formed between the heated surface and the bulk liquid rises and carries away the heat from the wall.

After some time, as the temperature of the liquid in the boundary layer is increased fractionally above the corresponding saturated temperature, bubble formation on the heated surface occurs, and saturated and later subcooled nucleate boiling takes place (Fig. 1). During boiling, the heat flux on the wall causes vapor generation; natural convection, and subcooling cause reduction of the liquid phase core. In the boundary layer, various phenomena occur: a thermal conduction transient, nucleation and bubble growth, bubble departure from the wall or condensation of bubbles and heat transfer to the bulk liquid at the outer edge.

Boiling starts with the growth and condensation of individual bubbles due to the presence of a thin superheated liquid layer near the heated surface. Initially, the bubbles cannot grow sufficiently large to leave the wall because of the subcooling, and the bubbles condense; the void fraction in this case is usually considered to be negligible. As the difference between the saturation temperature and the bulk liquid temperature decreases, the bubbles formed can depart from the wall and rise along the thin superheated layer adjacent to the wall. Although some bubbles still condense, the condensing rate is sufficiently low to generate a significant void fraction with most of the bubbles staying in the boundary layer for a significant amount of time due to entrainment in the high velocity caused by the greater buoyancy effect of the

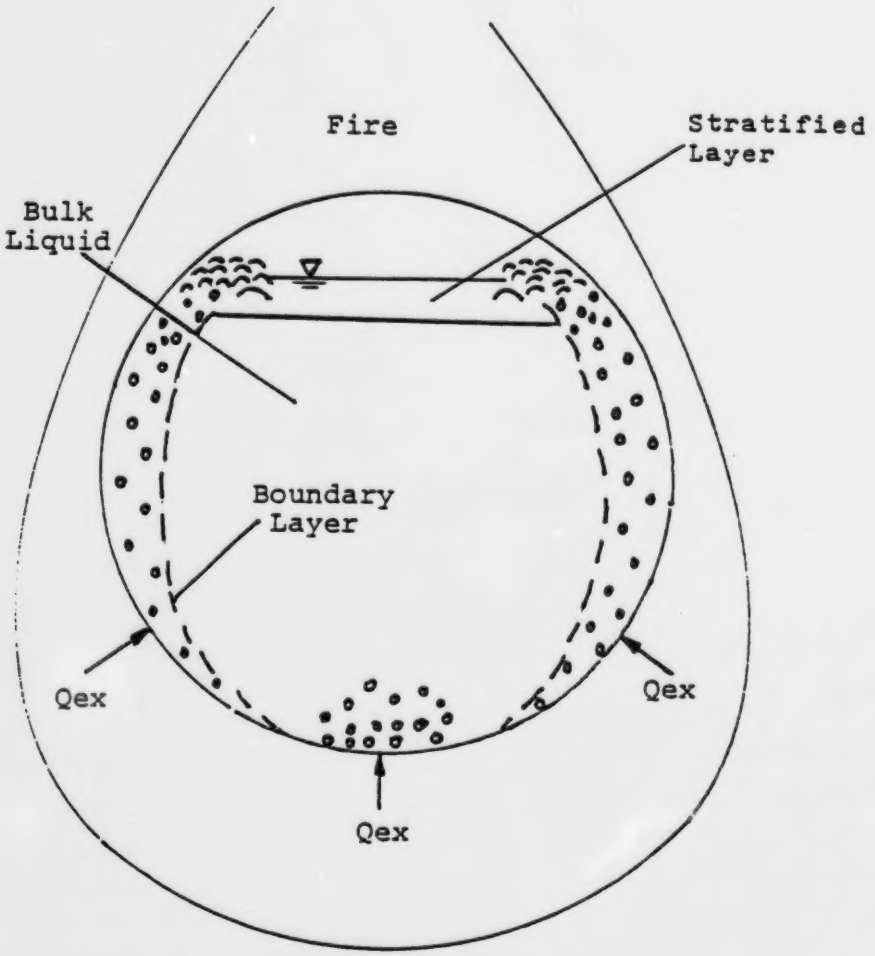


Fig. 1. Physical Model for Subcooled Boiling

bubbles. Since the vessel is hermetically sealed, with the increasing fluid temperature, the pressure in the vessel rises approximately along the pressure-temperature saturation curve (Fig. 2). During this process, the fluid in the boundary layer and at the free surface is at saturation conditions, and is a two-phase mixture. The bulk liquid is however subcooled.

When the pressure in the vessel exceeds some level above a set maximum value predetermined by the design of the pressure relief valve, the valve opens and fluid vents directly into the atmosphere. Hence the pressure drops and a flashing phenomenon begins (Fig. 3). Depending on the valve location and size and the initial loading condition, this depressurization and the resulting flashing can differ considerably.

When a high-pressure, high-temperature vessel is suddenly decompressed, tne depressurization is generally very strong and causes considerable disturbance within the vessel. When the liquid in the vessel is decompressed to a pressure below the saturation pressure corresponding to its initial temperature, the liquid passes from an initial subcooled or saturated condition to a superheated state. During the depressurization processes, the liquid in the boundary layer adjacent to the wall also boils due to heating and depressurization. The bulk liquid above the saturation temperature boils homogeneously due to the pressure drop across the core. Compared with ordinary or heterogeneous boiling, phase change under depressurization causes vapor generation in the superheated liquid body rather than only in the

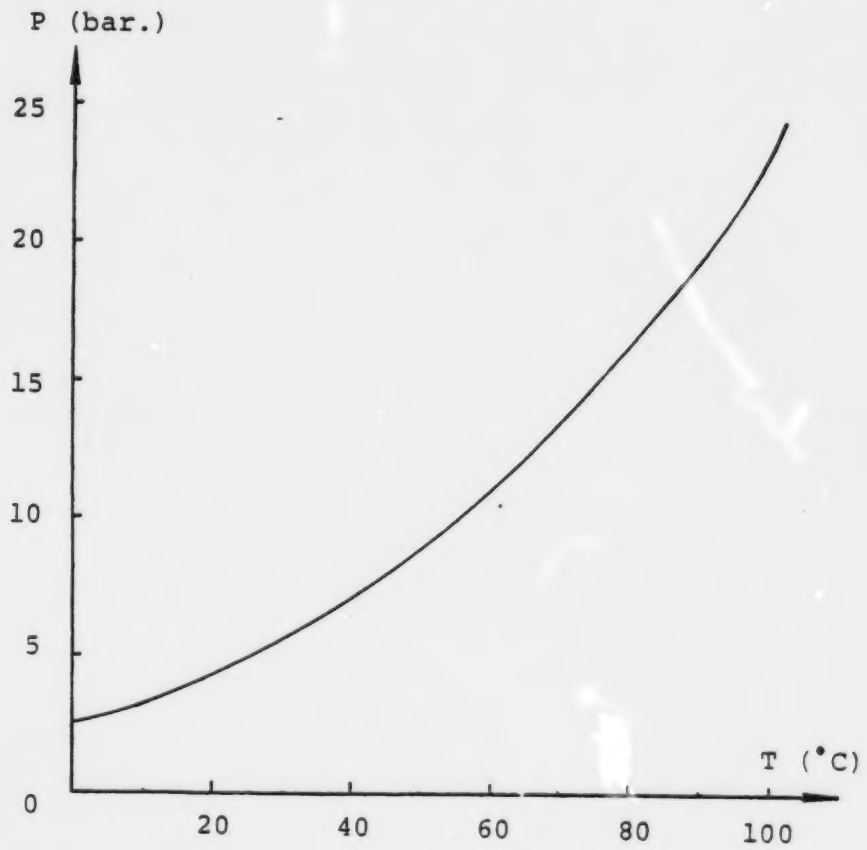


Fig. 2. Pressure-Temperature Saturation Curve (R-11)

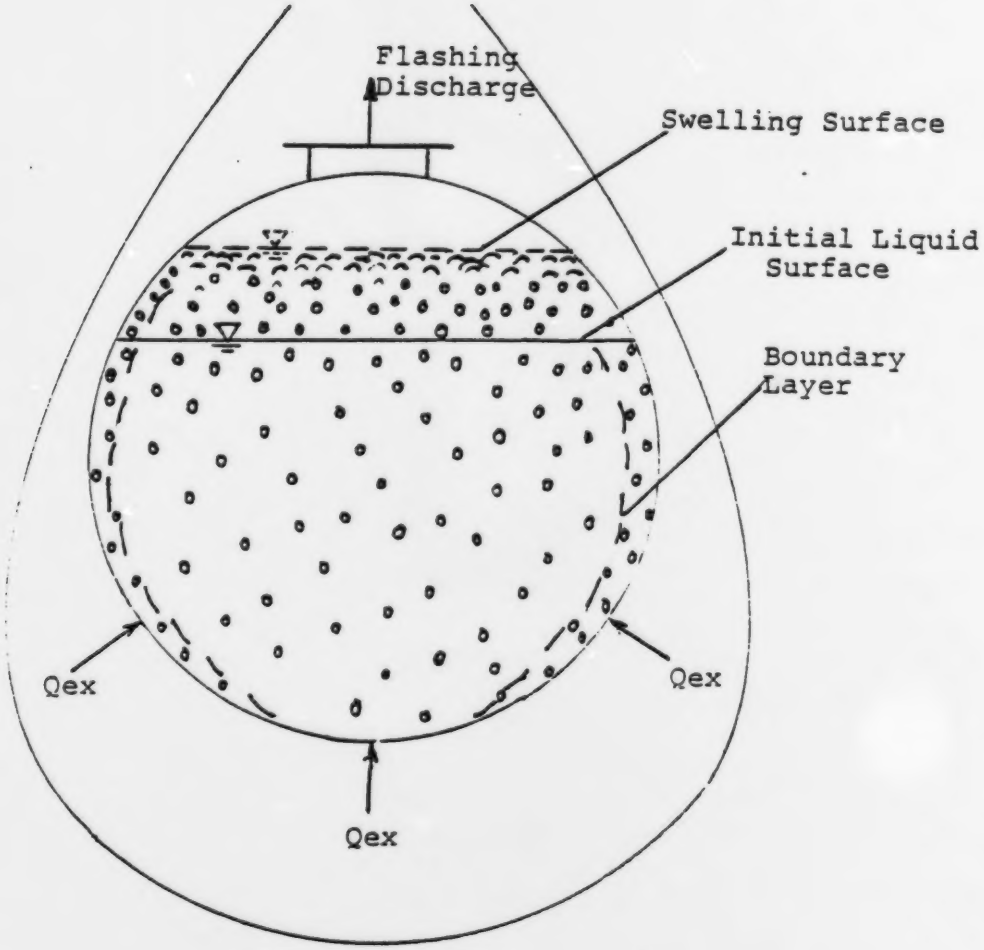


Fig. 3. Physical Model for Flashing

superheated layer adjacent to the heated surface. The process exhibits a transient decay rather than a continuous effect. During the depressurization process, the vessel void fraction therefore changes with time and space.

When the pressure decreases to some set lower value, which is determined by the design of the pressure relief valve, the valve closes. The fluid at the wall then reverts to subcooled boiling corresponding to the pressure in the vessel until such time as the core reaches saturation conditions.

## 1.3 OBJECTIVES

The purpose of the present study is to analyze and measure the characteristics of the flashing phenomena, including the void fraction development, in a partially filled horizontal cylinder containing a pressure liquefied gas subjected to external heating with controlled pressure relief.

Methods of analysis are proposed for the flashing process during depressurization. These comprise the transient void fraction development, the mass flux, and the fluid swell height. Experiments were carried out to observe the mechanism of the subcooled boiling in the boundary layer adjacent to the heated wall and the flashing phenomena both in the bulk liquid and the boundary layer during rapid depressurization. The results in the bulk liquid from these two methods are compared against each other.

# CHAPTER 2

# LITERATURE REVIEW

## 2.1 SUBCOOLED BOILING

The subject of subcooled boiling has been treated by many investigators. Most works deal, however, with studies of heat transfer and surface temperature but not void fraction. Studies on void fraction determination concentrate in the area of forced convection subcooled boiling - a situation quite different from the free convective subcooled boiling situation of with the present problem.

Griffith, Clark and Rohsenow [1] performed experiments at high pressure. Bubble populations were obtained from photographs taken during experiments to evaluate void fraction in subcooled boiling on a test strip in a rectangular flow channel. They considered the subcooled boiling region as two regions. In the first region, the liquid is highly subcooled so that vapor generation at the surface could be neglected in the calculation of void fraction. In this case the heat transferred is used to change the enthalpy of the liquid and to condense the bubbles. In the second region, the surface is covered by several layers of bubbles. They assumed here that the area of condensing vapor no longer changes with length, so that a constant condensing film coefficient can be assumed. In this case, vapor generation is included in the heat balance calculation. According to Rohsenow [2], it was assumed that when the boiling heat flux is five times the convective

heat flux, the boiling region will be "fully developed", and the fluid is in the second boiling region.

According to a balance of the forces exerted on the bubbles in contact with the wall and the temperature distribution in the liquid away from the wall, Levy [3] suggested a calculation method for predicting the point of bubble departure from heated surfaces. He developed a model in which the local vapor weight fraction was calculated from a heat balance at thermal equilibrium. According to the non-thermal equilibrium condition in subcooling and its decaying trend with time. he introduced a simple relation between the local vapor weight fraction and the true local vapor weight fraction. The basis and the form of the relation are very similar to those obtained by Zuber and Findlay [8]. The relation proposed in Ref. [7] was used to obtain the corresponding void fraction.

Zivi [4] assumed that idealized two-phase flow can be described by the linear phenomenological laws derived by Prigogine [5]. Based on this assumption and the principle that the rate of entropy production is minimum in a steady-state thermodynamic process, he formulated the rate of energy dissipation in terms of void fraction and sought a void fraction which minimizes the dissipation.

Bankoff [6] set up a physical model for the bubble flow regime of two-phase flow by considering the flow as a single-phase fluid whose physical properties are a function of cross-sectional position. He neglected the effect of the local slip between phases, but his model

contained the effect of the slip due to cross-sectional averaging of the void fraction profile.

In order to obtain analytical expressions to predict void fraction in subcooled boiling, Zuber et al. [7,8] considered four effects, namely the flow profile, the vapor concentration profile across the cross section, the relative velocity and the non-uniform temperature distribution. They accounted for these effects by means of a concentration parameter which quantifies the effect of the cross-sectional void and volumetric flux distribution, the vapor drift velocity which is a measure of local slip [8], and a dimensionless axial temperature distribution [7].

Kroeger and Zuber [9] evaluated the physical variables affecting void fraction, including the four effects mentioned above and the local conditions of the heated surface. They determined that the point of bubble detachment greatly affects the void fraction, and that axial temperature distribution has a little significance in the forced convective subcooled boiling regime. In the absence of an accurate method of estimating flow profile in various flow regions, they suggested that a constant distribution parameter be taken for all conditions.

Rouhani [10] also made use of the concept of two regions in subcooled boiling. He considered that heat is removed by single-phase heat transfer, vapor generation, heating of the liquid which replaces the detached bubbles, and vapor condensation which transfers the heat

from the vapor to the subcooled liquid. The relative velocity between the two phases is, however, neglected. A criterion was provided for obtaining the limiting value of subcooling between the two regions. He presented some methods for the calculation of void fraction and true liquid subcooling. Compared with experimental data, these methods do not yield satisfactory results in the case of very low mass velocity. Another limitation to the analysis is that some correlations in the model are only valid in certain ranges of heat flux.

By considering the rate of vapor condensation in the liquid, Rouhani and Axelsson [11] obtained an equation for the differential changes in the true steam quality throughout the boiling regimes in the first region. They hence obtained an expression of the vapor weight fraction at any position. In the second region, they used the results of Zuber and Findlay [8] and determined the void fraction corresponding to the calculated steam qualities.

A semi-analytical model by Larsen and Tong [12] is based on the formation and growth of a bubble boundary layer adjacent to the heated surface. They considered that once the bubble layer has been formed near a surface, the imposed wall heat transfer is transmitted across the bubble layer by liquid convection and latent heat transfer within the bubbles to the liquid core-bubble layer interface.

Foster [13] considered a heated vertical plane wall system. On the wall, a two-phase boiling boundary layer is postulated. The general boundary layer theory was used to solve this free-convective boiling

phenomenon. The boundary layer thickness was considered as a linear function of height and external heat flux. The effect of shear stress at the wall was considered to be only a function of the mass and volumetric fluxes of the mixture. The friction factor was also assumed as a constant. They obtained a set of rather simple semi-analytical expressions and compared these results with the data of Cheung and Farhadieh [14] who used an agron blown boundary layer in water.

## 2.2 HOMOGENEOUS BOILING

Flashing or homogeneous boiling is caused by large pressure drops during which a subcooled or saturated liquid becomes superheated. Many experiments have been carried out to study this phenomenon. Analytical models were developed to predict the various parameters in this transient two-phase flow.

Edwards and O'Brien [15] used a concept which is based on the conduction-controlled heat transfer to a cloud of bubbles to predict the phase change effects associated with sudden depressurization. They assumed that the hydrodynamic effects of slip between the phases can be neglected, and that nucleation occurs in the core when the local pressure falls below the saturation value, with no further nucleation subsequently occurring. Experimental results obtained from the depressurization tests on a simple pipe system showed that excessive mass losses were being predicted by the theoretical calculations at later stages of flashing. Hence, they decided that it was necessary to

provide a more appropriate droplet model for the high void fraction condition in order to reduce the rate of mass discharge.

Premoli and Sandri [16] performed experiments in a vessel filled with saturated water to observe the thermohydraulic transients of blowing down through breaks simulated at different positions. The transient pressure and mass histories were recorded during the experiments.

Miyatake et al. [17] carried out experiments to describe the physical mechanism of flashing evaporation. They obtained two exponential decaying curves which describe the two different flashing evaporation processes during depressurization. One decaying curve represents a violent boiling period in the liquid mainly due to depressurization with ordinary boiling neglected. Another curve describes a later boiling period near the liquid free surface when the effects of ordinary boiling are more pronounced. They considered the crossing point of these two exponential curves as the time for completion of the flashing process.

Hooper and Aldelmessih [18] made photographic studies of water flashing caused by suddenly decompressing a heated pool. From this investigation, they introduced a "law of flashing" [19], which stated that during the early part of the transient flashing period, the internal static pressure within the liquid remains nearly constant. This static pressure is determined only by the initial liquid temperature and the physical properties of the liquid, and is

independent of the initial blowdown pressure and the shape of pool.

Lienhard, Alamgir and Trela [20] focussed attention on the early response to depressurization and considered that the rate of despressurization was a strong function of the initial temperature and pressure. They observed that the liquid pressures reached a level far below saturation before nucleation occurred and that most depressurization, about 80 percent, occurred at great speed in the early stage. A sudden pressure recovery then occurred due to the great number of bubbles generated by the resulting superheating of the liquid.

Nariai [21] compared the void distributions in water from simple volume blowdown experiments with the distribution predicted by his bubble gradient model. He found that when the discharge position was in the upper region of the vessel, the real void fraction could be estimated very well by the analytical calculations. When the break position was under the free surface of the liquid, due to the non-equilibrium effects, the real void fractions were smaller compared with those predicted by his analytical calculations.

Hutcherson, Henry and Wollersheim [22] divided the two-phase blowdown process into three parts. Initially, the surface voids grew into the superheated liquid, later, the fluid near the surface was virtually completely dispersed and the expandig voids originating from the walls propagated over large distances into the superheated liquid. Finally, all the fluid in the vessel became dispersed as a two-phase mixture. Three analytical models were developed for the different

decompression regimes. The three models are namely, subcooled blowdown, bubble growth, and dispersion. They were combined to predict the overall two-phase decompression phenomena.

Saha, Abuaf and Wu [23] presented a non-equilibrium vapor generation model for forced flashing flow which includes a flashing inception point, a bubbly flow regime, a bubbly slug regime, an annular regime and a dispersed-droplet regime. Only the first three regimes were, however, analysed. For these three regimes, they obtained different analytical expressions. When void fraction was very low, it was assumed that the bubbles were spherical and they moved with the liquid without slip. When void fraction was a little higher, but less than 0.3, a two-fluid model was used to adapt the vapor drift velocity for calculating the relative velocity. To calculate void fraction, an equation for the conservation of bubble number was utilized. Between void fractions 0.3 to 0.8, they assumed that bubbles nucleated at the wall migrated into the center of the channel and then coalesced. When area-averaged void fraction distributions obtained from experiments were compared with the calculated results from the bubbly-slug model, the results were not in agreement.

In order to explain the flashing phenomena and the differences between flashing and evaporation, Peterson et al. [24] performed two sets of experiments. They determined that surface evaporation took place when the pressure drop was small. When pressure drop was quite large, flashing occurs with mass transfer rates 10-12 times the rates

due to evaporation alone.

Woodford and Scriven [25] developed a mathematical model based on vapor bubble rise velocity. Their physical model is a semi-infinite pool during depressurization, in which the liquid and vapor are at the saturation temperature corresponding to the instantaneous pressure. They obtained a rather simple equation for the void fraction. This simplified correlation is, however, only applicable to shallow pools in thermodynamic equilibrium and when the inertia forces are negligibly small. The analytical model is based on a correlation of vapor rise velocity which is a strong function of the void fraction. Void fractions measured were compared with values calculated using a steady-state correlation for vapor rise velocity in an attempt to determine the validity of the correlation in the transient case. It was found that for small void fraction change with height, the correlation might be accurately applied to transient studies; however, the larger the vertical gradient of void fraction, the greater the overestimate of vapor rise velocity predicted by the correlation. This was considered possible because newly formed bubbles do not immediately agglomerate in the transient case.

Vea and Lahey [26] presented an exact analytical solution of the two-phase system based on a one-dimensional drift-flux technique. The depressurization of a large saturated pool of liquid was studied. They used a void propagation equation derived previously by Zuber and Staub [27]. From this equation and a mass balance in a duct of constant cross

section, an exact solution was obtained. In their physical model of pool swell, they considered that the continuity wave from the bottom of the pool was a very important factor in the boiling regime during early depressurization. The void fraction varies with vertical position and with time below the continuity wave. It was only a function of time above this wave. When the continuity wave reached the pool swell surface, the entire pool was in a transient state. Their calculations indicated that the void fraction profile was strongly dependent upon the vapor drift velocity correlation. Wall heat fluxes affected only weakly the pool swell transient.

# CHAPTER 3

# PHYSICAL MODEL AND MATHEMATICAL DESCRIPTION

## 3.1 INTRODUCTION

The basic conservation equations of two-phase flow can be derived in many different ways [28,29,30]. In the present study, it is assumed that each phase can be described as a continuum governed by the respective partial differential equations from continuum mechanics. The assumptions for this are:

(1). The fluid follows a Newton-Fourier fluid behavior.

(2). The fluid properties are independent of the space field.

(3). The kinetic and potential energy terms are neglected.

(4). The work done by the the system is negligible.

In the following section, assumptions simplify the general equations to that of an actual model are studied.

## 3.2 HOMOGENEOUS BOILING IN A BULK LIQUID DURING DEPRESSURIZATION

### 3.2.1 General

During depressurization, there are two different boiling regions in the space filled by fluid in the vessel. In the region adjacent to the wall, there is a boundary layer. This boundary layer forms and grows not only due to heating by the external heat source but also due to considerable pressure drop in the boundary layer. The effect of homogeneous boiling by depressurizing the boundary layer may be very

strong compared with ordinary boiling due to external heating; it is however a function of the external heat flux.

In the bulk of the liquid, only homogeneous boiling due to depressurization occurs. During this process, the pressure in the vessel is suddenly lowered to a level substantially below the saturation pressure corresponding to the initial liquid surface temperature, resulting in a seemingly explosive phase transition. Since the pressure reduction takes place over the entire superheated liquid space, one can consider that the heat sources are not only on the wall but also distributed throughout the vessel. Throughout the volume superheated liquid transforms its superheat into latent heat. Across the vessel, a great number of bubbles will therefore nucleate and grow. Depending upon the external heat flux, the bubble numbers generated may be much greater than the bubbles generated on the wall by the external heating. The boundary layer region, in which two types of boiling (ordinary boiling due to external heat flux and homogeneous boiling due to flaming) occur, can under certain conditions, be thought to be much less than in the bulk region, thus the effect of the wall region can be neglected in any analysis. The void fraction and velocity of each phase are functions of both space and time. The buoyancy forces will be supplemented by inertia forces due to the verticle acceleration of vapor. Since a considerable amount of the vapor is generated, the single phase fluid in the bulk becomes a two-phase fluid and its volume will swell. If bubble velocity is less than the downward liquid

velocity being caused by the stratification process, vapor or bubble hold up occurs increasing locally the void fraction.

### 3.2.2 Analysis of Conservation of Energy and Mass

With the balances of energy and mass of the fluid in the vessel, a simple model for a horizontal cylinder is developed. During depressurization, void fraction will vary in the vertical direction and with time. One must divide the space into many small elemental layers in x-direction, and assume that the average void fraction in an elemental layer is only a function of time. When the bubbles are generated in the elemental layer, due to the density difference between the two phases and the vertical acceleration of vapor, the buoyancy and inertia forces on a bubble overcome the surface tension and viscous forces on the bubble, and thus the bubble is driven upward. After the bubble has risen from the layer, the liquid mass in the layer reduces. With pressure decreasing, the remaining liquid again becomes superheated relative to the present saturation temperature. The heat from the superheated liquid is then released in the layer and new bubbles form.

In a particular time step, it is assumed that the pressure reduction is linear with respect to time and that the fluid immediately reaches saturation. Thus vapor generation is also uniform with respect to time. From experiments, both here and elsewhere [37], [38], it has been observed that the initial temperature distribution varies linearly in the vertical direction. Thus with time the homogeneous boiling

region will progress from the liquid free surface to the bottom of the vessel step by step. When the bubbles form in an elemental layer, bubbles rise from the lower layers and pass through this layer. Thus the void fraction in this layer depends not only on the newly formed vapor in the layer but also on the rising bubbles from the lower layers. During depressurization, it is assumed that all the heat released from the liquid is used to change a part of the liquid into vapor. In an elemental layer, 2y*dx*1 (Fig. 4), one can perform an energy balance as follows.

The heat released from the liquid is:

$$dQ_\ell = dx\ 2y\ \rho_\ell\ Cp_\ell\ (T_s - T_s') \qquad (3.1)$$

where $T_s$ is the saturated temperature corresponding to the initial pressure within the time interval and $T_s'$ is that corresponding to the final pressure.

The heat transformed into latent heat is:

$$dQ_g = m_g\ h_{fg} \qquad (3.2)$$

where $m_g$ is the mass of vapor produced, $h_{fg}$ is the latent heat for vaporization.

An expression for the mass of vapor produced is obtained by equating the two expressions above,

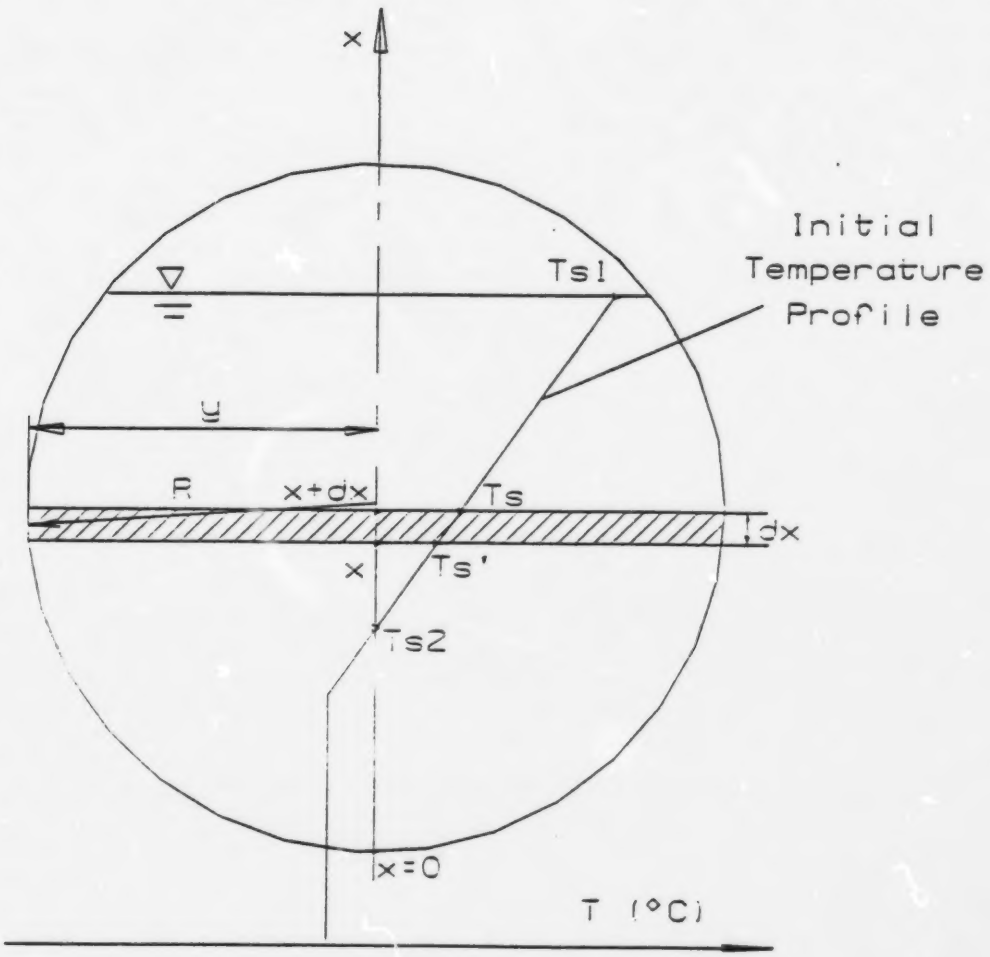


Fig.4. Mathematical Model for
Conservation of Mass and Energy

$$m_g = \frac{dx\ 2y\ \rho_\ell\ Cp_\ell\ (T_s - T_s')}{h_{fg}} \qquad (3.3)$$

The liquid remaining in the volume is given by,

$$m_\ell = dx\ 2y\ \rho_\ell - m_g$$

or

$$m_\ell = dx\ 2y\ \rho_\ell \left[1 - \frac{Cp_\ell}{h_{fg}} (T_s - T_s')\right] \qquad (3.4)$$

In the next time step, the thickness of the liquid elemental layer used for vaporization is given by,

$$dx' = dx\ \frac{\rho_\ell}{\rho_\ell'} \left[1 - \frac{Cp_\ell}{h_{fg}} (T_s - T_s')\right] \qquad (3.5)$$

where $dx'$, $\rho_\ell'$ are the liquid layer thickness and liquid density in the next time step respectively.

According to the definition of void fraction, a solution to the above equations is obtained and presented in section 4.2.1.

### 3.2.3 Drift Flux Two-Phase Flow Model

A simplified one-dimensional homogeneous flow model is also developed to describe the homogeneous boiling in the bulk liquid. The model is based upon the following assumptions:

(1) The shear stress and heat flux at the wall are neglected.

(2) Cross-sectional thermal equilibrium is considered.

(3) The axial pressure is considered constant and varies only with time.

Since the two-phase mixture is considered as a continium a two-phase flow drift flux model will greatly simplify the analytical process.

In a one-dimensional situation, we have [30],

$$\frac{\partial[\rho_g \alpha\, S]}{\partial t} + \frac{\partial[\rho_g \alpha\, Ug\, S]}{\partial x} = Mg\, S \tag{3.6}$$

$$\frac{\partial[\rho_\ell\, (1-\alpha)\, S]}{\partial t} + \frac{\partial[\rho_\ell\, (1-\alpha)\, U_\ell\, S]}{\partial x} = M_\ell\, S \tag{3.7}$$

The one-dimensional mixture energy equation is [30]

$$\frac{\partial[\alpha\, \rho_g h_g S]}{\partial t} + \frac{\partial[(1-\alpha)\, \rho_\ell h_\ell S]}{\partial t}$$

$$+ \rho_g \frac{\partial[\alpha\, Ug\, h_g S]}{\partial x} + \rho_\ell \frac{\partial[(1-\alpha)\, U_\ell\, h_\ell S]}{\partial x}$$

$$= \frac{\partial p}{\partial t} S + Q + Hg + H_\ell \tag{3.8}$$

where S is the cross-section area. Since the wall heat flux is neglected, Q = 0 and for thermal equilibrium, Hg = $H_\ell$ = 0.

Substituting (3.6) and (3.7) into Eq. (3.8), one obtains,

$$\alpha\,\rho_g S\left[\frac{\partial h_g}{\partial t} + Ug\,\frac{\partial h_g}{\partial x}\right] + (1-\alpha)\,\rho_\ell S\left[\frac{\partial h_\ell}{\partial t} + U_\ell\,\frac{\partial h_\ell}{\partial x}\right]$$

$$= \frac{\partial P}{\partial t}\,S - Mg\,(h_g - h_\ell)\,S$$

that is,

$$\alpha\,\rho_g\,\frac{dh_g}{dt} + (1-\alpha)\,\rho_\ell\,\frac{dh_\ell}{dt} = \frac{dP}{dt} - Mg\,(h_g - h_\ell) \qquad (3.9)$$

and

$$Mg = \frac{1}{h_{fg}}\left[1 - \alpha\,\rho_g\,\frac{dh_g}{dP} - (1-\alpha)\,\rho_\ell\,\frac{dh_\ell}{dP}\right]\frac{dP}{dt} \qquad (3.10)$$

where $h_{fg}$ is the latent heat ($h_{fg} = h_g - h_\ell$).

Combining Eqs. (3.6) and (3.7) as in Ref. [25], a mixture continuity equation results,

$$\frac{1}{1-\alpha}\,\frac{\partial \alpha}{\partial t} + \frac{1}{S}\left[Ug + \frac{\alpha}{1-\alpha}\,U_\ell\right]\frac{\partial(\alpha S)}{\partial x} + \alpha\,\frac{\partial(Ug - U_\ell)}{\partial x}$$

$$+ \alpha\left[\frac{1}{\rho_g}\,\frac{d\rho_g}{dP} - \frac{1}{\rho_\ell}\,\frac{d\rho_\ell}{dP}\right]\frac{dP}{dt} \qquad (3.11)$$

$$= Mg\left(\frac{1}{\rho_g} + \frac{1}{\rho_\ell}\,\frac{\alpha}{1-\alpha}\right)$$

From the definition of drift velocity,

$$Vgj = \frac{\overline{\alpha(Ug - J)}}{\overline{\alpha}} \qquad (3.12)$$

where the bar above each function means that it is a cross-section average quantity, and $J=J_\ell + Jg$ represents the total volumetric flux of the mixture.

From Ref. [7], the average void fraction was given as:

$$\overline{\alpha} = \frac{\overline{Jg}}{C_o\overline{J} + Vgj} \qquad (3.13)$$

where $C_o$ is a void concentration parameter. Since we may assume a developing bubbly profile in the boiling region, then $C_o \triangleq 1.0$, as taken from Ref. [31]

Hence,

$$(1-\overline{\alpha})\ \overline{Jg} - \overline{J}_\ell\ \overline{\alpha} = \overline{\alpha}\ Vgj\ ,$$

with:

$$\overline{Jg} = \overline{\alpha}\ \overline{Ug}$$

$$\overline{J}_\ell = (1-\overline{\alpha})\ \overline{U}_\ell\ ,$$

and the relative velocity,

$$\overline{Ug} - \overline{U}_\ell = \frac{Vgj}{1-\overline{\alpha}} \qquad (3.14)$$

For churn-turbulent bubbly flow, the drift velocity is equal to the bubble terminal rise velocity. The terminal rise velocity is obtained

through an analysis of the forces exerted on the bubble. Its general expression is of the following form:

$$U_\infty = k_3 \left[\frac{(\rho_\ell - \rho_g)\ \sigma\ g}{\rho_\ell^2}\right]^{1/4} \qquad (3.15)$$

where $k_3$ is a constant.

Since $U_g = U_\ell + U_b$ and $U_b = \frac{V_{gj}}{1-\alpha}$, it follows that

$$\frac{1}{1-\alpha}\left[\frac{\partial \alpha}{\partial t} + \frac{1}{S}\left(U_\ell + \frac{2-\alpha}{1-\alpha} V_{gj}\right)\frac{\partial(\alpha S)}{\partial x}\right] + \left(A - \frac{\alpha}{1-\alpha} B\right) = 0 \qquad (3.16)$$

where:

$$A = \left[\frac{\alpha}{\rho_g}\frac{d\rho_g}{dP} - \frac{1}{h_{fg}\rho_g} + \frac{\alpha}{h_{fg}}\frac{dh_g}{dP} + \frac{1-\alpha}{h_{fg}}\frac{\rho_\ell}{\rho_g}\frac{dh_\ell}{dP}\right]\frac{dP}{dt} \qquad (3.17)$$

and,

$$B = \left[\frac{1-\alpha}{\rho_\ell}\frac{d\rho_\ell}{dP} + \frac{1}{h_{fg}\rho_\ell} - \frac{\alpha}{h_{fg}}\frac{\rho_g}{\rho_\ell}\frac{dh_g}{dP} - \frac{1-\alpha}{h_{fg}}\frac{dh_\ell}{dP}\right]\frac{dP}{dt} \qquad (3.18)$$

By integrating Eqs. (3.6) and (3.7) from 0 to x, the following expressions are obtained.

$$\rho_g\left[(\alpha U_b S) - (\alpha U_b S)_{x=0^+} \alpha U_\ell S\right] + \rho_g \int_0^x \frac{\partial \alpha S}{\partial t}\, dx + \frac{d\rho_g}{dt}\int_0^x \alpha\, Sdx = \int_0^x MgSdx$$

$$\rho_\ell (1-\alpha) U_\ell S - \rho_\ell \int_0^x \frac{\partial \alpha S}{\partial t}\, dx + \frac{d\rho_\ell}{dt}\int_0^x (1-\alpha)\, Sdx = \int_0^x M_\ell\, Sdx$$

Combining these two equations and using Eqs. (3.17) and (3.18), an expression for $U_\ell$ is obtained as follows,

$$U_\ell = \frac{1}{S}\left[(\alpha\, U_b S)_{x=0} - (\alpha\, U_b S) - \int_0^x S\,(A+B)\,dx\right] \qquad (3.19)$$

It is known that the temperature distribution in the vertical direction is not uniform [37]. However, the above equations are valid only in the case where the initial temperature profile is uniform in the x-direction. As in Section 3.2.2, the liquid space is divided into many small layers, each with a uniform temperature profile.

The region of uniform temperature profile initially only includes a small regime close to the liquid surface (Fig. 5). With the pressure decreasing, this region descends to lower layers (Fig. 6).

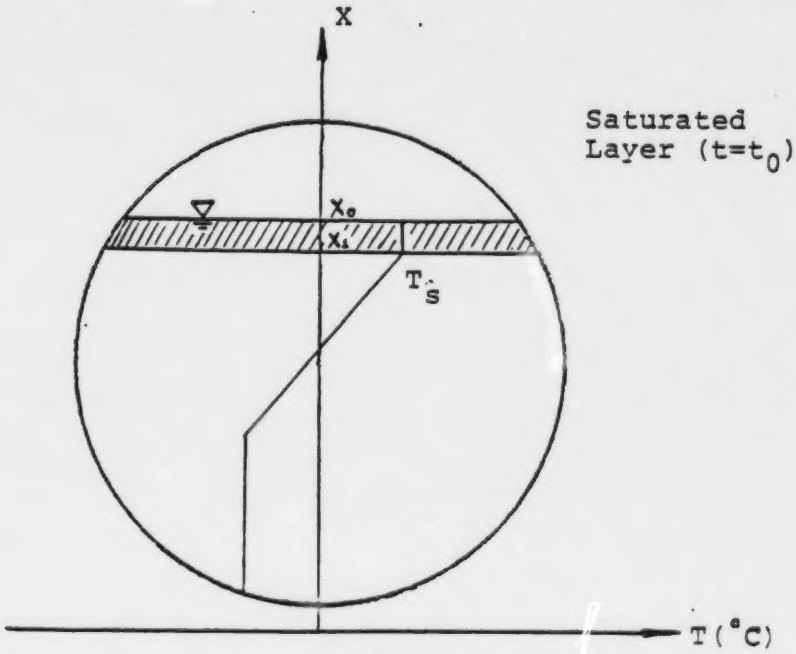


Fig.5. Saturation Region
for $t=t_0$

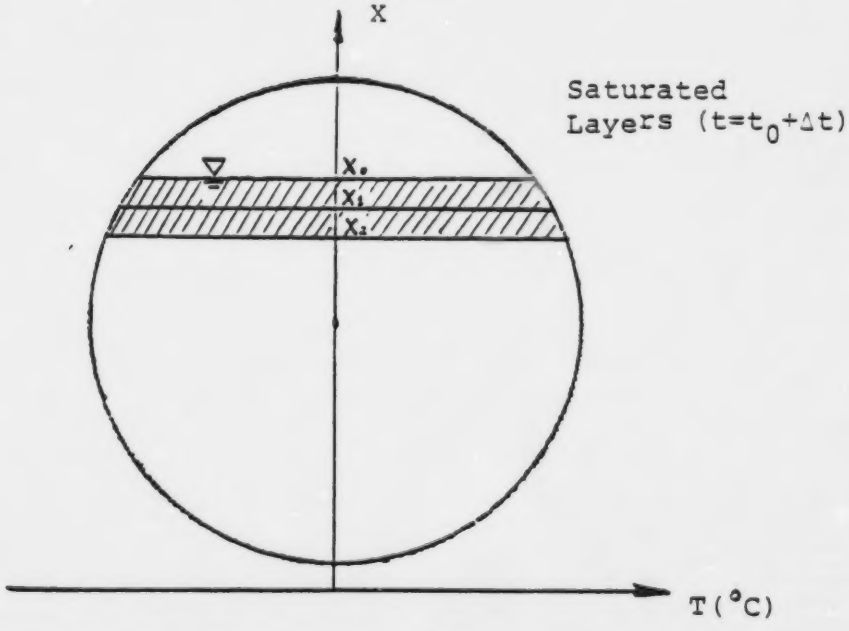


Fig.6. Saturation Region
for $t=t+\Delta t$ $(\Delta t>0)$

# CHAPTER 4

# ANALTYICAL AND NUMERICAL SOLUTIONS

## 4.1 THEORETICAL SOLUTION ANALYSIS

### 4.1.1 Overall Average Void Fraction during Depressurizaton

From the conservation of energy and mass, the expressions of overall average void fraction may be obtained. To simplify the analytical process, a linear relation between the pressure and time during depressurization was assumed, namely,

$$\frac{dP}{dt} = - C \qquad (C > 0) \tag{4.1}$$

where C is a constant determined from the PRV characteristics. When t equals 0, P equals $P_1$ and when flashing finishes, P equals $P_2$, therefore,

$$P = P_1 - C\,t \qquad (0 \leq t \leq \frac{P_1 - P_2}{C}) \tag{4.2}$$

In Section 3.2.2., the initial temperature distribution may be considered as a linear function of the vertical height,

$$T = \frac{T_1 - T_2}{x_1 - x_2}(x - x_2) + T_2 \tag{4.3}$$

The relation between the pressure and temperature will be expressed by the Clausius-Clapeyron equation,

$$\left(\frac{dP}{dT}\right)_S = \frac{h_{fg}}{T_s V_{fg}} \tag{4.4}$$

Hence, the saturated temperature in the vessel varies only with time corresponding to the following equation,

$$T_s(t) = T_{s1} \exp\left[-\left(\frac{V_{fg}}{h_{fg}}\right)_m (C\ t)\right] \tag{4.5}$$

Supposing that the latent heat is immediately released by the superheated liquid during depressurization; the region in which flashing occurs will develop downward with time according to

$$x(t) = \frac{x_1 - x_2}{T_{s1} - T_{s2}} \left\{T_{s1} \exp\left[-\left(\frac{V_{fg}}{h_{fg}}\right)_m (C\ t)\right] - T_{s2}\right\} + x_2 \tag{4.6}$$

According to Eqn. (3.3), from time to t to t+Δt, the vapor generated in an elemental layer will be,

$$dMg\ (t+\Delta t) = \frac{dx\ 2y\ \rho_\ell(t)\ Cp_\ell[T_s(t) - T_s(t+\Delta t)]}{h_{fg}(t)} \tag{4.7}$$

In the vessel, the vapor mass generated in the time interval Δ t is:

$$Mg\ (t+\Delta t) = \frac{2\rho_\ell(t)\ Cp_\ell[T_s(t) - T_s(t+\Delta t)]}{h_{fg}(t)} \int_{x(t+\Delta t)}^{x_1} \frac{}{\sqrt{2xR - x^2}}\, dx$$

that is,

$$Mg(t+\Delta t) = \frac{\rho_\ell(t)\ Cp_\ell[T_s(t)-T_s(t+\Delta t)]}{h_{fg}(t)}$$

$$* \quad \{[(x_1-R)\ \sqrt{2x_1R-x_1^2} + R^2 \arcsin\ (\frac{x_1}{R} - 1)] \qquad (4.8)$$

$$- [(x(t+\Delta t)-R)\ \sqrt{2x(t+\Delta t)R-x(t+\Delta t)^2} + R^2 \arcsin\ (\frac{x(t+\Delta t)}{R} - 1)]\}$$

The liquid remaining above $x(t+\Delta t)$ will be:

$$M_\ell(t+\Delta t) = 2\ \rho_\ell(t)\ (1 - \frac{Cp_\ell}{h_{fg}(t)}\ [T_s(t)-T_s(t+\Delta t)]$$

$$* \quad \{[(x_1-R)\ \sqrt{2x_1R-x_1^2} + R^2 \arcsin\ (\frac{x_1}{R} - 1)] \qquad (4.9)$$

$$- [(x(t+\Delta t)-R)\ \sqrt{2x(t+\Delta t)R-x(t+\Delta t)^2} + R^2 \arcsin\ (\frac{x(t+\Delta t)}{R} - 1)]\})$$

According to the definition of void fraction:

$$\bar{\alpha}\ (t+\Delta t) = \frac{Vg(t+\Delta t)}{V_\ell(t+\Delta t)+Vg(t+\Delta t)} \qquad (4.10)$$

where $Vg(t+\Delta t) = \frac{Mg(t+\Delta t)}{\rho_g(t+\Delta t)}$ , $V_\ell(t+\Delta t) = \frac{M_\ell(t+\Delta t)}{\rho_\ell(t+\Delta t)}$

Substituting Eqs. (4.8) and (4.9) into (4.10) results in:

$$\bar{\alpha}(t+\Delta t) = \frac{\frac{\rho_{\ell}(t+\Delta t)}{\rho_g(t+\Delta t)}}{\frac{h_{fg}(t)}{Cp_{\ell}[T_s(t)-T_s(t+\Delta t)]} - 1 + \frac{\rho_{\ell}(t+\Delta t)}{\rho_g(t+\Delta t)}} \qquad (4.11)$$

This is the average void fraction in the vessel above $x(t+\Delta t)$ from time $t$ to $t+\Delta t$. From this result an expression of swell height may be obtained.

4.1.2 Swell Height and Total Vapor Mass Flux

During depressurization the swell height of the fluid and total mass flux are only functions of time. Above $x(t+\Delta t)$, the volume of the two-phase fluid is:

$$V(t+\Delta t) = V_{\ell}(t+\Delta t) + Vg(t+\Delta t) \qquad (4.12)$$

which should equal the volume between $x(t+\Delta t)$ and $x'(t+\Delta t)$ in the vessel:

$$V = 2\int_{x(t+\Delta t)}^{x'(t+\Delta t)} \sqrt{2xR-x^2}\, dx$$

where $x'(t+\Delta t)$ is the swell height at time $t+\Delta t$. That is,

$$[x'(t+\Delta t)-R]\sqrt{2x'(t+\Delta t)R-x'(t+\Delta t)^2}$$

$$+ \frac{R^2}{2} \arcsin \left(\frac{x'(t+\Delta t)-R}{R}\right) \qquad (4.13)$$

$$= [x(t+\Delta t)-R] \sqrt{2x(t+\Delta t)R-x(t+\Delta t)^2}$$

$$+ \frac{R^2}{2} \arcsin \left(\frac{x(t+\Delta t)-R}{R}\right) + V_\ell(t+\Delta t) + Vg(t+\Delta t)$$

During the whole process of depressurization, the total vapor mass is:

$$d\bar{M}g = \frac{2y\ dx\ \rho_{\ell m} Cp_\ell (T_s - T_{s2})}{h_{fgm}} \qquad (4.14)$$

Substituting Eq. (4.3) into Eq. (4.14) and integrating,

$$\bar{M}g = \frac{2\rho_{\ell m} Cp_\ell}{h_{fgm}} \frac{T_{s1}-T_{s2}}{x_1-x_2}$$

$$* \left(\frac{1}{3}\sqrt{2Rx_2-x_2^2} + (x_2-R)\left[\frac{x_2-R}{2}\sqrt{2x_2R-x_2^2} + \frac{R^2}{2}\arcsin\left(\frac{x_2}{R}-1\right)\right]\right. \qquad (4.15)$$

$$\left. - \left\{\frac{1}{3}\sqrt{2Rx_1-x_1^2} + (x_2-R)\left[\frac{x_1-R}{2}\sqrt{2x_1R-x_1^2} + \frac{R^2}{2}\arcsin\left(\frac{x_1}{R}-1\right)\right]\right\}\right)$$

The final liquid mass in the vessel will be thus:

$$\bar{M}_\ell = \rho_{\ell m} \int_0^{x_1} 2\sqrt{2Rx-x^2}\,dx - \bar{M}g$$

that is,

$$\overline{M}_{\ell} = \rho_{\ell m}[(x_1-R)\sqrt{2Rx_1-x_1^2} + R^2 \arcsin\left(\frac{x_1}{R} - 1\right) + R^2\frac{\pi}{2}] - \overline{M}g \quad (4.16)$$

The total mass of vapor produced over the entire period of flashing in the vessel therefore may be represented with an overall averaged void fraction,

$$\overline{\alpha} = \frac{\dfrac{\rho_{\ell m}}{\rho_{\ell m}}}{\dfrac{\overline{M}_{\ell}}{\overline{M}_g} + \dfrac{\rho_{\ell m}}{\rho_{\ell m}}} \quad (4.17)$$

The comparison of results obtained from Eq. (4.17) with some test data is presented in Appendix 1.

## 4.2 NUMERICAL SOLUTION PROCEDURES

### 4.2.1 Energy and Mass Analysis in the Bulk Liquid

In Section 3.2, with the assumptions of no heat and mass loss, the energy and mass balances in an elemental layer were set up. Since the effect of an external heat source is neglected here, the physical model may be simplified into a horizontal pressure cylinder. The pressure in the vessel varies only with time and the properties of the fluid depend on the different pressure values. Since the initial temperature distribution is not uniform in the vertical direction, the region in which liquid temperature exceeds the saturation point corresponding to

the pressure will vary with time during depressurization. With pressure reducing from $P_{t-\Delta t}$ to $P_t$ between time t-Δt to t, the corresponding saturation temperature will change from $T_{st-\Delta t}$ to $T_{st}$. Considering that the temperature of the ith elemental layer is above $T_{st}$, the produced vapor mass and remaining liquid mass in that same layer during time interval Δt are given by the following two equations respectively,

$$Mg_{t,i} = \frac{\Delta x_{t-\Delta t} 2y_i \rho_{\ell t-\Delta t} Cp_\ell (T_{st-\Delta t} - T_{st})}{h_{fgt-\Delta t}} \qquad (4.18)$$

$$M_{\ell t,i} = \Delta x_{t-\Delta t} 2y_i \rho_{\ell t-\Delta t} \left[1 - \frac{Cp_\ell (T_{st-\Delta t} - T_{st})}{h_{fgt-\Delta t}}\right] \qquad (4.19)$$

Assuming that vapor generation is uniform the pressure reduction is linear with time during time Δt. The vapor mass generation rate is,

$$m_{gt,i} = \frac{Mg_{t,i}}{\Delta t} \qquad (4.20)$$

$$\delta t = \frac{\Delta x_{t-\Delta t}}{U_{bt}} \qquad (4.21)$$

During Δt, the bubbles are rising upward while the vapor mass is produced continuously. Since the rate of generation has been assumed to be a constant, a running balance will be set up between the bubbles generated and those leaving in the element volume. The vapor mass in the elemental layer is,

$$m_{gt,i} = \frac{M_{gt,i}}{\Delta t}\,\delta t \qquad (4.22)$$

Since some liquid is evaporated, the liquid mass in the vessel decreases. In the next time step, the volume of liquid is changed and the thickness of the elemental layer becomes

$$\Delta x_t = \Delta x_{t-\Delta t}\,\frac{\rho_{\ell t-\Delta t}}{\rho_{\ell t}}\left[1 - \frac{Cp_\ell}{n_{fgt-\Delta t}}\,(T_{st-\Delta t} - T_{st})\right] \qquad (4.23)$$

From Fig. 4, the widtn of the itn elemental layer may be expressed as,

$$2y_i = 2\sqrt{R^2 - [R - x_i + \Delta x_i/2]^2} \qquad (4.24)$$

When the vapor rising from the lower layers into this elemental layer is considered, according to the definition of void fraction, the following expression of void fraction at the jtn time and in the itn layer is obtained,

$$\alpha_{i,j} = \frac{Sg}{(1/A_j - 1)\,y_i + Sg} \qquad (4.25)$$

where

$$Sg = \frac{\rho_{\ell j}}{\rho_{gj}}\left\{\left[\left(\frac{1}{1-A_{j-1}}\,\frac{\rho_{\ell j-1}}{\rho_{\ell j-2}}\,y_{j-1} + y_{j-2}\right)\frac{1}{1-A_{j-2}}\,\frac{\rho_{\ell j-2}}{\rho_{\ell j-3}} + y_{j-3}\right]\frac{1}{1-A_{j-3}}\,\frac{\rho_{\ell j-3}}{\rho_{\ell j-4}}\right.$$

$$+ \ldots + y_i \} \frac{\delta_{tj}}{\Delta t_j}$$

$$A_k = \frac{Cp_\ell (T_{sk-1} - T_{sk})}{h_{fg\ k-1}} \qquad \begin{matrix} (k= i,\ i+1,\ i+2,\ \ldots,\ j) \\ (i= 1,\ 2,\ 3,\ \ldots) \end{matrix}$$

The calculating procedure is as follows. From time $t_{j-1}$ to $t_j$, the pressure in the vessel will be reduced from $P(t_{j-1})$ to $P(t_j)$. The region, in which vapor mass is generated, will spread downward to the ith layer. Eq. (4.25) is used to obtain the void fraction distribution during $\Delta t = t_j - t_{j-1}$. From Eq. (4.23), the thickness of each layer may be obtained. Eqs. (4.19) and (4.20) give the remaining liquid mass and escaped vapor mass in each layer.

The initial conditions are:

t=0, (j=1), the void fraction in the vessel is 0, and other variables are set to suitable initial values.

From the obtained void fraction distribution, the swell height is

$$H_j = x_j + \sum_{i=1}^{j} \frac{1}{1-\alpha_{i,j}} \Delta x_{i,j} \qquad (4.26)$$

### 4.2.2 Solution of the Drift Flux Model

In Section 3.2.3, Eq. (3.16) gives the differential relation between the void fraction and the vertical space and time. From Fig. 7, Eq. (3.16) is discretized to obtain a numerical solution. The finite-difference representation of Eq. (3.16) in the ith control volume and

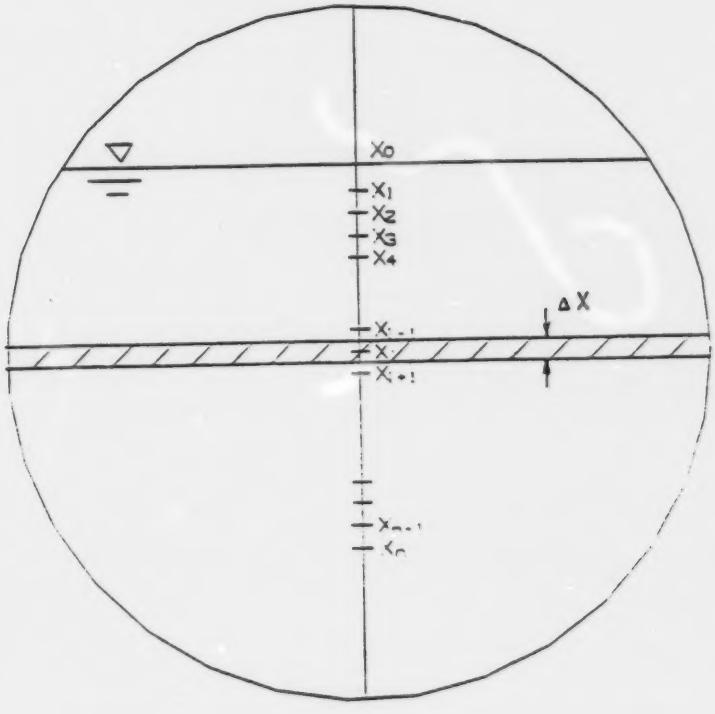


Fig.7. Drift Flux Two-phase Fluid Model

jth time step is:

$$\alpha_{i,j} = \frac{S_{i+1}}{S_i}\,\alpha_{i+1,j} - \frac{\dfrac{\alpha_{i,j}-\alpha_{i,j-1}}{\Delta t_j} + A_{i,j}(1-\alpha_{i,j}) - B_{i,j}\alpha_{i,j}}{U_{\ell k,j} + \dfrac{2-\alpha_{i,j}}{1-\alpha_{i,j}}\,Vgj}\,\Delta x \qquad (4.27)$$

where subscript i indicates that the variables are in the control volume, i+1 is defined as the lower layer, j is the time step considered, and j-1 is the former time step. By Euler's method, the predicted void fraction in the ith level, $\alpha^{o}_{i,j}$, can be obtained with the value at the (i+1)th level:

$$\alpha^{o}_{i,j} = \frac{S_{i+1}}{S_i}\,\alpha_{i+1,j} - \frac{\dfrac{\alpha_{i+1,j}-\alpha_{i,j-1}}{\Delta t_j} + A_{i+1,j}(1-\alpha_{i+1,j}) - B_{i+1,j}\alpha_{i+1,j}}{U_{\ell i+1,j} + \dfrac{2-\alpha_{i+1,j}}{1-\alpha_{i+1,j}}\,Vgj_j}\,\Delta x \qquad (4.28)$$

The void fraction in the ith level may then be calculated from $\alpha_{i+1,j}$ and $\alpha^{o}_{i,j}$:

$$\alpha_{i,j} = \frac{S_{i+1}}{S_i}\,\alpha_{i+1,j} - \frac{\Delta x}{2}\left[\frac{\dfrac{\alpha_{i+1,j}-\alpha_{i,j-1}}{\Delta t_j} + A_{i+1,j}(1-\alpha_{i+1,j}) - B_{i+1,j}\alpha_{i+1,j}}{U_{\ell i+1,j} + \dfrac{2-\alpha_{i+1,j}}{1-\alpha_{i+1,j}}\,Vgj_j}\right.$$

$$+\frac{\frac{\alpha^{o}_{i,j}-\alpha_{i,j-1}}{\Delta t_j}+A^{o}_{i,j})1-\alpha^{o}_{i,j})-B^{o}_{i,j}\alpha^{o}_{i,j}}{U^{o}_{\ell i,j}+\frac{2-\alpha^{o}_{i,j}}{1-\alpha^{o}_{i,j}}Vgj_j}] \tag{4.29}$$

where A, B, $U_\ell$ and $V_{gj}$ are defined by Eqs. (3.17), (3.18), (3.19) and (3.12), respectively, $A^o$, $B^o$, and $U_\ell{}^o$ indicate that $\alpha_{i,j}$ is replaced by $\alpha^o_{i,j}$ in the defining equations.

# CHAPTER 5

# EXPERIMENTAL APPARATUS, PROCEDURES, AND MEASUREMENTS

## 5.1 INTRODUCTION

The object of the present section is to develop a simple technique to measure the void fraction. Of all the void fraction measurement techniques available, the following two kinds of methods are the most widely used [32]. The first type is based on nuclear engineering applications such as gamma attenuation, x-ray attenuation, etc. The second one is based on the principle that the electrical impedance between two electrodes filled by a two-phase fluid changes due to the different vapor content in the fluid.

The electrical impedance methods are more suitable and less expensive for most investigations compared with nuclear techniques. Generally speaking, electrical impedance methods have the following advantages: i) most economical, ii) simple apparatus, iii) applicable to transient phenomena due to its fast response to void variation, and iv) the output is an analog voltage suitable for process control.

The conductivity of a fluid is strongly influenced by temperature and ion concentration, which can be difficult to control, and can be changed by orders of magnitude. The dielectric constant, however, is relatively insensitive to these effects. It is obvious that measurements based on capacitance are easier and more convenient and

generally provide better reproducibility than those based on conductance.

## 5.2 TEST INSTRUMENTS

### 5.2.1 Apparatus

Fig. 8 shows the test pressure vessel and instrument arrangement. All of the results reported herein were obtained by using this set-up. The apparatus is described in detail elsewhere [37], [38]; only a general outline will be given here. It consists of an electrically heated horizontal double walled cylinder, variable area pressure relief valve (PRV) orifices (6 - 25 mm dia.), two 25 mm thick observation windows, and instrumentation.

The inner stainless steel cylinder is heated by nine individual heater elements located between the inner cylinder and a mild steel argon cooled pressure ballasted outer cylinder. Heater power can range between 0 to 80 $kw/m^2$, and is maintained by the use of three manually controlled 220v 3-phase variacs. When the pressure in the inner vessel reaches a predetermined initial value, the pressure relief valve opens under computer control. After the pressure drops to a predetermined level (approximately 95% of the initial pressure), the valve is closed. If necessary, the valve can be controlled to open until the pressure decreases to atmospheric pressure. The change in the liquid level and flashing phenomena in the vessel can be recorded by a time synchronized video system positioned in front of the observation

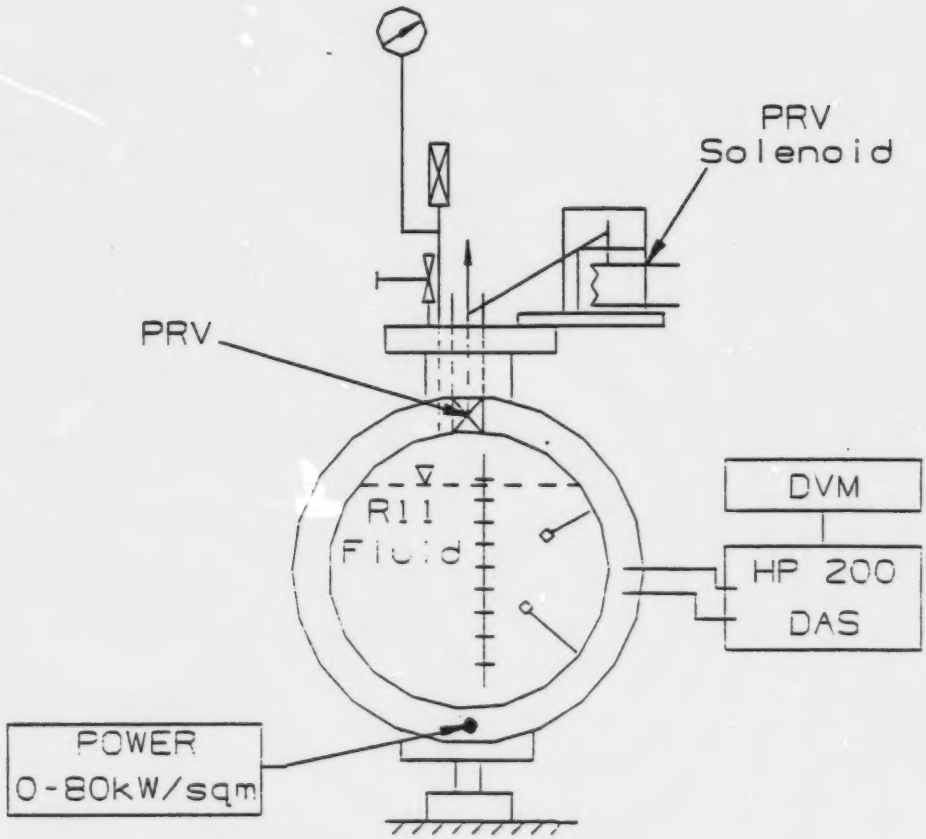


Fig.8. Experimental Apparatus

windows.

The instrumentation used here for void fraction determination includes nine central rod-ring capacitance sensors, four radio-frequency boundary layer probes and some shielded and stainless steel sheathed iron or copper constantan thermocouples and pressure transducers in the vessel (Fig. 9). An automatic data acquisition and control unit was used for overall system control, data reduction, and recording. The system includes a fast reading scanner, an HP-3437 High Speed Voltmeter, the system mainframe, an HP-3497A Data Acquisition/Control Unit, and a program performer (the HP-9920 system Computer). The HP-3437 can provide precisely timed sample and hold readings. The sampled readings are transferred into the HP-9920 using a high speed buffered transfer in packed output format. The data are then converted to ASCII format and stored onto a disc for future use.

### 5.2.2 Capacitance Transducers and Electrical Circuit

As stated above, by utilizing the difference between the dielectric constants of liquid and vapor, it is possible to detect changes in relative phase concentration by measuring the electric capacitance between two electrodes in a two-phase mixture. The design of the central rod-ring sensor was based on this principle and was used to measure the overall void fraction, which is an averaged vapor content in a certain volume of space enclosing the internal cross-sectional area of the sensor over some axial distance. Fig. 10 shows the sensors'

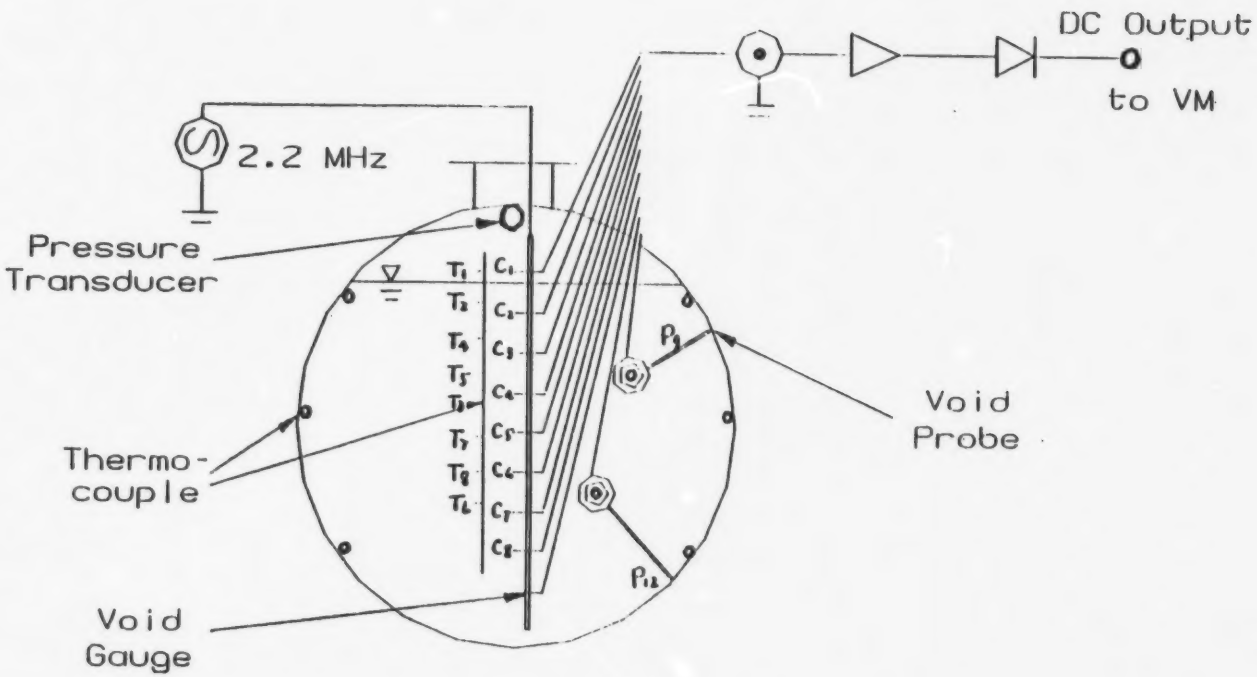


Fig.9. Experimental Instrumentation

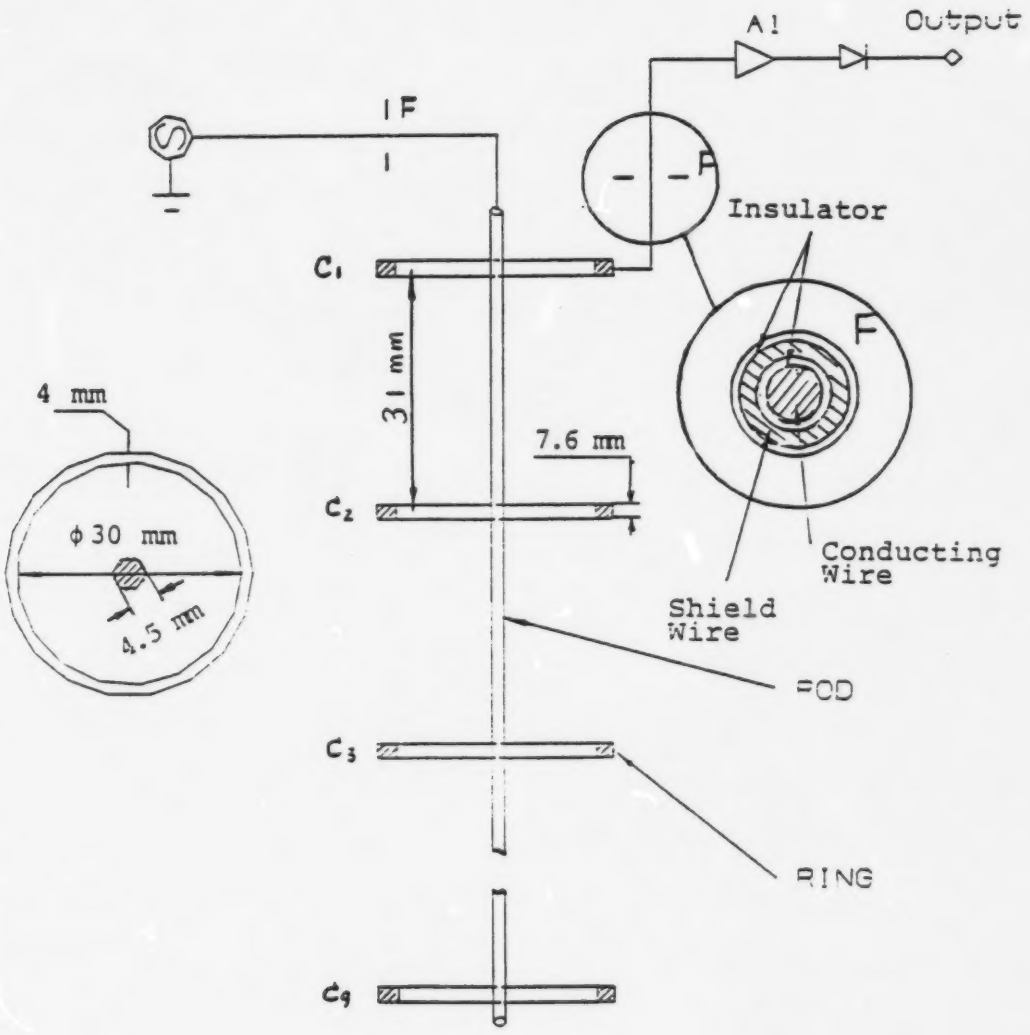


Fig. 10 Central Rod-Ring Sensor

configuration and arrangement. A high frequency (2.2 MHz) sine wave is applied to the central rod and the input wave is changed through the capacitance sensor immersed in the working fluid. From the ring the output signals are received. Quite sensitive responses can be obtained when the components of mixture vary as has been shown by others [39].

To measure the local void fraction in the boundary layer adjacent to the wall, a radio-frequency probe was used (Fig. 11). From this probe, the void fraction is obtained according to the relative amount of time spent as liquid and vapor bubbles cross the probe tip. The sensing tip of the probe is made of two wires. One of the wires is used as a transmitter to which a sine wave is applied from a generator as above. The other wire is used as a receiving antenna, and its output is sent to the measurement circuit. The signal received by the antenna maintains a constant voltage level while the sensing tip is completely immersed in liquid. Since liquid and vapor have different electrical properties, whenever the probe tip comes in contact with, or penetrates into, a bubble, its electrcal capcitance will be altered and the output decreases from its liquid level to the vapor level and stays almost constant during the passage of the bubble. A similar probe design has been used by others [33].

Since the transducers are located in the vessel, cables must travel some distance to the outside and equivalent cable capacitance may be greater than the probe capacitance. By use of a circuit configuration which maintains the cable shield at the same potential as the central

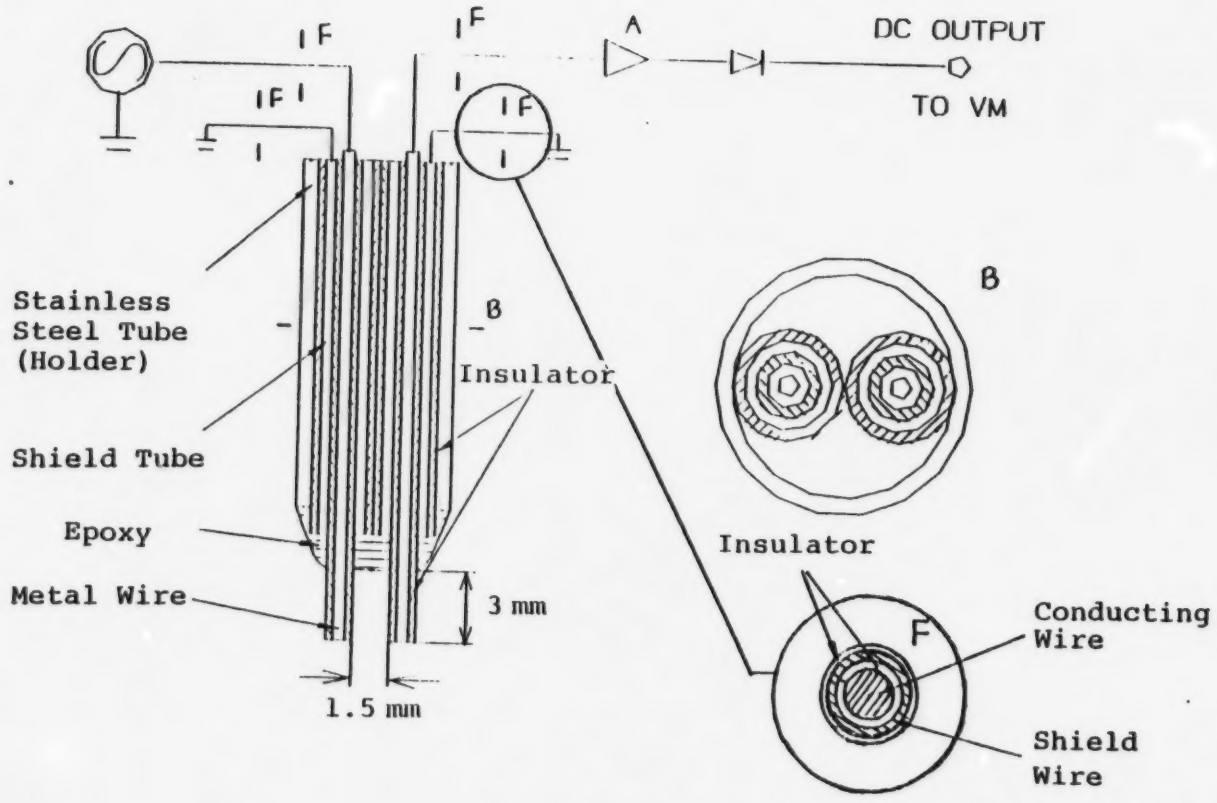


Fig. 11 Radio-Frequency Probe

conductor, this effect can be minimized and a capacitance charge is not built up.

The input end of the transducer is placed in parallel with a high frequency generator. When measuring with a.c. voltage and high frequency, the disturbing influences of electrolysis and polarization can be avoided. With frequency increasing, the admittance between the electrode which can be represented by tne vector sum of two components - a conductance (1/R) and a susceptance ($\omega C$) - the latter can be much greater than the former, so that when the frequency is high enough, the conductance component can be neglected and only the capacitance between the electrode is measured. These effects are discussed further in Appendix 2.

As shown in the experimental circuit diagram, Fig. 12, the a.c. voltage signal coupled to the transducer output end is amplified by an amplifier and rectified by a diode, and the corresponding d.c. voltage signals are received by the voltmeter. The amplifier is constructed around a Motorola MC1350P Video I.F. amplifier integrated circuit. In the amplifier, the a.c. signal first passes through FIL.1, which is a 2.2 MHz ceramic filter to block out unwanted high frequency signals. It next goes to the MC1350P which increases the signal level, and the output from this is coupled by the transformer T1 to the rectifier D1 which converts the a.c. signal to the necessary d.c. signal.

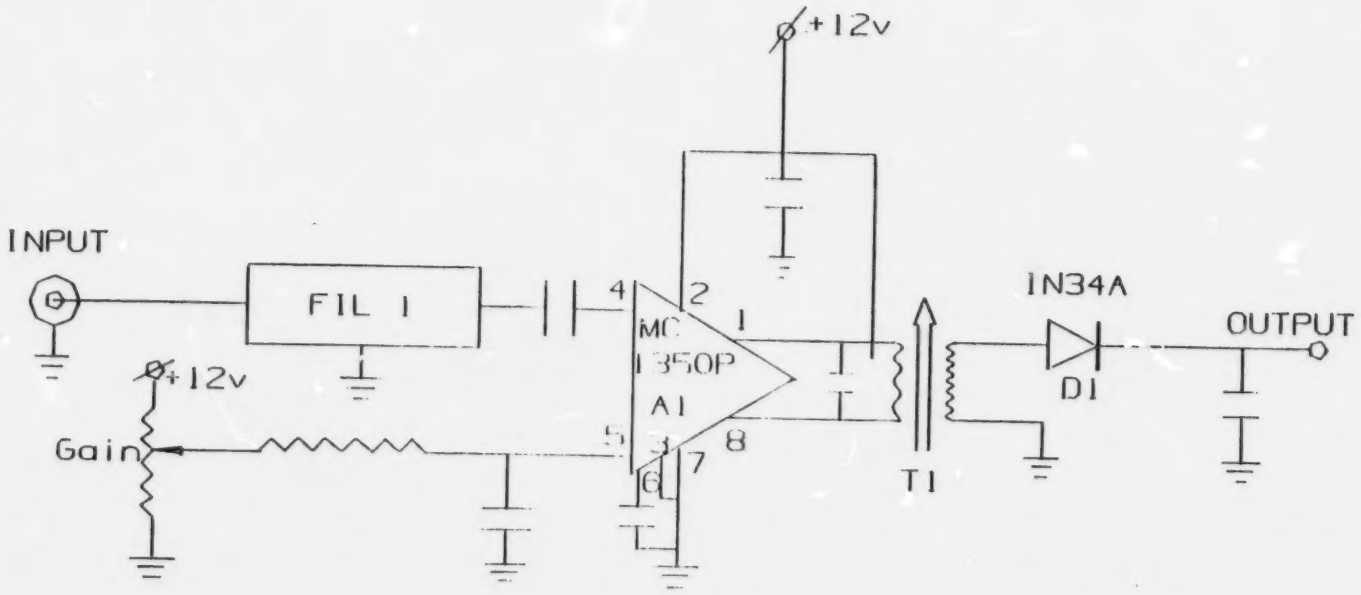


Fig.12. Experimental Circuit

## 5.3 EXPERIMENTAL PROCEDURES

1). Test on the interference between the capacitance transducers

If there is only one ring electrode in the vessel during the experiments, there will be no mutual interference to the ring. However, in order to determine the average void fraction distribution in the vertical direction of the vessel, several rings are required and the multiple electrodes provide interference between the rings. This effect causes the electric field to be essentially three dimensional. Hence, before the transient experiments were performed, some tests were done to study this effect.

2). Program for experiments

R-11 was used as the working fluid in all of the experiments. Two initial liquid levels (The proportion between the level and the diameter of the vessel is: 50% and 75%, respectively) were selected. The pressure relief valve orifice diameter was 9.53 mm. The power supply value was 80 $kw/m^2$. Experiments were carried out for both subcooled and saturated intitial conditions.

In the experiments, the procedures were the same in terms of setting test points and taking data, and all data were taken at the same initial pressure value.

3). Experimental method

After setting up and checking all the instrumentation, the distilled R-11 was allowed to flow into the test vessel until it was filled with a specified quantity of liquid. The vessel was then sealed

and the liquid heated. The pressure in the vessel increased gradually with time. Subcooled wall boiling occurred in the vessel before reaching the specified pressure. Radio-frequency probes were used to measure the cross-sectional void fraction distribution in the boiling boundary layer adjacent to the wall and its development along the wall. In the bulk liquid, the fluid was still single-phase, therefore, the output from the central rod-ring sensors maintained at a constant value.

Upon reaching the expected pressure, the pressure and temperature profiles were adjusted by means of each responding instrument. Immediately after the pressure relief valve opened, the liquid in the vessel flashed and the observation of the transient void fraction development began. The central rod-ring sensors responded to transient void variation in the liquid core and gave the void fraction distribution on each test time point. Meanwhile, the pressure and temperature profiles were obtained from the corresponding transducers. The signals from various transducers were recorded on magnetic disc.

The experimental electrical circuit designed provided one analog output signal. After appropriate filtering and demodulation, the a.c. voltage output from the capacitance transducers were presented as a d.c. voltage output proportional to the magnitude of the transducer susceptance. In the next section, the measurement program for scanning data will be discussed.

## 5.4 MEASUREMENTS AND DATA REDUCTION

### 5.4.1 Measurements

A test to examine the influence between the sensors was made. Fig. 13 shows the response of each central rod-ring sensor with varying liquid surface level. A normalized result from the voltage output is shown in Fig. 14. It can be seen that the working characteristics of each sensor are similar and that the response of each sensor only depends on its own working conditions. The effects from other sensors, whose working conditions may vary, do not appear to influence others and thus mutual interference between the sensors can be ignored although each individual characteristic differs.

The central rod-ring sensors were set at nine positions, which were 30.4 cm (C1), 27.44 cm (C2), 24.3 cm (C3), 21.52 cm (C4), 18.75 cm (C5), 15.8 cm (C6), 12.57 cm (C7), 9.72 cm (C8), and 7.03 cm (C9) from the bottom of the pressure vessel. Each pair of radio-frequency probes was fixed on two probe holders. The two holders were positioned at -45° and 40° with the central horizontal line. The probes could be moved normal to the curved surface, and along the wall of the vessel. Thus, the void fraction profile in the boundary layer and along the wall could be measured.

The pressure transducer was situated on the top of the vessel. Six thermocouples in the bulk liquid were located at 13.53 cm (T6), 16.16cm (T7), 18.64 cm (T3), 20.90 cm (T5), 23.58 cm (T4), and 31.38 cm (T1) from the bottom of the vessel. On the wall of the vessel, six

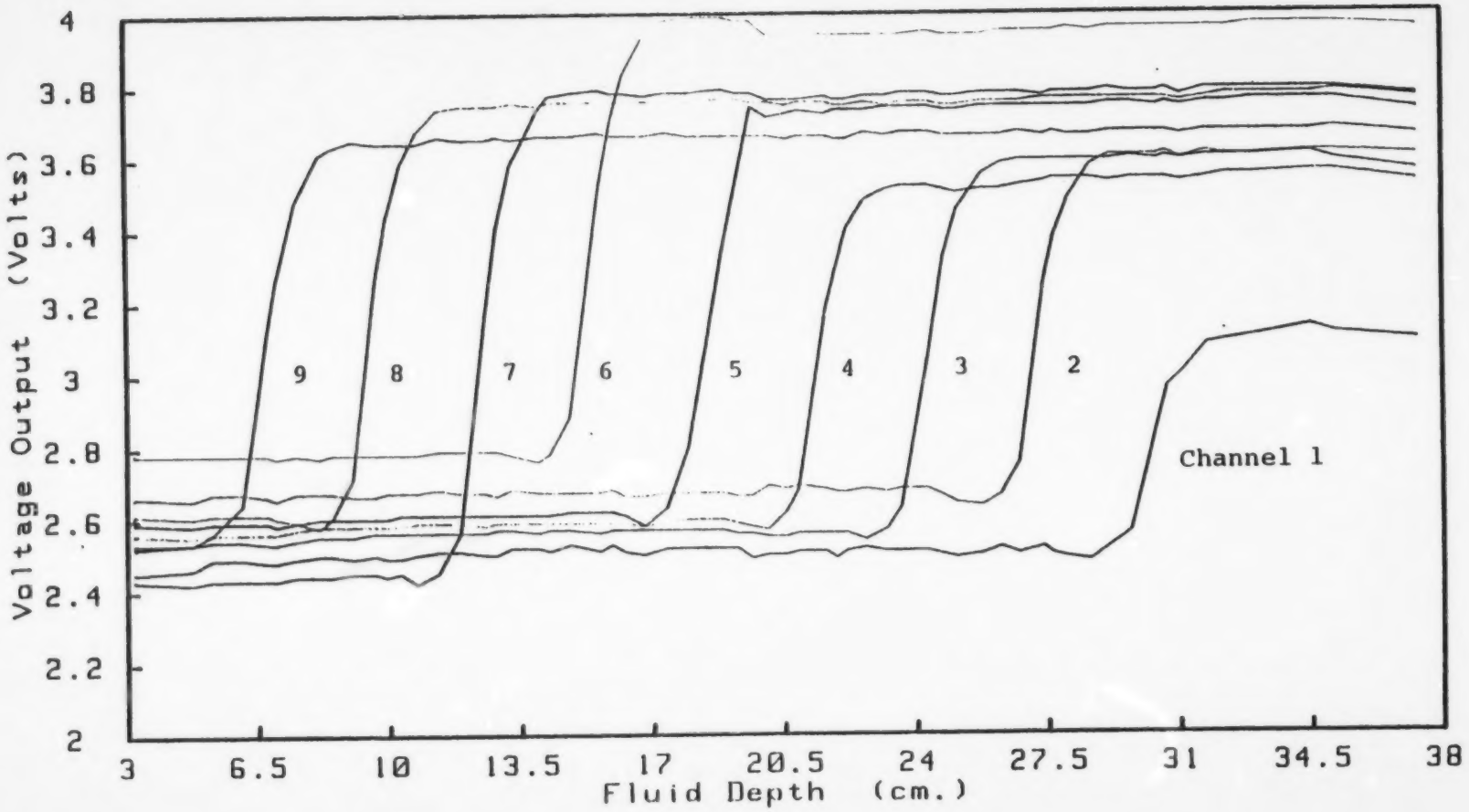


Fig.13. Measurement for Depth Effect

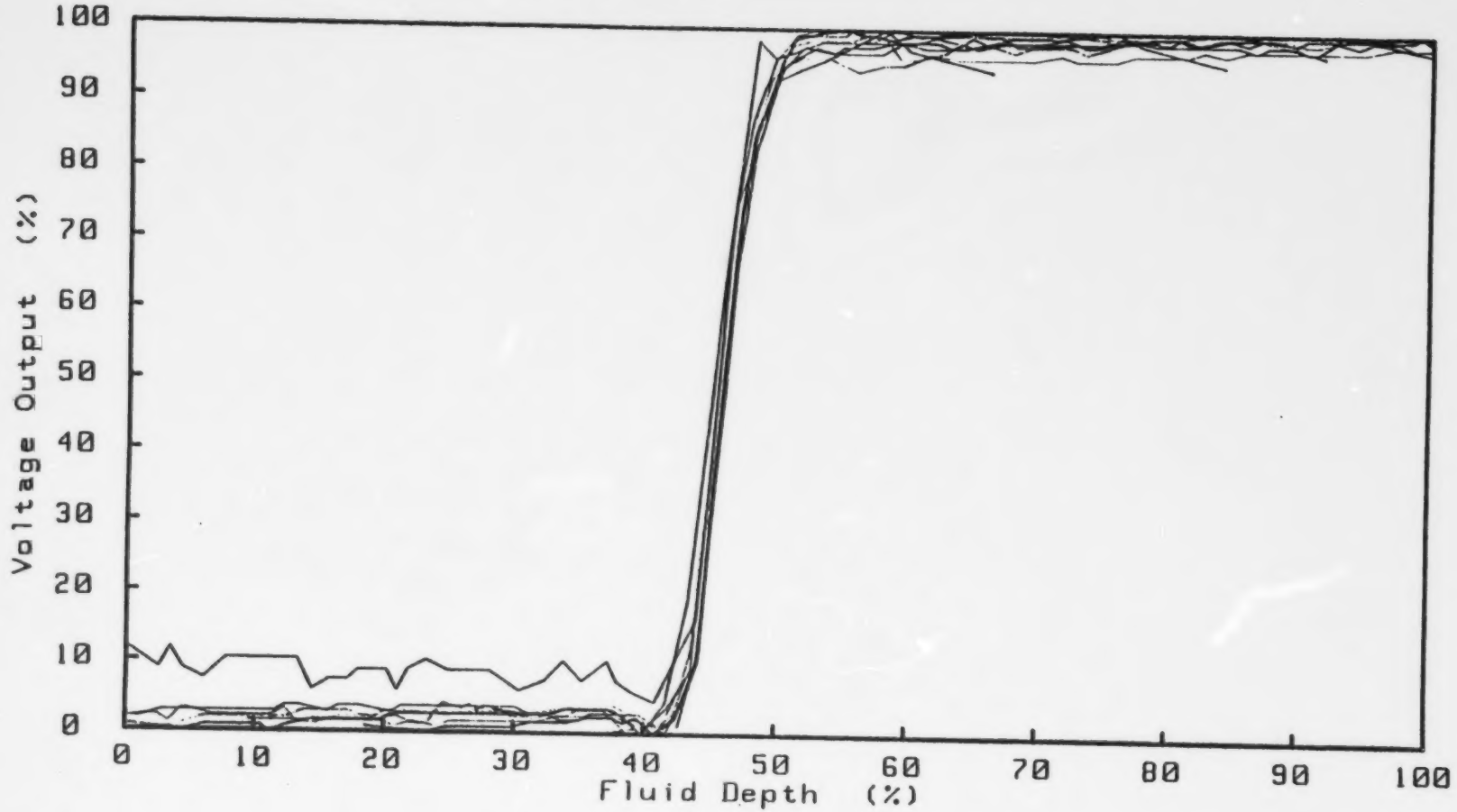


Fig.14. Normalized Results of Depth Effect

thermocouples used to measure the wall temperature were symmetrically distributed over the positions of 45°, 5°, and -40° with the central horizontal line of the vessel.

When heating of the liquid was started, one pressure, a set of temperatures and 100 sets of voltage output from the capacitance transducers were taken in each one-second period. Since the process of scanning the readings was not continuous, the flashing phenomena were assumed to be at steady-state for each scanning time period; thus, the void fraction and other parameters were constant and were found by using the data obtained. A computer program (Appendix 3) was designed to control the experimental process with the following sequence of operations being carried out automatically.

1). Before filling the liquid into the vessel, the signals from the capacitance transducers filled by vapor were recorded. After the vessel was filled to a specific level, the output from the capacitance transducers were recorded once more.

2). The heaters were started. Scanning of the pressure, temperature and voltage output responding to the variation of the capacitance started. In this period, the measurements were used to study the void fraction distribution in the boundary layer adjacent to the wall and the influence upon the bulk liquid due to the circulation caused by the two-phase flow along the wall.

3). Immediately after the pressure reached 342.7 kPa, the pressure relief valve opened and flashing phenomena began until the end of

flashing.

4). Depending upon the data recorded from the experiment, the computer plotted the corresponding characteristic curves and presented the results of all measured parameters.

### 5.4.2 Data Reduction

With each test run, the data obtained consisted of the temperature profile in the vessel, the test vessel pressure and the response signal from all the capacitance transducer on each time point. The data could be calculated and plotted by using the designed computer program to obtain the experimental results.

When vapor bubbles having a dielectric constant, $\varepsilon_g$, are between two electrodes separated by a liquid having a dielectric constant, $\varepsilon_\ell$, one will measure an effective dielectric constant, $\varepsilon_\alpha$, which will depend not only on the proportion of $\varepsilon_g$, $\varepsilon_\ell$ and sizes of bubbles but also the electrode spacing and the bubble distribution. According to the fundamental definition of capacitance:

$$C = A * \varepsilon \qquad (5.1)$$

where C is the capacitance and A is a geometric parameter. The value of A is specific for a particular capacitor, thus, by using Eq. (5.1), there is a unique relation between the capacitance and dielectric constant.

The simplest relationship between the void fraction and dielectric constant is a linear expression, in which $\varepsilon_\alpha$ is assumed to vary linearly between $\varepsilon_\ell$ and $\varepsilon_g$. By using Eqn (5.1),

$$\alpha = \frac{1 - C\alpha/C_\ell}{1 - Cg/C_\ell} \tag{5.2}$$

The dielectric constant of a two-phase mixture depends strongly on the flow pattern, sizes and distribution of bubbles. From the results of Hylton and Mcgill [34], the linear relationship is a good approximation for slug flow and annular flow. However, as the portion of the dispersed liquid droplets increases or the void fraction is relatively lowered, this relationship is not valid.

For small size bubbles dispersed in a liquid matrix, one possible method of relating $\alpha$ to the relative capacitance is the Maxwell law from the approximate formula [40]:

$$\alpha = \frac{(1 - C\alpha/C_\ell)\ (2 + Cg/C_\ell)}{(1 - Cg/C_\ell)\ (2 + C\alpha/C_\ell)} \tag{5.3}$$

This relation can only applied to low void fractions. However, when the sizes of bubbles are smaller than the characteristic size of the sensor in the direction of the electric field, Subbotin et al. [41] has experimentally shown that Eq. (5.3) holds (within 0.5% accuracy) up to volumetric proportions of inclusions of about 62%. Thus, Eq. (5.2) is valid within a very wide range of void fractions, and it can almost

include all situations in the present work.

When the void fraction is quite high, in a homogeneous field, the Rayleigh expression can be considered [35]:

$$\frac{C_\alpha}{C_\ell} = 1 - \frac{3\,\alpha}{\dfrac{2+Cg/C_\ell}{1-Cg/C_\ell} + \alpha - \dfrac{3.919\,\alpha^{\frac{10}{3}}}{\dfrac{4+3Cg/C_\ell}{1-Cg/C_\ell} + 1.22\,\alpha^{\frac{7}{3}}}} \qquad (5.4)$$

It is important to note that this expression reduces to the Maxwell formula when void fractions are quite small.

An expression given by Bruggmen [36] may be used to determine the void fraction of a medium consisting of spheres of varying sizes randomly distributed in a continuum, which is considered to have the properties of a homogeneous medium:

$$1 - \alpha = \frac{1 - C_\alpha/Cg}{1 - C_\ell/Cg} \left(\frac{C_\ell}{C_\alpha}\right)^{\frac{1}{3}} \qquad (5.5)$$

# CHAPTER 6

# DISCUSSION AND COMPARISONS OF MEASUREMENTS AND MODELS

## 6.1 EXPERIMENTAL RESULTS

Data from two experiments will be discussed. These two tests were carried out at approximately 75 percent (Experiment 2) and 50 percent (Experiment 3) fill of liquid respectively. In both cases, the PRV opening pressure was about 343 kPa. Immediately after the PRV opened for the first time, the outputs from the pressure transducer, thermocouples and void fraction elements were scanned once every second. The PRV closed when the pressure dropped to about 308 kPa.

### 6.1.1 Pressure

The results of the pressure measurements from the tests are shown in Figs. 15 and 16. Before flashing began, the pressure rose along a smooth curve with time in each experiment. When pressure reached about 343 kPa., the PRV opened and flashing in the vessel occurred. From the results at the early stage of each experiment, the pressure was observed to have decompressed linearly with time for every flashing step. The variation range in Experiment 2 (75% fill of liquid), however, was larger than that of Experiment 3 (50% fill of liquid). This variation gradually reduced with time due to the successive decrease of subcooling in the bulk liquid.

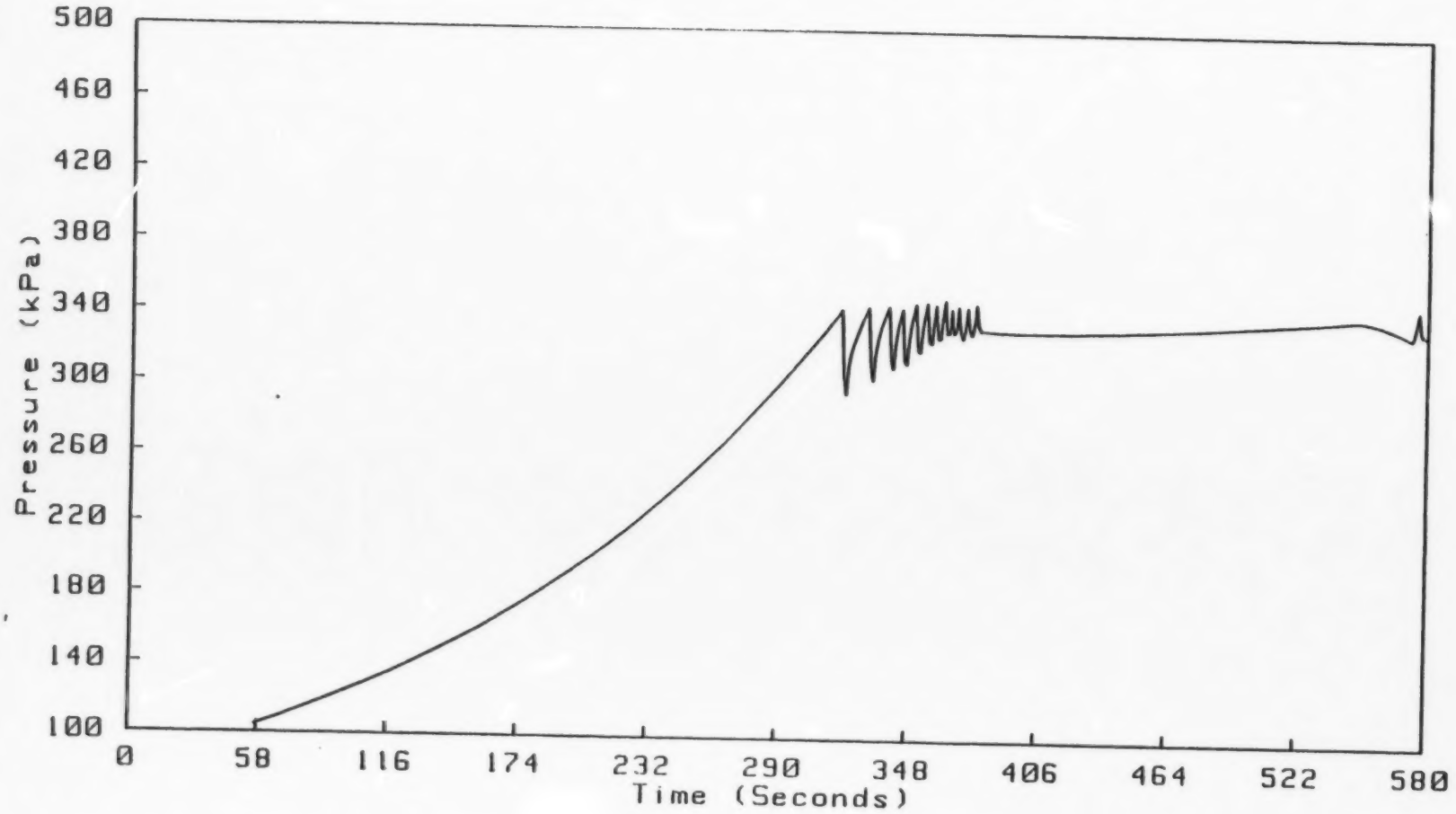


Fig. 15 Pressure vs. Time (Experiment 2)

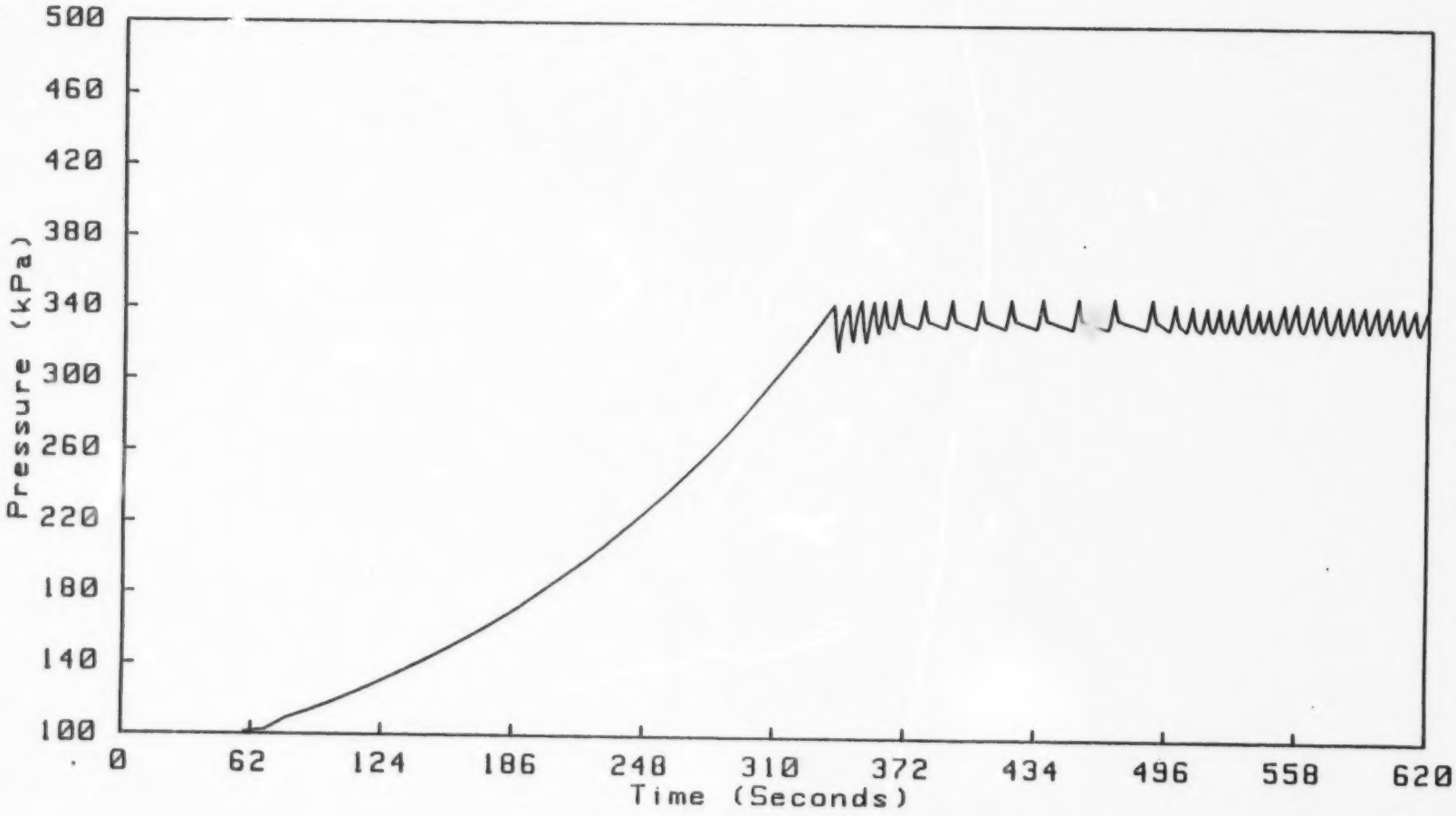


Fig. 16. Pressure vs. Time (Experiment 3)

After having reached pseudo-thermal equilibrium at the latter stage of each experiment, the pressure variation of the two experiments were quite different.

In Experiment 2, although the PRV opened and flashing was taking place, pressure was almost constant with time (Fig. 15). This is because of a balance, between the pressure drop due to flashing and volume swell due to a large bubble population generated. Due to flashing and vaporization, the mixture mass in the vessel was reduced successively. When the two-phase mixture mass took up about half of the vessel volume, the pressure variation with time became similar to that at the latter stage in Experiment 3.

In Experiment 3, pressure decreased sharply for the first few PRV openings; then it dropped at a slower rate due to the large number of bubbles being generated. Finally, less vapor was generated as the amount of liquid decreased steadily over time, therefore the pressure varied in a manner similar to that at the early stages of the experiment.

### 6.1.2 Temperature

Figs. 17 and 18 show the temperature profile variation with time. In both cases, the following temperature profile development was observed.

The temperature in the vessel gradually increased as the contents inside are progressively subcooled with time due to external heating. Subcooling in the bulk liquid was reduced after flashing began because

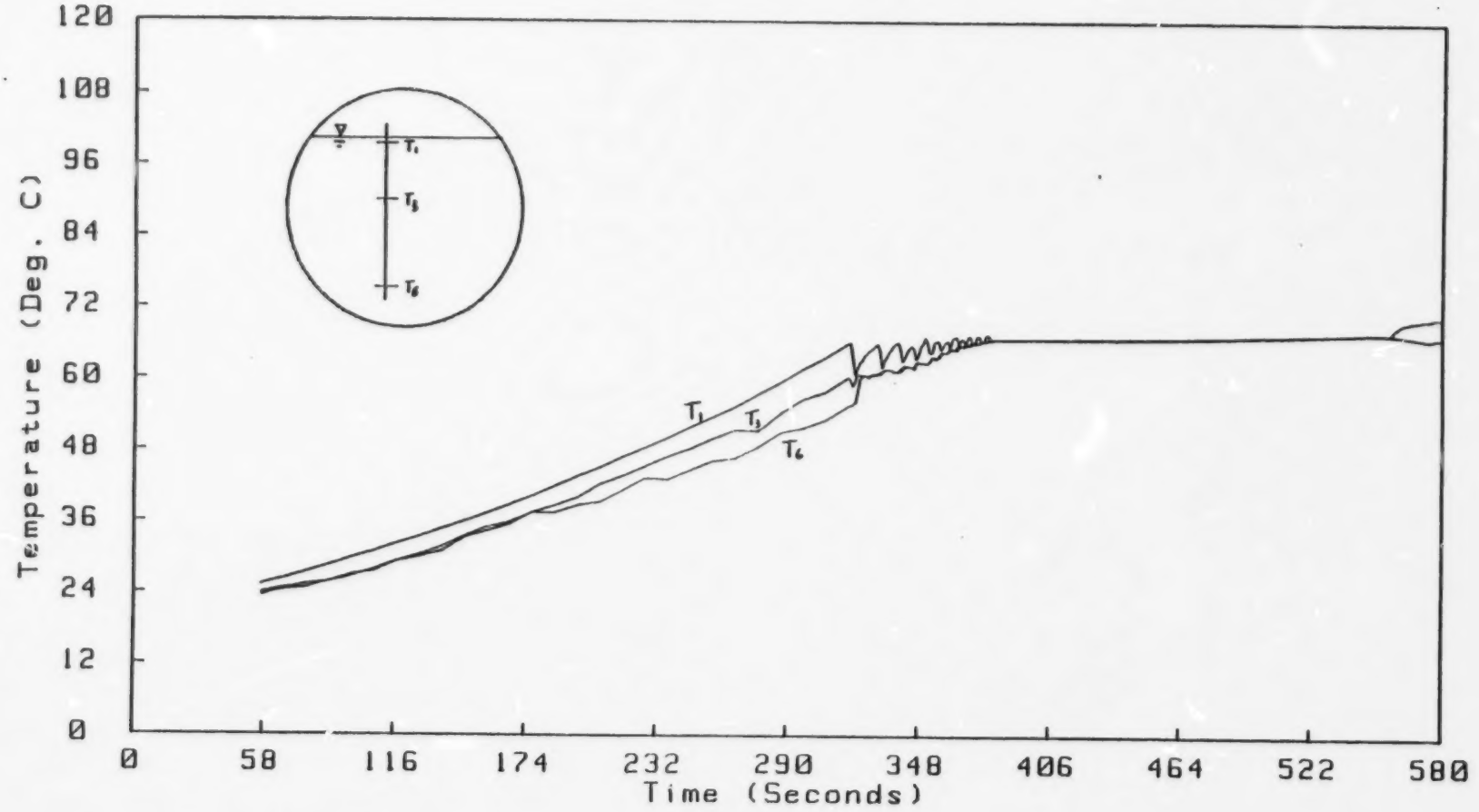


Fig.17. Temperature Profile vs. Time (Experiment 2)

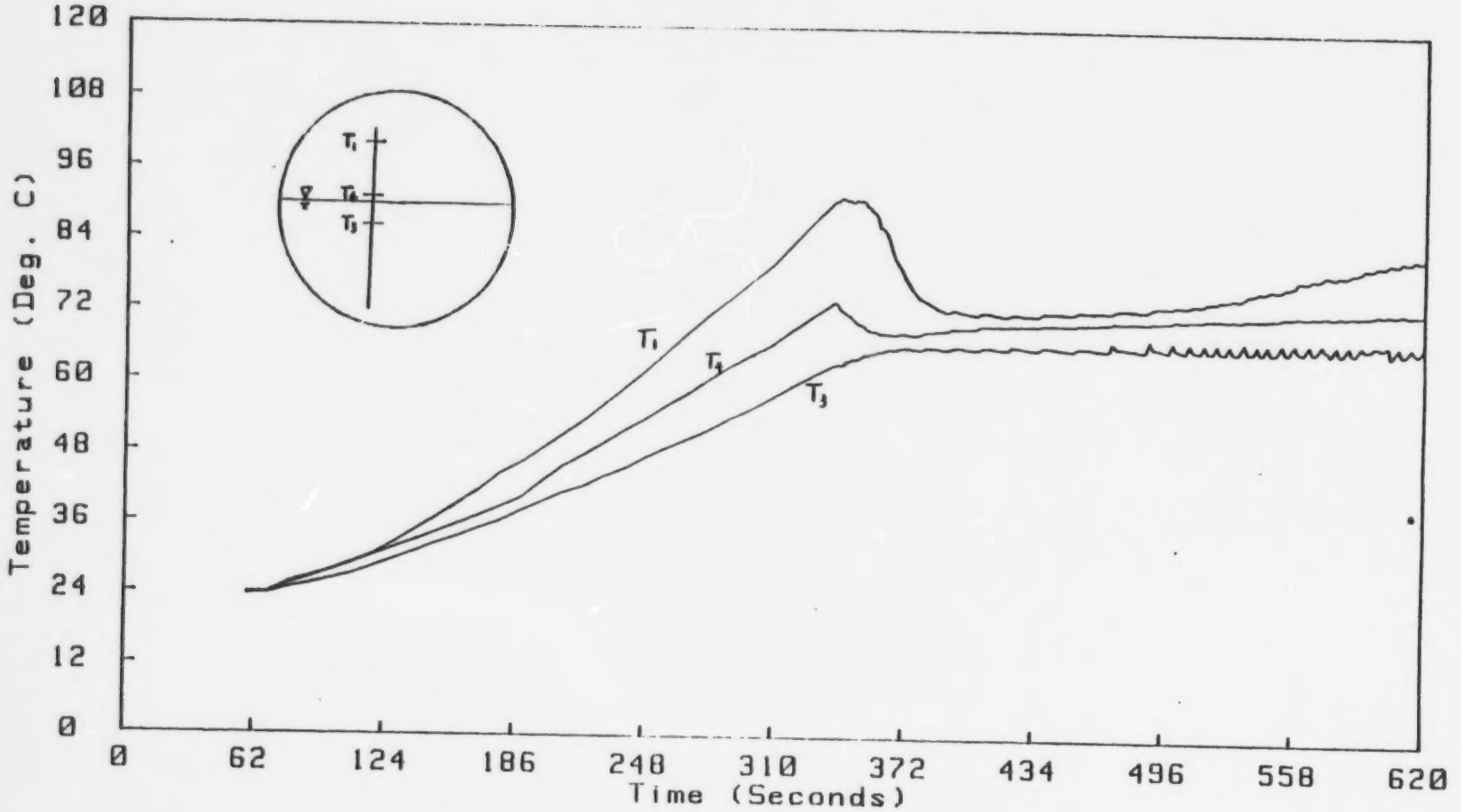


Fig.18. Temperature Profile vs Time (Experiment 3)

of the boiling disturbance created in the system. However, flashing occurred only for a short time during each depressurizing step at the early stage of the experiments, and the disturbance was not violent, hence subcooling was not affected significantly. Later in the experiments, the bulk liquid was saturated and under thermal equilibrium because of the increased disturbance. From the experiments, it was found that the temperature at the liquid surface was always saturated corresponding to pressure variation. Temperature in the vapor space was higher than that in the liquid space. In Experiment 3, the temperature of the vapor was much higher than the saturation temperature at the beginning of the first flashing. After this, since a large quantity of saturated vapor and liquid droplets was spread into the superheated vapor space, the temperature of the vapor dropped nearly to the saturation temperature.

### 6.1.3 Mass and Swell Height

Fig. 19 shows the variations of pressure, mass and swell height with time in Experiment 2. In the early stage, flashing was not fully developed in each depressurizing step. Although vapor was generated violently during flashing, the period for each step was very short and little liquid mass was lost because most of the droplets carried by the rising bubbles did not escape from the vessel. However, the swell height of fluid oscillated very violently corresponding to the pressure variations. Later, as the PRV kept open for a longer time smaller

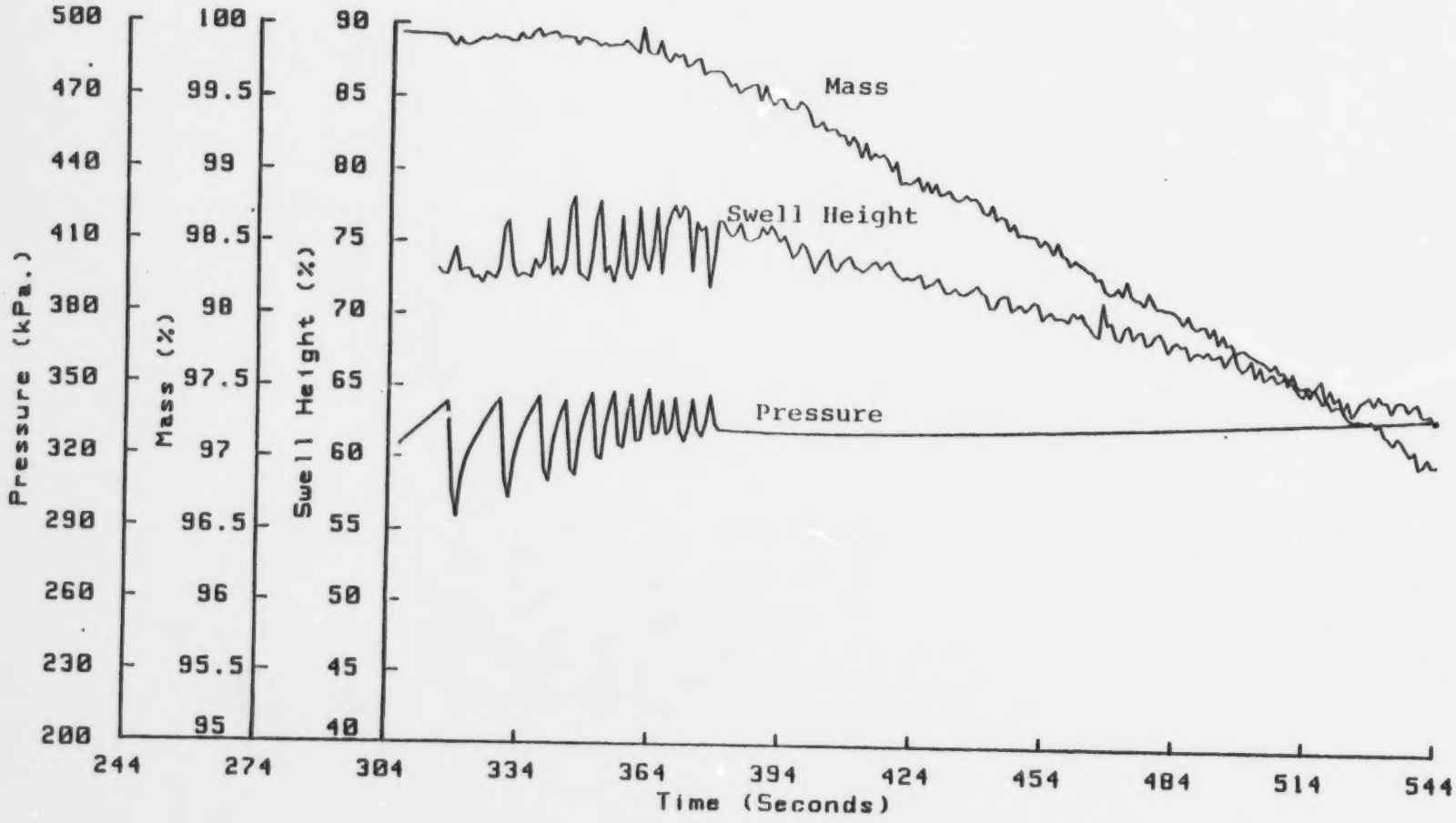


Fig. 19 Pressure, Mass and Swell Height Variations (Experiment 2)

oscillations in swell height were observed; but mass loss increased greatly, and hence the average swell height decreased. In Experiment 3 (Fig. 20), pressure decompression was relatively small in each flashing step, and the PRV opened and closed sequentially. The mass loss was less than that in Experiment 2. The fluctuation of swell height was large, but the decrease of its average value was minor. Figs. 21 and 22 show a comparison between the mass loss for the two experiments.

### 6.1.4 Void Fraction

Measurements of void fraction of the bulk liquid made in Experiment 2 are presented in Fig. 23. The initial liquid surface was just above Sensor 1. During flashing, Sensor 0 was filled by a two-phase mixture instead of only vapor due to fluid swelling. As the average swell height went down gradually with time, Sensor 0 was filled by vapor and a few rising liquid droplets. Sensor 1 was immersed in liquid initially. After some time, the swell height went below this sensor. Sensor 2 had a similar experience as Sensor 1 but it took more time for the swell height to drop below Sensor 2 as compared with Sensor 1. From the experimental results, since the pressure decompression is small, the void fraction was quite low in the bulk liquid. Only in the region close to the swelling surface, was the void fraction relatively high. The outputs from Sensors 6 and 8 show that the void fraction in the bulk liquid increased with the upward height coordinate. The void fraction profiles and their comparison with numerical calculation will be further

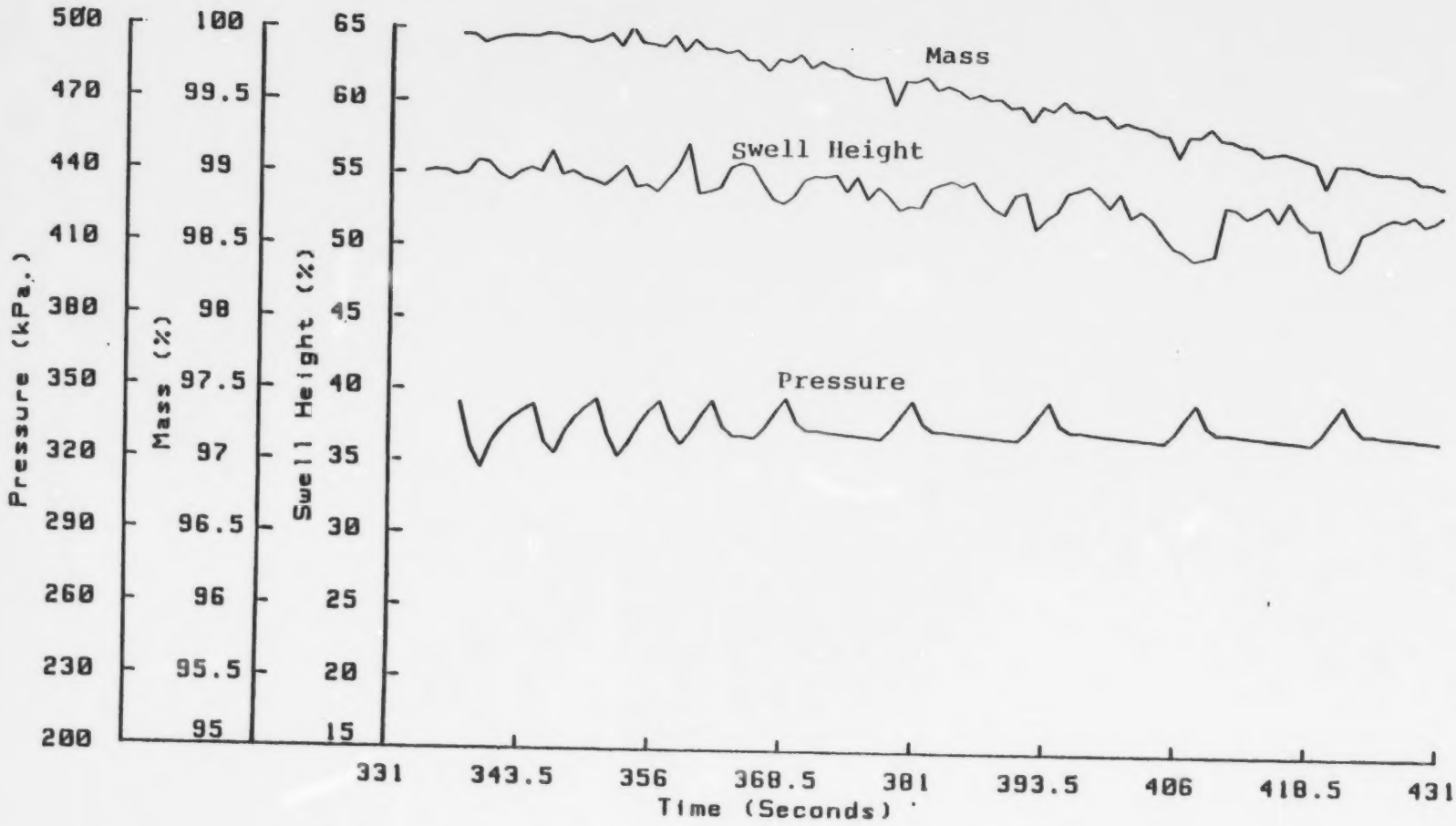


Fig. 20 Pressure, Mass and Swell Height Variations (Experiment 3)

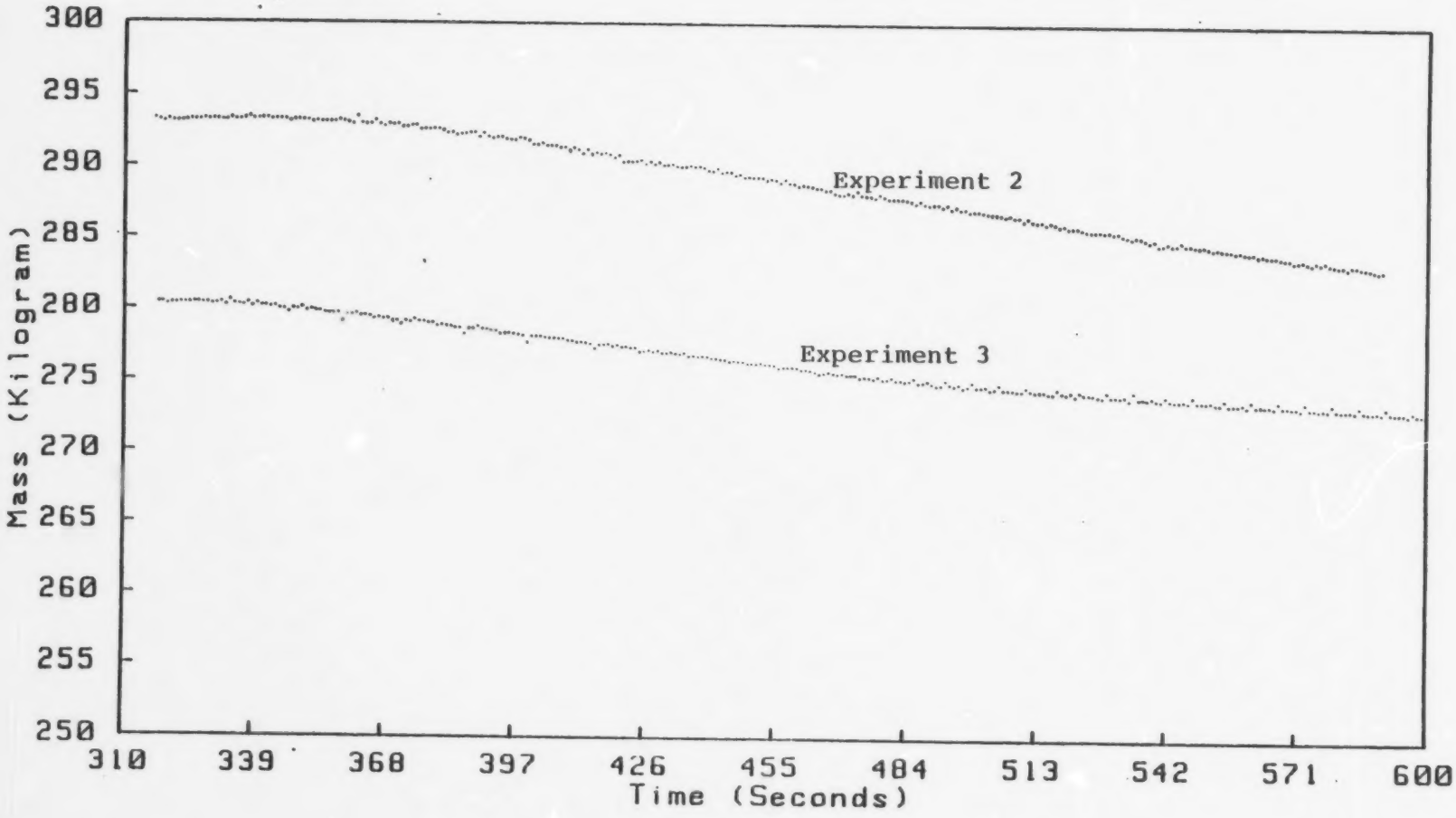


Fig.21. Mass Variation

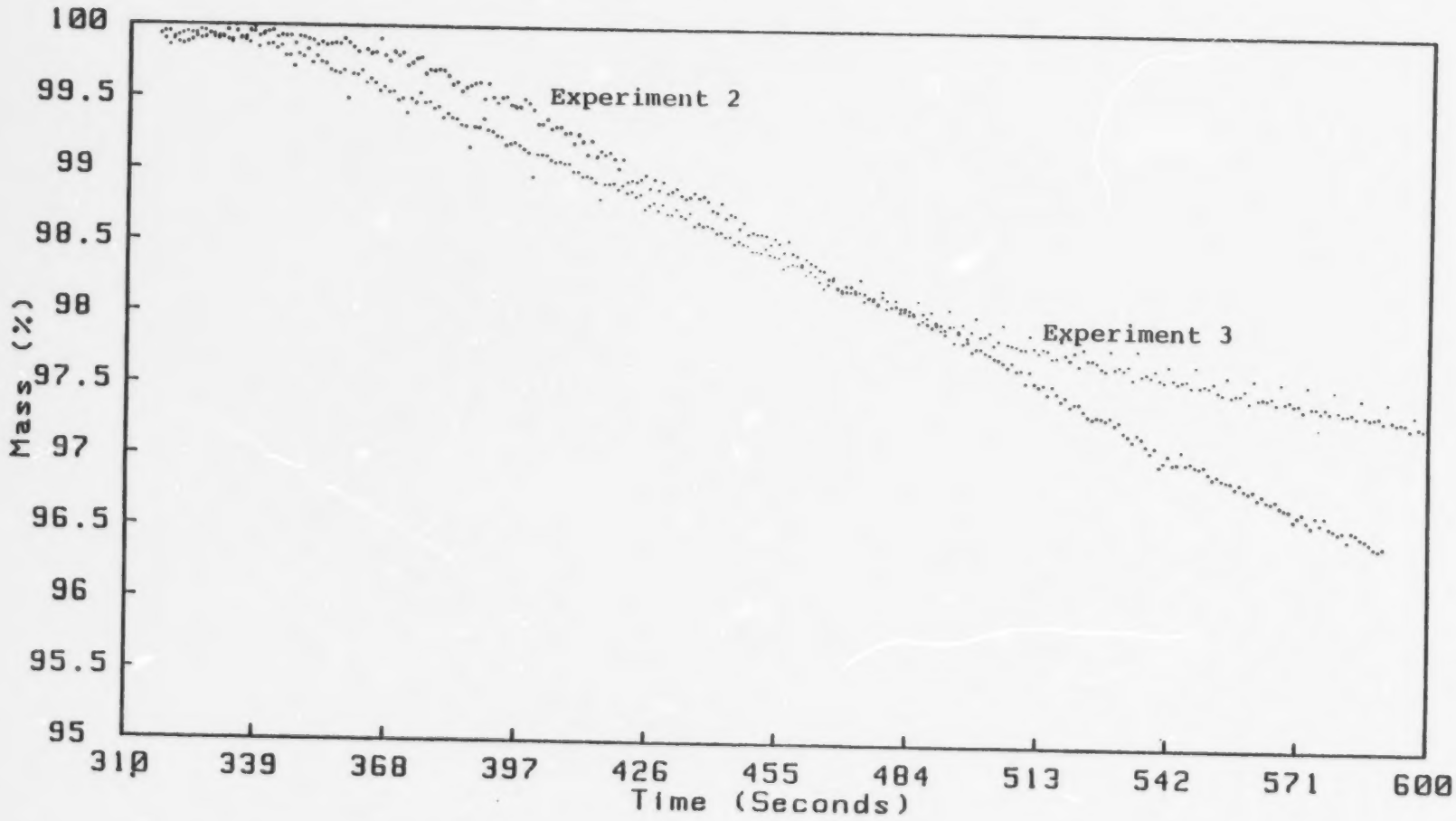


Fig.22. Relative Mass Variation

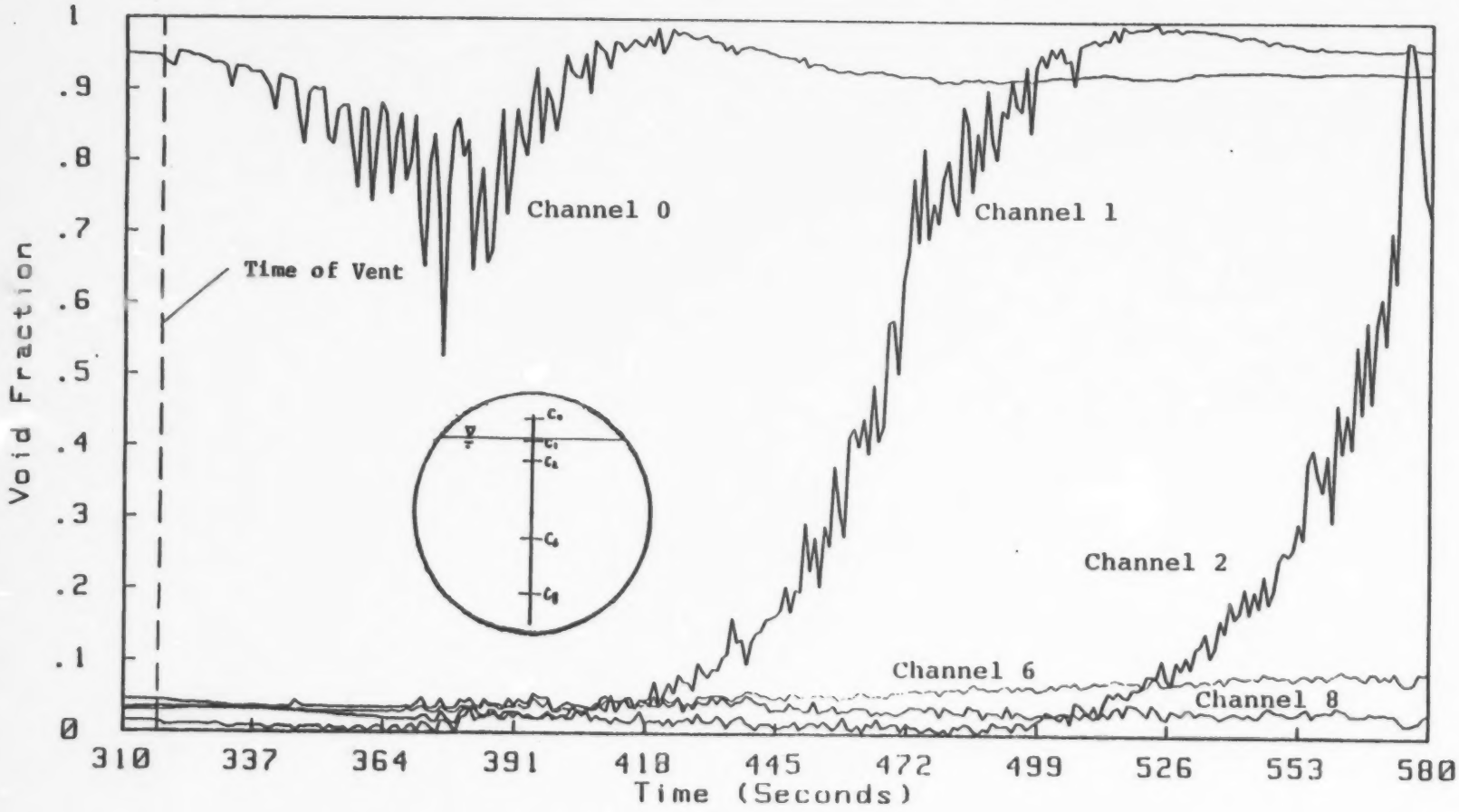


Fig.23 Void Fraction Profile with Time (Experiment 2)

discussed in Section 6.2.

In Experiment 3 (Fig. 24), half of Sensor 3 was initially immersed in the liquid. Response of Sensor 2 showed that there were not many liquid droplets entrained in the vapor space during flashing. The droplets only took up less than 5% of the volume of the sensor. During flashing Sensors 3 and 4 were filled by liquid-vapor bubble mixtures, and then by vapor-liquid droplets as time progressed due to the average swell height variation. In the bulk liquid, void fraction was still quite low. From experiments, in the case of low void fractions, the effect of the external wall heat source was noticeable.

Fig. 25 shows the comparison of void fractions between the two experiments. In plots (1), (2) and (3) the results are compared during the first flashing step at three time points (respectively valve opening, half of the flashing period and valve closing); plots (4), (5) and (6) compare those in the second flashing step at similar time points. In the lower positions in the vessel, there was little difference the void fraction in the two experiments. In the upper region below the fluid surface, Experiment 2 showed a slightly larger variation of void fraction as compared with Experiment 3.

Figs. 26 and 27 show the void fractions in the boundary layer adjacent to the wall. In both experiments, Probe 9 was positioned above the initial liquid surface and Probe 12 was immersed into the liquid (both at 2 mm from the wall). Before flashing began, the void fraction in the boundary layer increased gradually due to wall heat flux, and

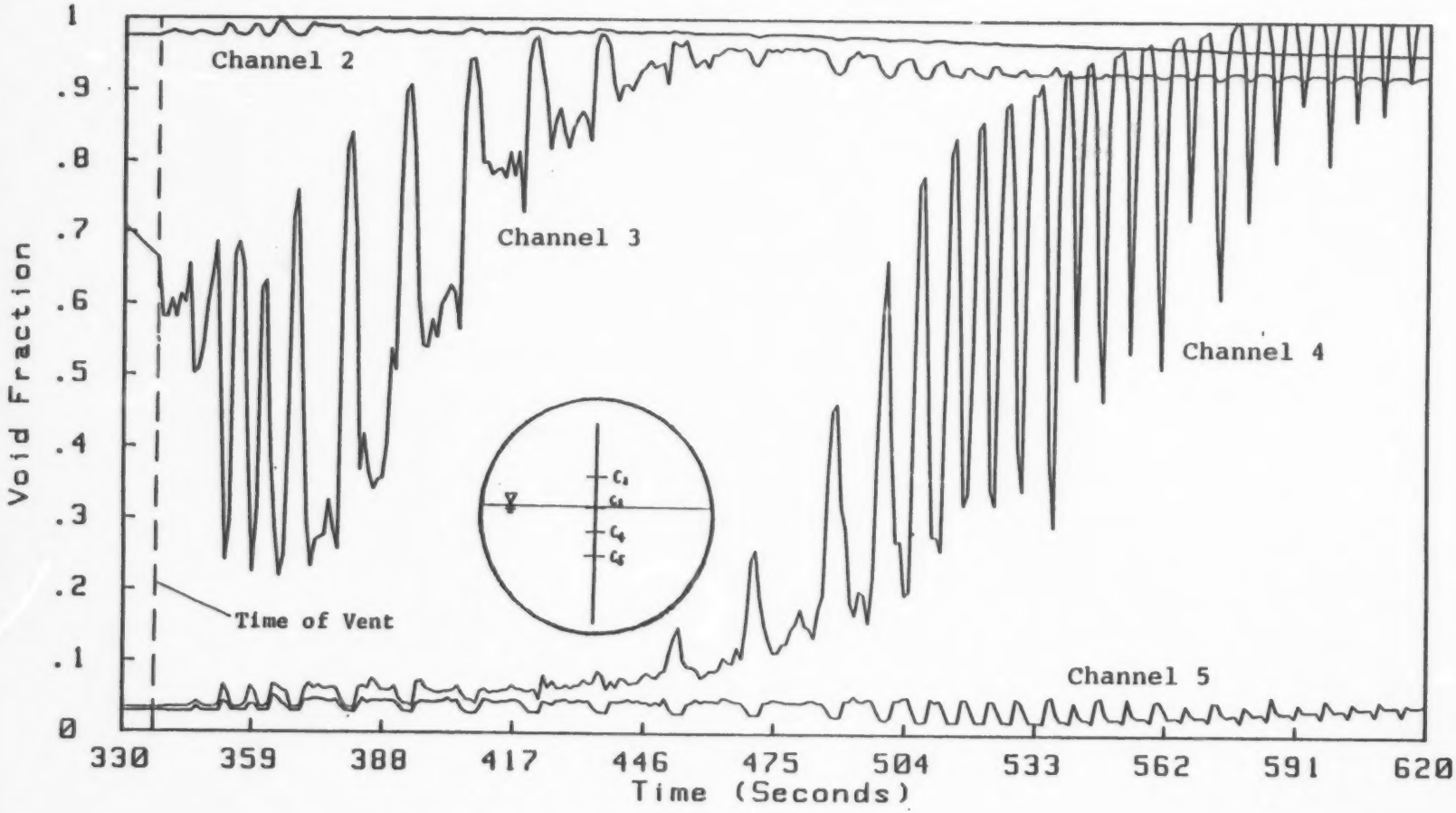


Fig. 24 Void Fraction Profile with Time (Experiment 3)

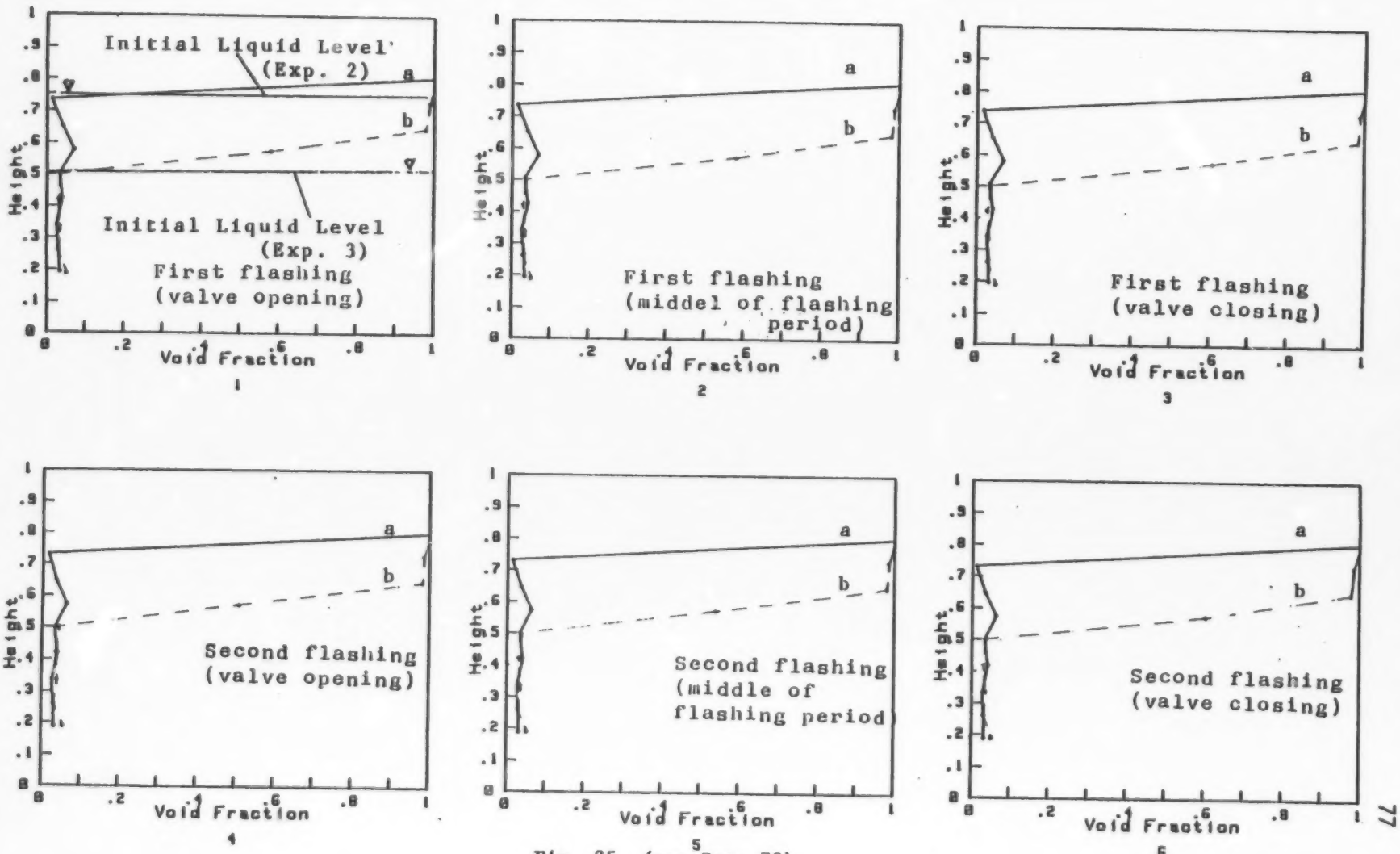


Fig. 25 (see Page 78)

Fig. 25 Comparison of Void Fractions from Experiments 2 and 3

a Line: In the case of 75% fill of liquid (Experiment 2).

b Line: In the case of 50% fill of liquid (Experiment 3).

In the Figure:

Plots 1,2,3: Times are flashing begining, half of flashing period and flashing finishing respectively in the first step of flashing in the two experiments. (Flashing period is two-second)

Plots 4,5,6: Times are flashing begining, half of flashing period and flashing finishing respectively in the second step of flashing in the two experiments. (Flashing period is two-second)

(Absolute experimental times are different in the two experiments. In figure 1, for example, time is 318 sec. in the case of 75% fill of liquid; however, time is 338 sec. in the case of 50% fill of liquid)

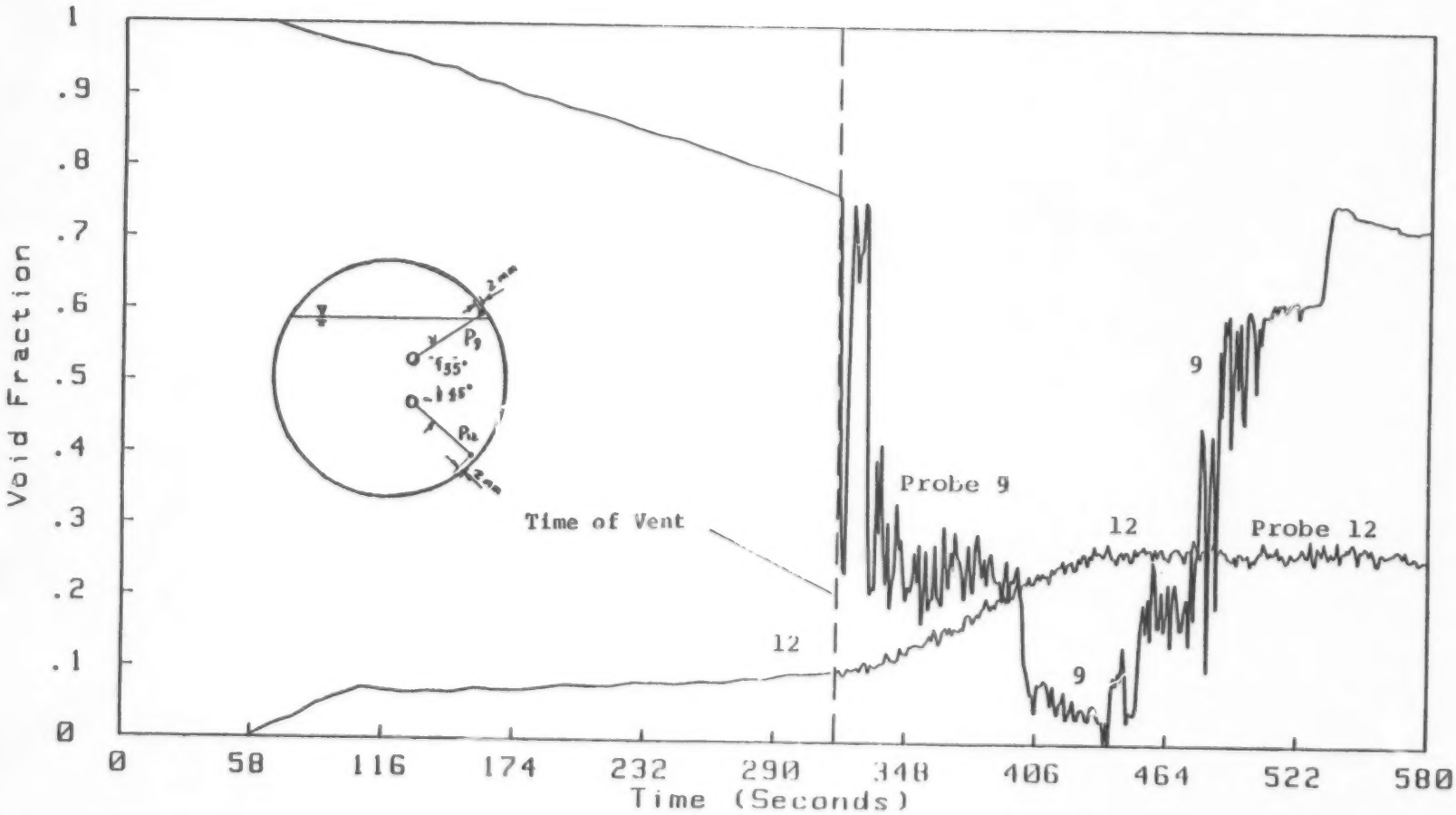


Fig. 26. Void Probes Response (Experiment 2)

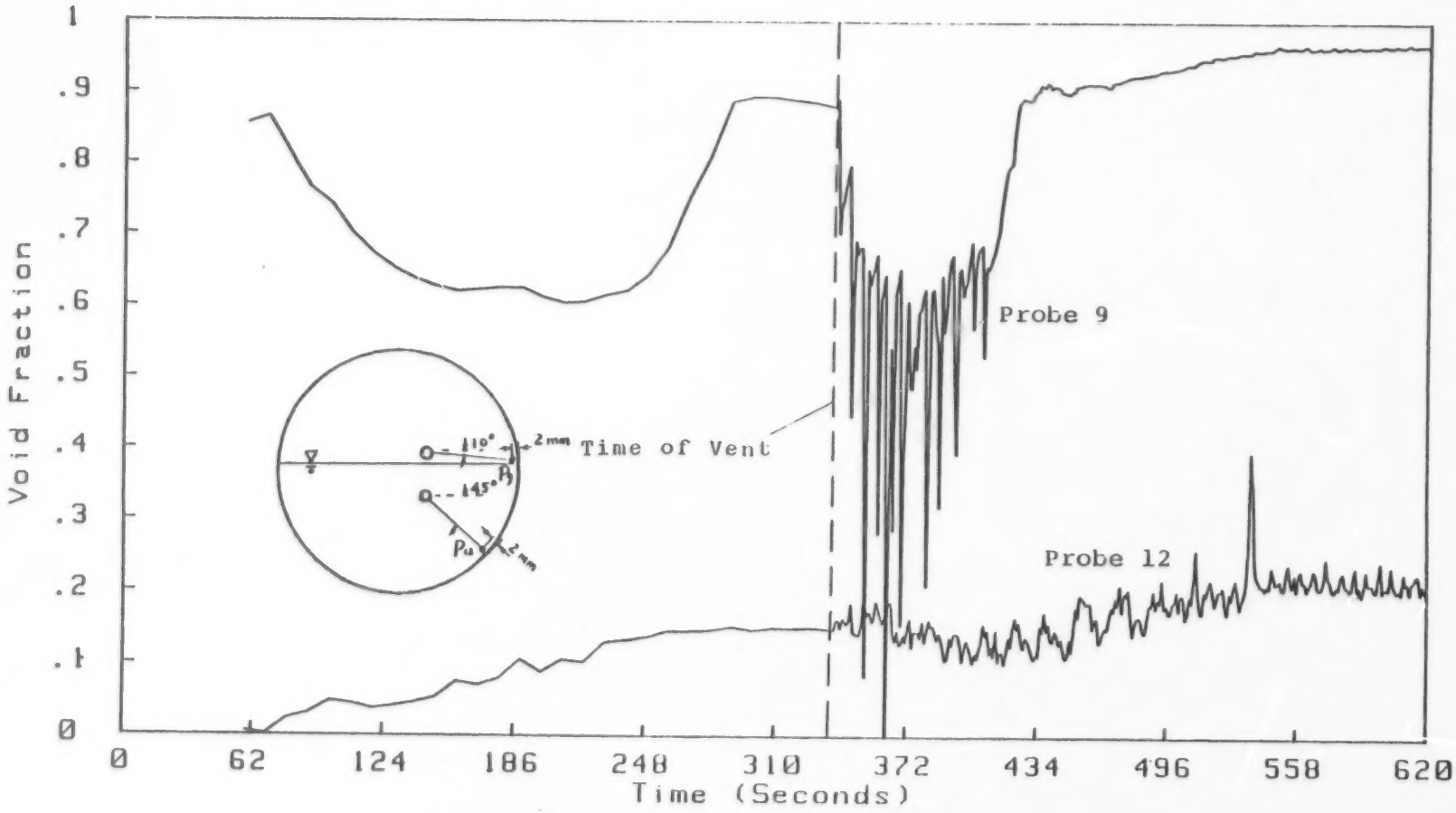


Fig. 27 Void Probes Response (Experiment 3)

liquid droplets rose into the vapor space along the wall due to bubble disengagement from the interaction of the bubble boundary layer and the surface. During depressurization the void fraction increased in the boundary layer until a value of about 0.3 was reached. In the upper position, the void fraction was higher. Response of Probe 9 showed that in the beginning of flashing, with the swell height increasing, the probe tip was immersed in a two-phase mixture; with the swell height dropping, the liquid droplets were less and less passing through the probe tip. Compared with the bulk liquid, the void fraction development in the boundary layer was higher as would be anticipated since the liquid close to the wall was superheated rather than saturated.

## 6.2 COMPARISON OF EXPERIMENTS AND CALCULATIONS

The two numerical methods discussed in Chapter 5 were applied in the early stage of the two experiments just discussed. A linear temperature distribution was assumed for the calculations, based on the initial temperature profile at the beginning of each flashing step. Pressure variation was considered only in the transient process. The value of the pressure used in the calculations was taken directly from the experimental pressure results.

In Figs. 28(a), 28(b) and 28(c) a comparison of the void fractions between Experiment 2 and the numerical calculations was made. In the figures, the dotted line represents the results from the method of energy and mass conservation without the effect of external heating, and

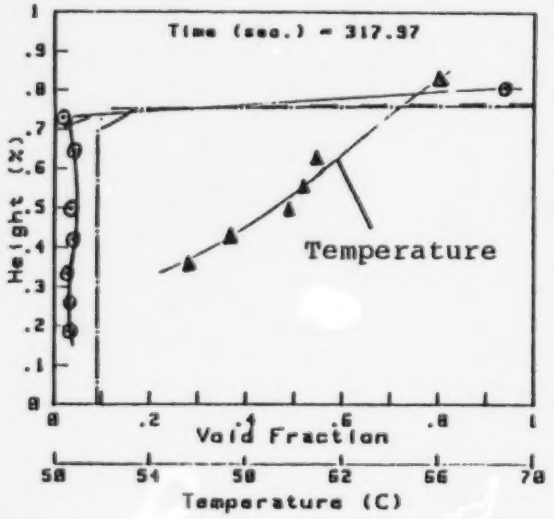


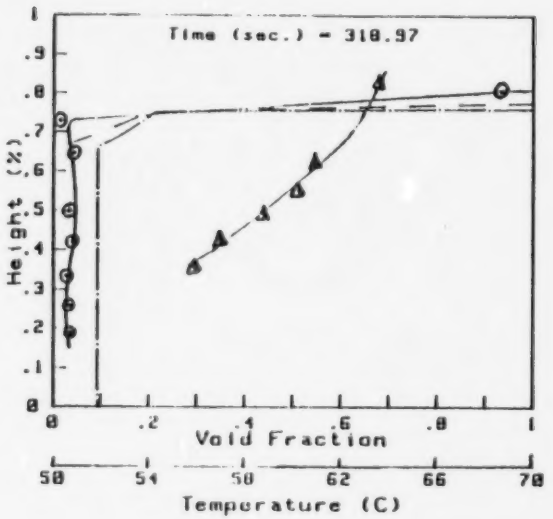


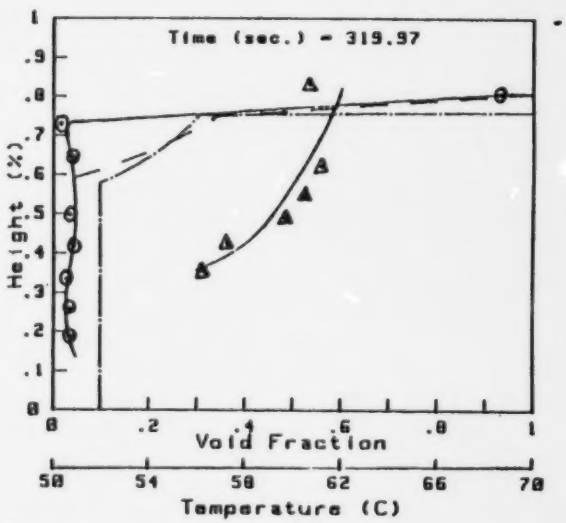


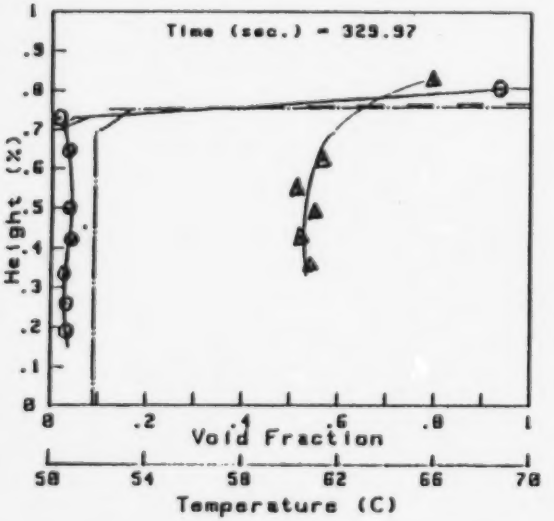


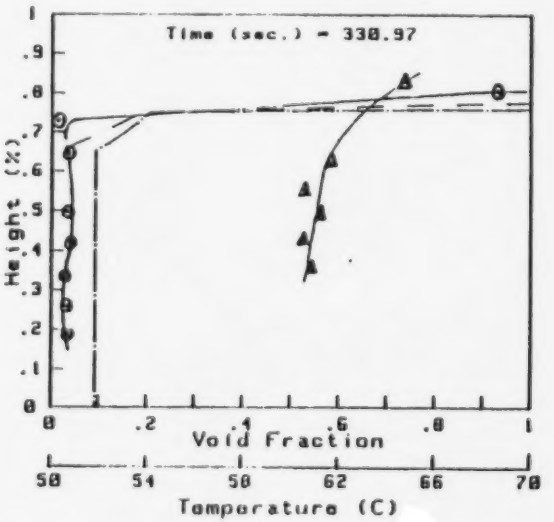


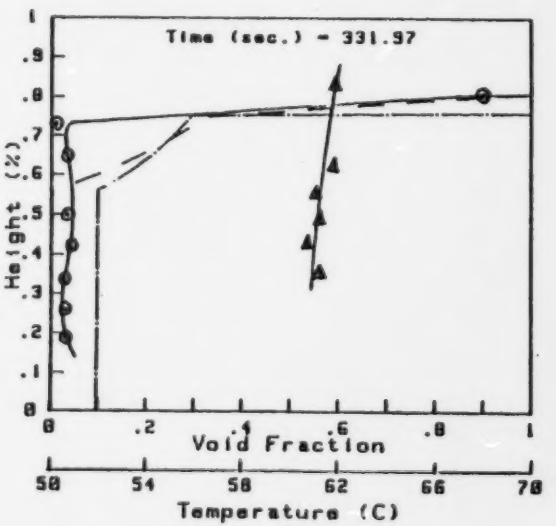


Fig. 28 (a) (See Page 87 )

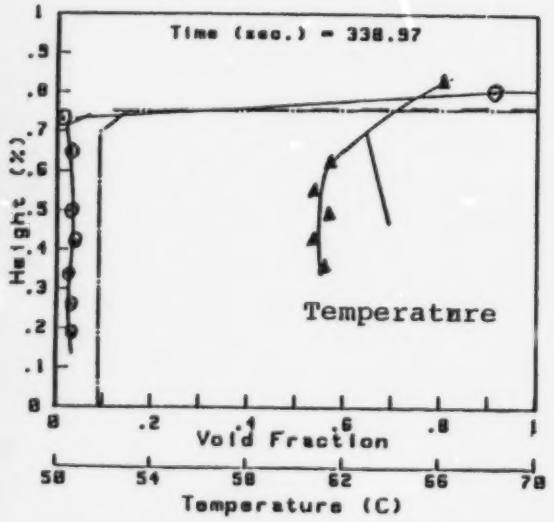


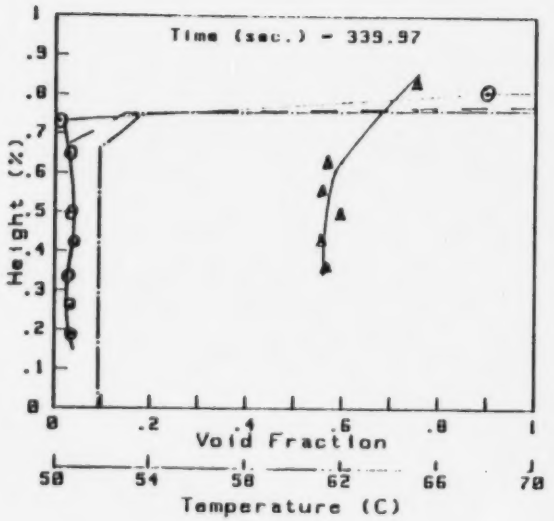


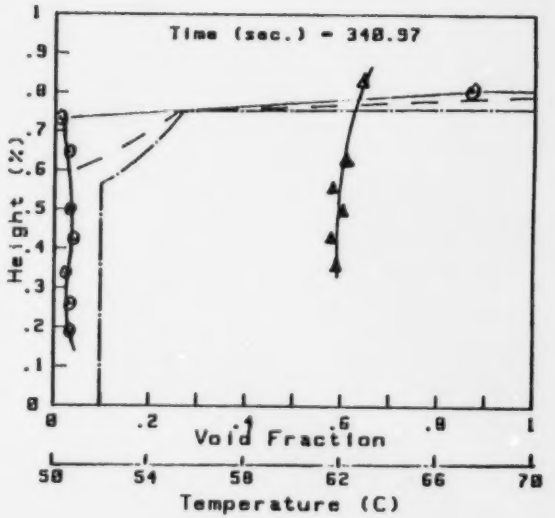


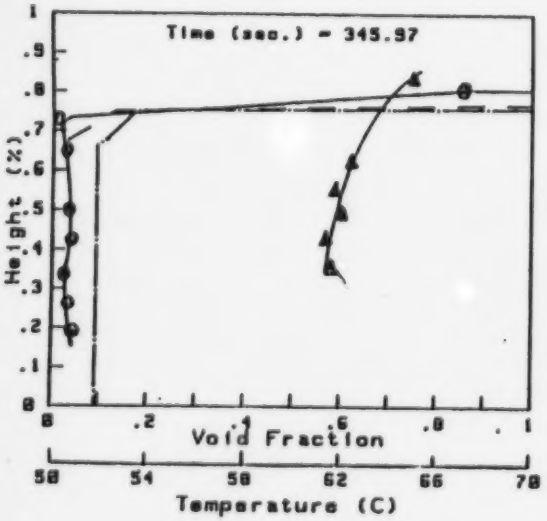


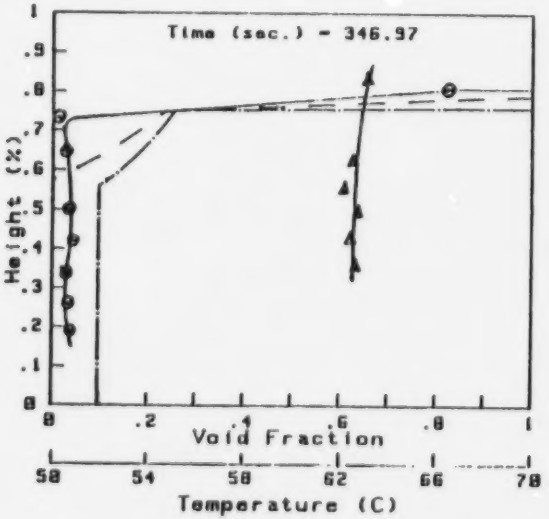


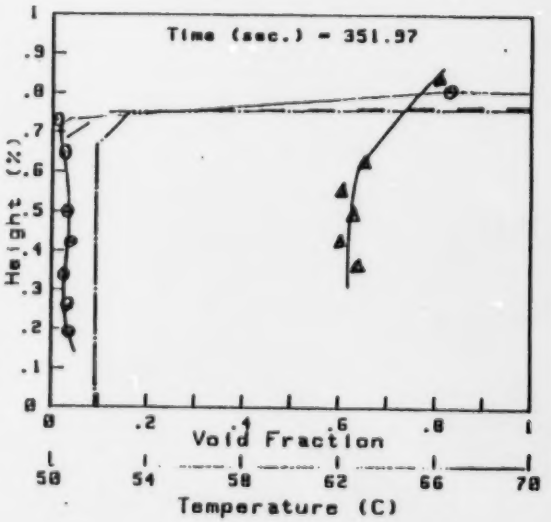


Fig. 28 (b) (See Page 87 )

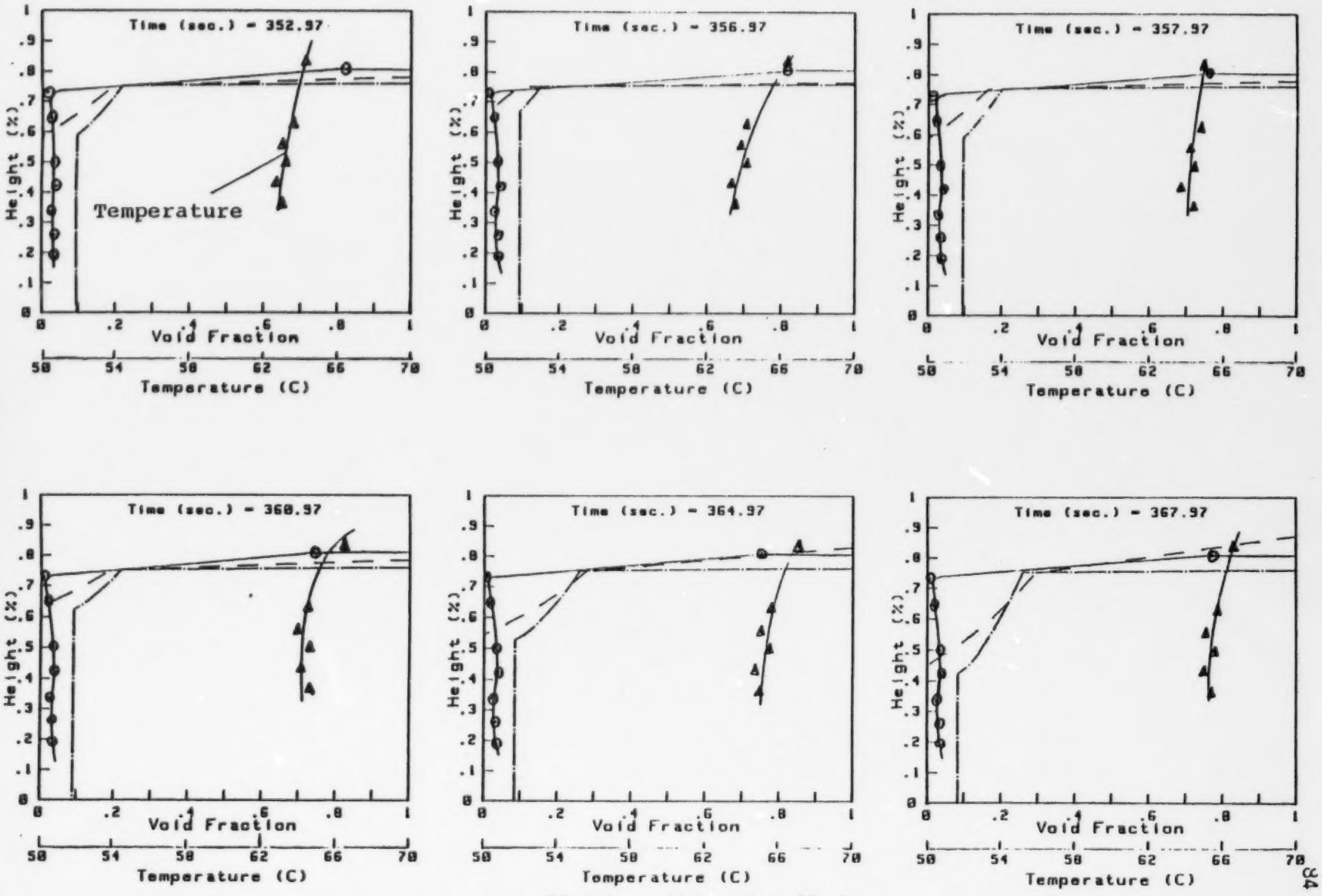


Fig. 28 (c) (See Page 87 )

void fraction below the saturated liquid level was neglected. The dot-and-dash curve indicates the results of the drift flux model calculations, in which the effect of void fraction due to external heating was considered.

In the region close to the liquid surface, the results obtained from these two numerical calculations agreed very well with those from the experiments. However, when the void fraction was quite low, the experimental results were between the two numerical results, indicating that when void fraction is quite low, the effect of the rising wall generated bubbles should be considered. This effect can be neglected only in the case of high void fraction. Since flashing occurred in a short period, there was not enough time for void fraction to become fully developed. In the figures, there was very little difference observed in the void fraction profiles for each flashing step. The observed experimental temperature distribution is also shown in the figures. It can be seen that temperature distribution in the bulk liquid develops from an initial subcooled state to a subsequent saturated state.

Fig. 29 shows the comparison between the results of experment 3 and the calculations. Similar conclusions, as for experiment 2 above, can be drawn for this test; however, the results from the experiment 3 and the calculations are quite different near the swell surface. This is beacuse the mass loss obtained by these two methods is different due to the part of vapor condensing. It will be discussed in the following.

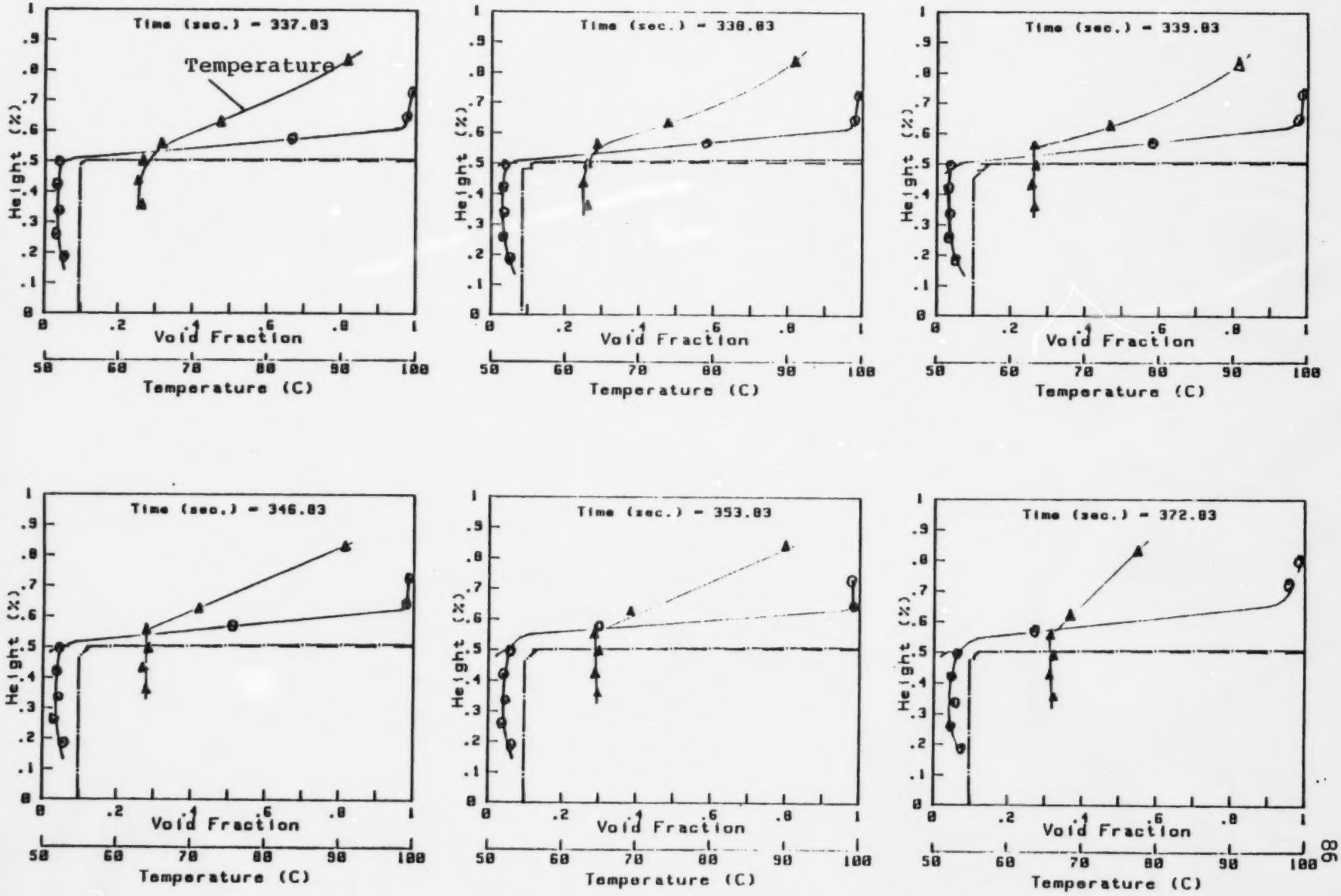


Fig. 29 (See Page 87 )

Fig. 28 (a) Comparison of Numerical Calculations and Experimental Data (Experiment 2) (First and second steps of flashing)

Fig. 28 (b) Comparison of Numerical Calculations and Experimental Data (Experiment 2) (Third and fourth steps of flashing)

Fig. 28 (c) Comparison of Numerical Calculations and Experimental Data (Experiment 2) (Fifth and sixth steps of flashing)

Fig. 29 Comparison of Numerical Calculations and Experimental Data (Experiment 3) (First and second steps of flashing)

In the above figures:

——— Experiment's Results

------- Energy and Mass Conservation Model's Results

-·-·-·- Drift Flux Model's Results

o Experimental Data of Void Fraction

Δ Experimental Data of Temperature

From Figs. 28 and 29, it is concluded that the more the liquid filling in the cylinder, the less the difference between the results from two methods. It is obvious that the more the space above the swell surface, the more difficult the vapor escaping from the valve.

A comparison of the mass loss is described in Figs. 30 and 31. The remaining liquid mass obtained from the theoretical calculations is less than that from experiments. Due to mixing with liquid and cooling after the PRV closing, a portion of the vapor generated would be returned to the bulk liquid by condensation caused by recompression. In the calculations, however, this vapor was assumed to be lost, so that the mass loss calculated is higher than the experimental results.

In Figs. 32 and 33, the swell heights obtained from the experiments agree very well with calculation results. The fluctuation of swell height was quite large in Experiment 2, and the calculation results describe this variation quite well. In Experiment 3, the swell heights did not vary as much and the calculation yields a nearly constant swell height which fits the average value of swell heights determined from the experiment.

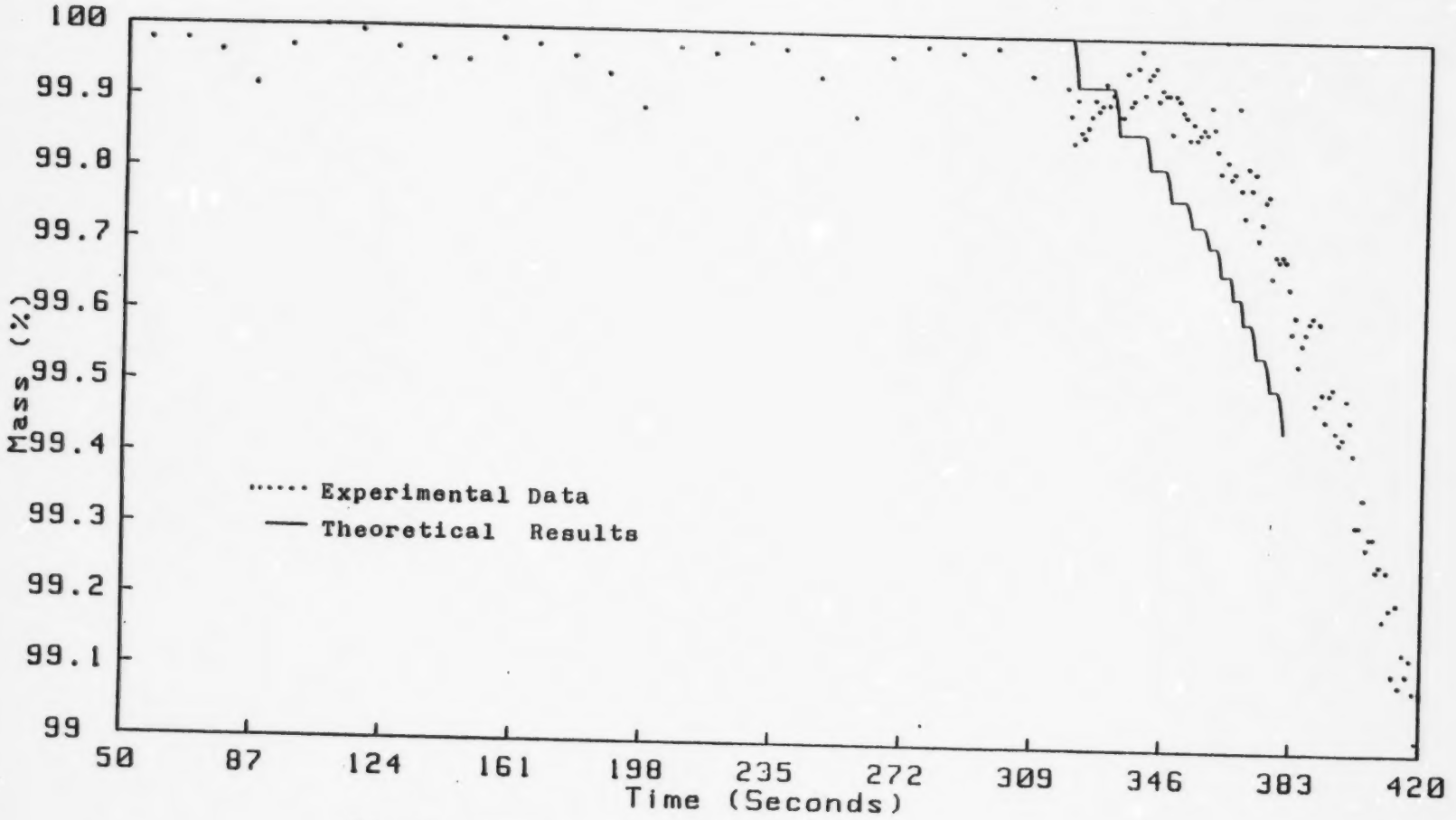


Fig.30 Comparison of Liquid Masses between Theoretical and Experimental Results (Experiment 2)

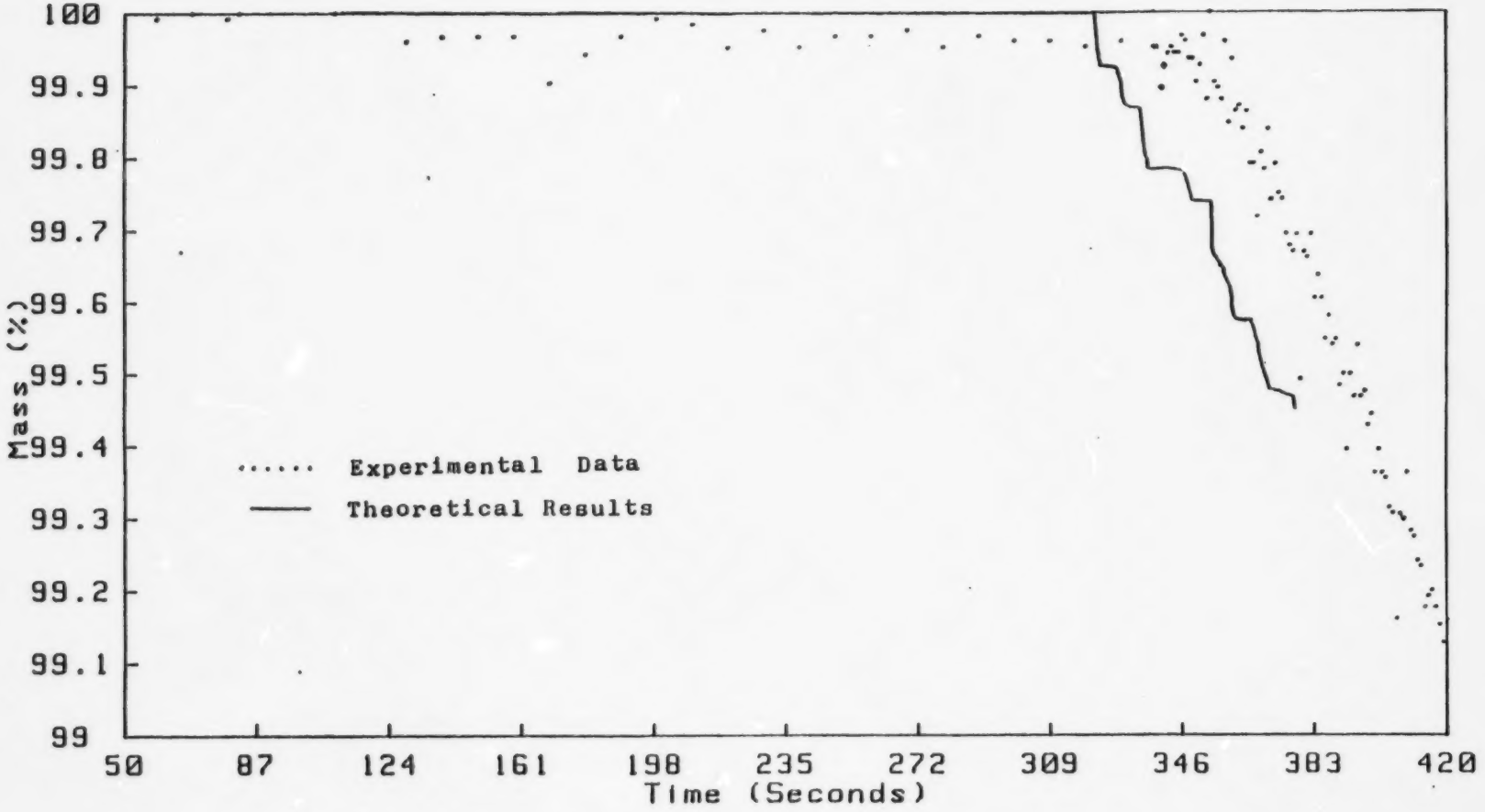


Fig. 31 Comparison of Liquid Masses between Theoretical and Experimental Results (Experiment 3)

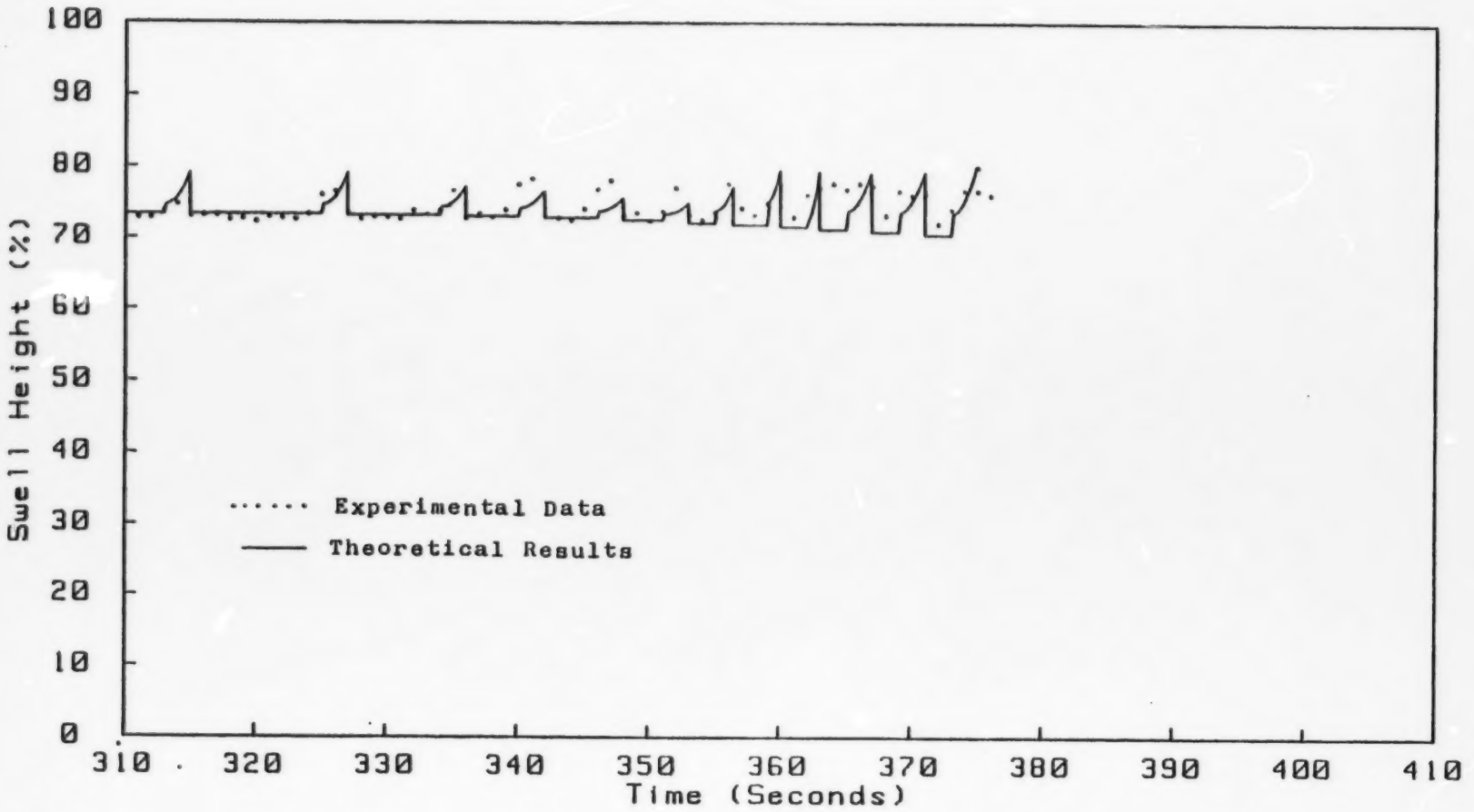


Fig. 32 Comparison of Swell Heights between Theoretical and Experimental Results (Experiment 2)

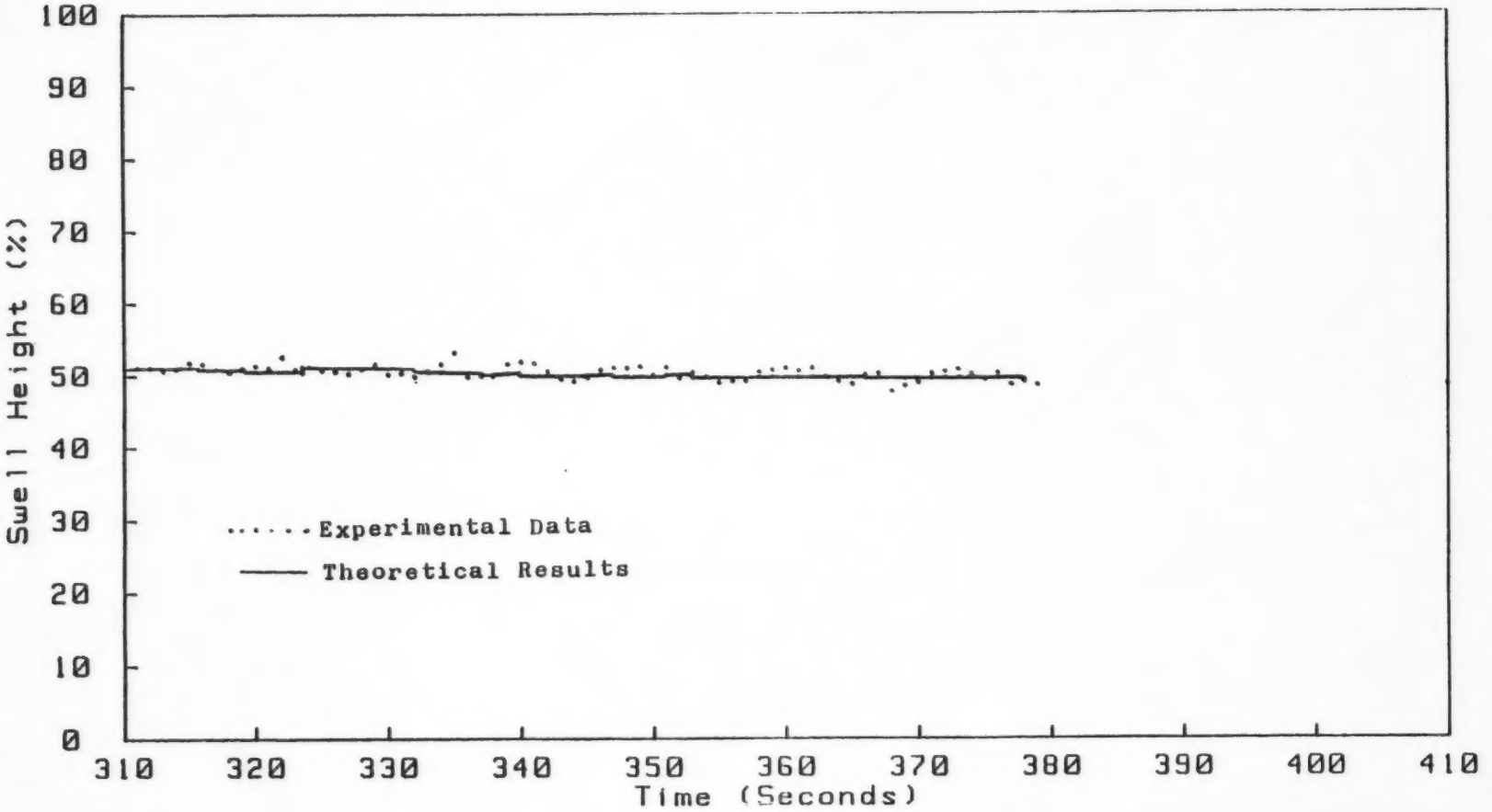


Fig. 33 Comparison of Swell Heights between Teoretical and Experimental Results (Experiment 3)

# CHAPTER 7

# CONCLUSIONS AND FUTURE WORK

## 7.1 CONCLUSIONS

Based on the experimental void fraction and swell height results for transient phenomena in a heated vessel during transient depressurization and the numerical calculations, the following conclusions can be drawn:

1). In the case of low void fraction, external heating has a noticeable effect on the void fraction profile. The number of bubbles generated at the wall by heating depends mainly on the amount of heat transferred from the wall. The amount of vapor may be quite small compared with the overall liquid mass; however, when the void fraction in the bulk liquid due to depressurization is low, this vapor generation cannot be neglected. Due to low void fraction, the four derived expressions (Eqs. (5.2), (5.3), (5.4) and (5.5)) gave almost the same results.

2). The fill of liquid in the vessel determines the number of bubbles produced. The change in bubble population affects both the pressure variation and the time of flashing. In the experiments, it was observed that the volumetric expansion due to the vapor generation restrained the pressure decompression due to flashing when the liquid filled more than half of the volume of the vessel.

3). During depressurization, the pressure drop depended to a large

extent upon the temperature distribution in the bulk liquid. Due to subcooling in the bulk liquid, depressurization was sharper at the early part of the experiment than at a latter stage where saturation situation occurred. This can also be explained by the effects of bubble population.

4). Considering the conservation of mass and energy in the two-phase mixture layer, an analytical method was developed for the change of void fraction in the mixed layer of vapor and liquid. For high void fraction, the calculated results agreed quite well with the experimental data. In the case of low void fraction, the numerical results were slightly higher in value than the experimental data, if the effect of heat flux from the walls was considered. This results from the subcooling in the bulk liquid. The analytical results of the fluctuation of swell height and mass loss showed good agreement with experimental findings.

## 7.2 FUTURE WORK

1). In order to study the full development of transient void fraction in a horizontal cylinder, experiments should be performed with the PRV kept opened.

2). A detailed investigatin of subcooled boiling in the boundary layer should be carried out, as it may affect the temperature distribution in the bulk liquid before flashing.

3). During flashing, the liquid circulation from the boundary

layer to the bulk liquid caused a great deal more disturbance in the vessel. This important factor should be taken into consideration in future transient phenomena studies.

## REFERENCES


[1]. Griffith, P., Clark, I.A., and Rohsenow, W.M., "Void Volumes in Subcooled Boiling Systems," ASME Paper No. 58-HT-19., 1958.

[2]. Rohsenow, W.M., "A Method of Correlating Heat Transfer Data for Surface Boiling of Liquids," Trans. ASME, J. Heat Transfer, Vol. 74, 1952, pp. 969.

[3]. Levy, S., "Forced convection Subcooled Boiling - Prodiction of Vapor Volumetric Fraction," Int. J. Heat and Mass Transfer, Vol. 10, 1967, pp. 951.

[4]. Zivi, S.M., "Estimation of Steady-State Steam Void-Fraction by Means of the Principle of Minimum Entropy Production," J. of Heat Transfer, Vol. 86, 1964, pp. 247.

[5]. Prigogine, I., "Introduction of Thermodynamics of Irreversible Processes," Interscience Publishes, a Division of John Wiley & Sons, Third Edition, 1967.

[6]. Bankoff, S.G., "A Variable Density Single-Fluid Model for Two Phase Flow with Particular Reference to Steam Water Flow," J. Heat Transfer, Vol. 82, 1960, pp. 265.

[7]. Zuber, N., Staub, F.W., and Bijwaard, G., "Vapor Void Fraction in Subcooled Boiling and in Saturated Boiling Systems," III International Heat Transfer Conference, ASME-154, Vol. 5, 1966, pp. 24.

[8]. Zuber, N., and Findlay, J., "Average Volumetric Concentration in Two-Phase Flow Systems," J. Heat Transfer, Vol. 87, 1965, pp. 453.

[9]. Kroeger, P.G., and Zuber, N., "An Analysis of the Effects of Various Parameters on the Average Void Fractions in Subcooled Boiling," Int. J. Heat and Mass Transfer, Vol. 11, 1968, pp. 211.

[10]. Rouhani, S.Z., "Calculation of Steam Volume Fraction in Subcooled Boiling," J. Heat Transfer, Vol. 90, 1968, pp. 158.

[11]. Rouhani, S.Z., and Axelsson, E., "Calculation of Void Fraction in the Subcooled and Quality Boiling Regions," Int. J. Heat and Mass Transfer, Vol. 13, 1970, pp. 383.

[12]. Larsen, P.S., and Tong, L.S., "Void Fraction in Subcooled Flow Boiling," J. Heat Transfer, Vol. 91, 1969, p. 471.

[13]. AIChE, "Externally Heated Vessels", "Design Institute for Emergen Relief System," Appendix A, Feb., 1984.

[14]. Cheung, F.B. and Farhadieh, G., "On the Formation of Bubble Boundary Layer over an Inclined Porous Plate," Trans. Am. Nucl. Soc., Vol. 32, 1979, pp. 526.

[15]. Edwards, A.R., and O'Brien, T.P., "Studies of Phenomena Connected with the Depressurization of Water Reactors," J. Br. Nucl. Energy Soc. 9, 1970, pp. 125.

[16]. Premoli, A. and Sandri, C., "A Study on the Blowdown of a Pressure Vessel Filled with Saturated Steam-Waterer," Energia Nucleare, Vol. 21, No. 11, 1974, pp. 625.

[17]. Miyatake, O., Murakami, K., Kawata, Y., and Fujji, T., "Fundamental Experiments with Flash Evaporation," Heat Transfer - Jap. Res., Vol. 2, 1973, pp. 89.

[18]. Hooper, F.C. and Aldelmessih, A.H., "The Flashing of Liquids at Higher Superheats," Proc. 3rd Int. Heat Transfer Conf., Vol. 4, No. 117, 1966, pp. 44.

[19]. Hooper, F.C., and Kerba, N.A., "A Law of Flashing," Proc. 2nd Can. Congr. of Appl. Mech. Waterloo, Ontario, 1969, pp. 259.

[20]. Lienhard, J.H., Alamyir, Md, and Trela, M., "Early Response of Hot Water to Sudden Release from High Pressure," J. Heat Transfer, Vol. 100, 1978, pp. 473.

[21]. Nariai, H., "Thermo-hydraulic Behavior of Fluid in Pressure Vessel during Blowdown," Heat & Fluid Flow in Water Reactor Safety, IMechE Conf. Puslic., Manchester, 1977, pp. 113.

[22]. Hutcherson, M.N., Henry, R.E., and Wollersheim, D.E., "Two-Phase Vessel Blowdown of an Initial Saturated Liquid," J. Heat Transfer, Vol. 105, 1983, pp. 687.

[23]. Saha, P., Abuaf, N., and Wu, B.J.C., "A Nonequilibrium Vapor Generation Model for Flashing Flows," J. Heat Transfer, Vol. 106, 1984, pp. 199.

[24]. Peterson, R.J., Grewal, S.S., and El-Wakil, M.M., "Investigations of Liquid Flashing and Evaporation due to Sudden Depressurization," Int. J. Heat Mass Transfer, Vol. 27, No. 2, 1984, pp. 301.

[25]. Woodford, D.J., and Scriven, A.H., "The Rising Velocity and Distribution of Vapor in a Liquid Pool during Depressurization," Int. Conf. on the Phys. Modelling of Multi-Phase Flow, Paper E3, April, 1983, pp. 199.

[26]. Vea, H.W. and Lahey, R.T., Jr, "An Exact Analytical Solution of Pool Swell Dynamics during Depressurization by the Method of Characteristics," Nuc. Eng. Design, Vol. 45, 1978, pp. 101.

[27]. Zuber, N. and Staub, F.W., "The Propagation and the Wave Form of the Vapor Volumetric Concentration in Boiling, Forced Convection System under Oscillatory Conditions," Int. J. Heat and Mass Transfer, Vol. 9, 1966, pp. 871.

[28]. Harlow, F.H., and Amsden, A.A., "Numerical Calculation of Multiphase Fluid Flow," J. Computational Physics, Vol. 17, 1975, pp. 19.

[29]. Solbrig, C.W., and Hughes, E.D., "Governing Equations for a Seriated Continuum,", "Two-Phase Transport and Reactor Safety," Vol. 1, 1980, pp. 307.

[30]. Spalding, D.B., "Numerical Computation of Multi-Phase Fluid Flow and Heat Transfer," "Recent Advanced in Numerical Methods in Fluids," Vol. 1, 1980, pp. 139.

[31]. Lahey, R.T., Jr., and Moodey, F.J., "The Thermal-hydraulics of a Boiling Water Nuclear Reactor", ANS Monography, 1977.

[32]. Rouhani, Z., "Measuring Techniques in Two-Phase Flows", "Two-Phase FLow and Heat Transfer with Applications to Nuclear Reactor Design Problems", 1978, pp. 329.

[33]. Jones, O.C., Jr., Abuaf, N., Zimmer, G.A., and Feierabend, T., "Void Fraction Dynamics and Measurement Techniques," Japan-U.S. Seminar 1979, pp. 145.

[34]. Hylton, J.O., and Mcgill, R.N., "Measurement of Velocity and Void Fraction in Steam-water Mixtures with Electrical Impedance Probes," Transient Two-phase Flow Proceedings of the Third CSNI Specialist Meeting, 1984, pp. 51.

[35]. Meredith, R.E., and Tobias, C.W., "Resistance to Potential Flow through a Cubical Array of Spheres," J. App. Phys., Vol. 34, No. 7, 1960, pp. 1270.

[36]. Bruggeman, D.A.G., "Berechnung Verschiedener Physikalischer Konstanten von Heterogenen Substanzen," Ann. Phys. Leipzig, Vol. 24, 1935, pp. 636.

[37]. Aydemir, N.U., M.Sc.E. thesis, Department of Mechanical Engineering, UNB, Fredericton, Canada, 1984.

[38]. Doyle, R., M.Sc.E. thesis, Department of Mechanical Engineering UNB, Fredericton, Canada, (in preparation Febs., 1985).

[39]. Friedel, L., and Purps, S., "Phase Distribution in Vessels during Depressurization," Int. J. Heat & Fluid Flow, Vol. 5, No. 4, 1984, pp. 229.

[40]. Maxwell, L., "A Treatise on Electricity and Magnetism, "Oxford University Press, Oxford, 1873.

[41]. Subbotin, V.I., Pokhvalov, Yu.E., Mikhailov, L.E., Leonov, V.A., and Kronin, I.V., "Resistance and Capacitance Methods of Measuring Steam Contents", Teploenergetika, Vol. 21, No. 6, 1974, pp. 63.

[42]. Orbeck, I., "Impedance Void Meter," Symposium on In-core Instrumentation, Oslo, 1964, pp. D-8.

# APPENDIX 1

## EXAMINATION OF THE EQUATION OF OVERALL AVERAGE VOID FRACTION

An examination of Eq. (4.17) is made as follows. A test was carried out in the UNB tank 2 with the working parameters listed below:

Heat power Qex = 65 kw/$m^2$

Initial liquid filled = 79%

Set pressure = 342.7 kPa

PRV orifice diameter = 6.35 mm

Initial liquid level = 350 cm

Tank diameter = 37.65 cm

A comparison between the empirical and theoretical results is presented below.

When flashing begins, the working fluid is saturated at $P_1$.

$T_{s1}$ = 63.3° C

$P_1$ = 342.7 kPa

$h_{fg1}$ = 164.4 kJ/kg

$\rho_{\ell 1}$ = 1379.1 kg/$m^3$

$\rho_{g1}$ = 18.44 kg/$m^3$

$Cp_{\ell 1}$ = 0.9402 kJ/kgK

When the flashing ends, fluid is saturated at $P_2$.

$T_{s2}$ = 23.8° C

$P_2$ = 1.013 kPa

$h_{fg2}$ = 180.3 kJ/kg

$\rho_{\ell 2}$ = 1478.5 kg/m$^3$

$\rho_{g2}$ = 5.86 kg/m$^3$

$C_{p\ell 2}$ = 0.8957 kJ/kgK

It is assumed that the pressure decrease from $P_1$ to $P_2$ immediately. The arithmetic mean value of each physical property is taken to calculate Eq. (4.17):

$$\bar{\alpha} = \frac{\frac{\rho_{\ell m}}{\rho_{gm}}}{\frac{h_{fgm}}{Cp_{\ell m}(T_{s1}-T_{s2})} - 1 + \frac{\rho_{\ell m}}{\rho_{gm}}} \qquad \text{(A1.1)}$$

For convenience in calculation, the above equation can be obtained from Eq. (4.17) by substitutions.

where: $\rho_{\ell m}$ = 1428.8 kg/m$^3$

$\rho_{gm}$ = 12.14 kg/m$^3$

$h_{fgm}$ = 172.4 kJ/kg

$Cp_{\ell m}$ = 0.918 kJ/kg K

Hence, $\bar{\alpha}$ = 97%

These results mean that when the saturated liquid is depressurized from $P_1$ to $P_2$, the volume of vapor produced makes up 97% of the total volume of vapor and liquid.

The initial liquid amounts to 79% of the volume of the tank, V. The mass is 0.79 V$\rho_{\ell}$1. During depressurization, the mass of the two-

phase mixture is $Mm=M_{\ell}+Mg$, and the volume is $Vm=M_{\ell}/\rho_{\ell 2}+Mg/\rho_{g2}$.

From the above:

$$\frac{Mg}{\rho_{g2}} = 0.97\ Vm$$

that is,

$$\frac{Mg}{M\ell} = 12.82\ \%$$

The mass balance between initial and final states is,

$$0.79\ V\ \rho_{\ell 1} = Mg + M\ell$$

Finally,

$$\frac{V_{\ell 2}}{V} = 65.76\ \%$$

Hence, it is known that after the flashing finishes, the volume of the remaining liquid in the tank amounts to 65.76% of the volume of the tank. The liquid level calculated is 29.67 cm. During depressurization, the liquid of 13.24% of the tank volume has been evaporated.

From the experimental results, the initial liquid level is 35 cm and the final liquid level is 30 cm. Thus, in the experiment, the

volume of remaining liquid takes up

$$\frac{V'_{\ell 2}}{V} = 65.56\ \%$$

of the tank volume.

The relative error between the theoretical and the experimental results is

$$\varepsilon = 1.2\ \%.$$

## APPENDIX 2

## ELECTRODE EFFECTS AND IMPEDANCE OF A TWO-PHASE MIXTURE

When a metal electrode is immersed in a fluid medium, an electric double layer is formed at the interface, which may cause an undesirable additional impedance. This may be due to the transfer of electrons from fluid to metal or vice versa. When a current equilibrium is reached, a potential difference exists between the metal and medium. Otherwise, when an a.c. voltage is applied to the electrode, the average energy level of the valence electrons of the metal is changed continuously, thus a charge transport goes on continuously. The above two ways make it possible for an electronic current to exist between the metal and medium. This effect can be replaced by an equivalent impedance. According to the electronic theory represented by the electric circuit in Fig. A1. Ce represents the latter factor, due to the application of the a.c. voltage to the electrode, and $R_\beta$ and $Z\omega$ represent the former factor, due to an electrochemical reaction at the interface between the electrode and medium. $Z\omega$ can be given by,

$$Z\omega = \frac{a}{\sqrt{\omega}} (1-j) \qquad (A2.1)$$

where a is a constant and $\omega$ is the angular frequency.

This impedance can be considered to be in series with the ohmic resistance of the two-phase mixture as shown in Fig. A2. $R\alpha$ and $C\alpha$ are

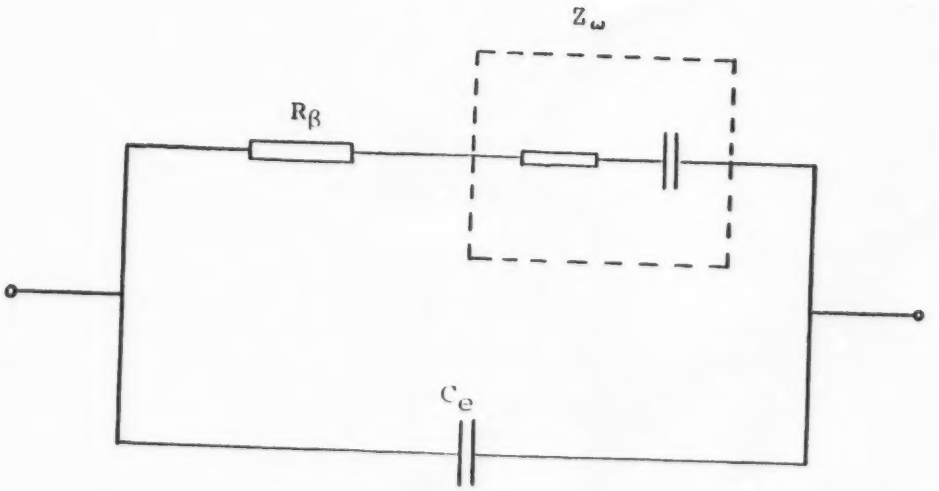


Fig. A1 Equivalent Circuit for Electrode Effect

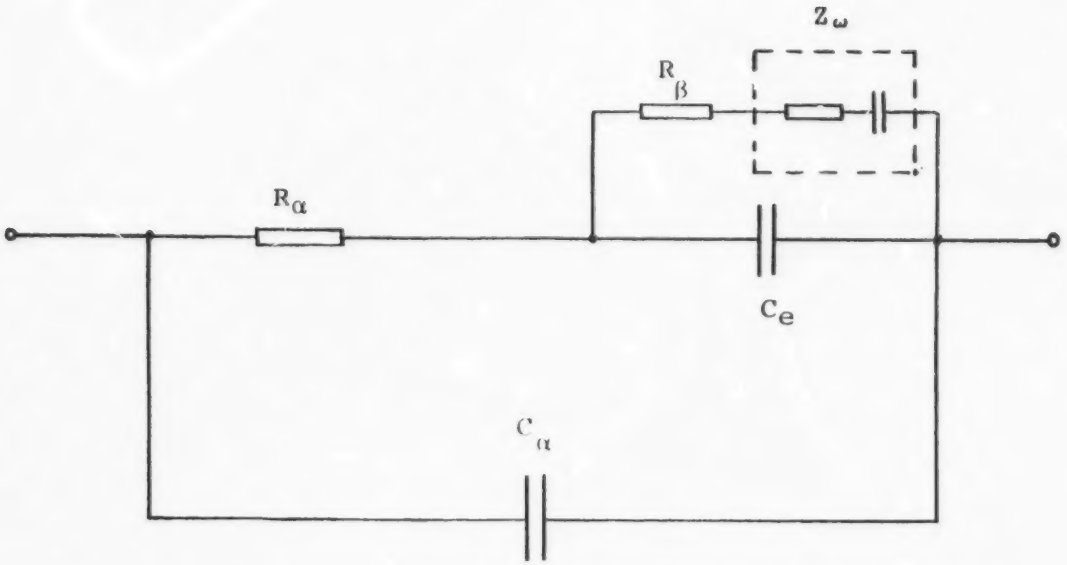


Fig. A2 Equivalent Circuit for Impedance of Void Sensor

the ohmic resistance and capacitance of the fluid, respectively.

The impedance of the electrode effects can be expressed as

$$Ze\omega = \frac{Z1 * Xce}{Z1 + Xce}$$

where $Z1=(R + a/\sqrt{\omega}) - j\ a/\sqrt{\omega}$ , and $Xce=1/(j\sqrt{\omega}\ Ce)$ .

or

$$Ze\omega = A - j\ B \qquad (A2.2)$$

where

$$A = \frac{(R_\beta + a/\sqrt{\omega})(a\ Ce/\sqrt{\omega} + 1/\omega) - a\ Ce/\sqrt{\omega}(R_\beta + a/\sqrt{\omega})}{(a\ \omega\ Ce + \sqrt{\omega})^2 + \omega^2\ Ce\ (\sqrt{\omega}\ R_\beta + a)^2}$$

$$B = \frac{a^2\ Ce/\omega + a/\omega^{3/2} + Ce\ (R + a/\sqrt{\omega})^2}{(a\ \sqrt{\omega}\ Ce + 1)^2 + \omega\ Ce^2(\sqrt{\omega}\ R_\beta + a)^2}$$

The total ohmic resistance and capacitance of a transducer are given as

$$R_T = R\alpha + (A + \frac{B^2}{A + R\alpha}) \qquad (A2.3)$$

$$C_T = C\alpha + \frac{B}{\omega\ [(A + R\alpha)^2 + B^2]} \qquad (A2.4)$$

It is easily found that when $\omega$ is high enough, A and B tend to be infinitely small, thus if an appropriate $\omega$ is chosen, the electrode

effects can be neglected. The two parts of impedance of the transducer are given by,

$$R_T = R\alpha \tag{A2.5}$$

$$C_T = C\alpha \tag{A2.6}$$

Hence, when the frequence $\omega$ is high enough, the impedance of a transducer can be represented as the equivalent circuit shown in Figure A3.

By analyzing the circuit in Fig. A3,

$$Z\alpha = \frac{1}{(1/R\alpha)^2 + (\omega\, C\alpha)^2} \left(\frac{1}{R\alpha} - j\ \omega\ C\alpha\right) \tag{A2.7}$$

With $\omega$ increasing, the $1/R\alpha$ terms in the demominator and numerator in Eq. (A2.7) can be neglected when a suitable frequency is reached. Then this equivalent circuit can be considered as a simple capacitance circuit and the impedance of a two-phase mixture is represented as the capacitance resistance:

$$Zc = \frac{1}{j\ \omega\ C\alpha} \tag{A2.8}$$

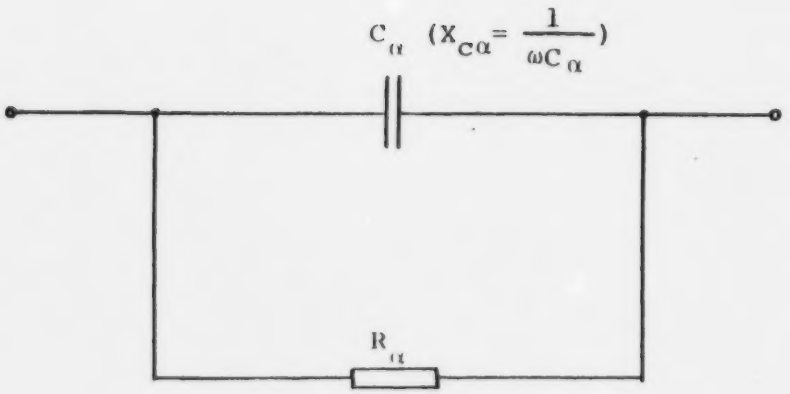


Fig. A3 Equivalent Circuit for Sensor
( High Freauency )

# APPENDIX 3

## COMPUTER PROGRAM FOR DATA ACQUISITION

```
3000 !*************************************************************************
3010 !*                                                                       *
3020 !*              Tank Car Test Data Acquisition Routine                   *
3030 !*                                                                       *
3040 !*                        Copyright 1985 By                              *
3050 !*                                                                       *
3060 !*                        Charles R. Dutcher                             *
3070 !*                                                                       *
3080 !*                    Void Fraction Test Version                         *
3090 !*                                                                       *
3100 !*               Date of Last Revision : July   18, 1985                 *
3110 !*                                                                       *
3120 !*************************************************************************
3130 !
3140 !
3150 !     This routine was developed by Charles R. Dutcher for use in
3160 !  data for the Tank Car Project. This routine is written to run
3170 !  on a Hewlett-Packard Model 9220 computer with Basic 3.0 opera-
3180 !  ing system with options :
3190 !
3200 !  Model HP89622 Serial Interface Card
3210 !  Model HP89624 HPIB Interface Card
3220 !
3230 !     Data is gathered using the following instruments :
3240 !
3250 !  Hewlett-Packard Model 3456 Digital Voltmeter   -   HPIB 822
3260 !  Hewlett-Packard Model 3437 System Voltmeter    -   HPIB 824
3270 !  Hewlett-Packard Model 3497 DACU                -   HPIB 809
3280 !  Hewlett-Packard Model 3497 DACU                -   HPIB 808
3290 !
3300 !*************************************************************************
3310 !
3320 OPTION BASE 0
3330 INTEGER Index1,Index2,Index3,Index4,Index5,Index6     ! Loop Indexes
3340 INTEGER Storage_flag,Store_counter,Fast_scan_flag     ! Scan Variables
3350 DIM Valve_state$[1],Void_info$[1300],Temp_info$[150] ! Scan Storage
3360 !
3370 DIM Void_data$(320)[1300],Temp_data$(320)[100]        ! Scan Dump
3380 REAL Total_time(320),Tank_pressure(320)               ! Scan Dump
3390 REAL Void_averages(12)
3400 DIM Emf(8)                                           ! Power
3410 !
3420 !*************************************************************************
3430 !*                                                                       *
3440 !*     OPEN UP I/O PATHS FOR CRT, KEYBOARD, BUS AND INSTRUMENTS          *
3450 !*                                                                       *
3460 !*************************************************************************
3470 !
3480 ASSIGN @Crt TO 1
3490 ASSIGN @Kbd TO 2
3500 ASSIGN @Instr_bus TO 8
3510 ASSIGN @Hispeed_scanner TO 824
3520 ASSIGN @Pressure TO 822
3530 ASSIGN @Scanner1 TO 809
3540 ASSIGN @Scanner2 TO 808
3550 !
```

```
3560 CLEAR @Instr_bus
3570 !
3580 !*************************************************************************
3590 !*                                                                       *
3600 !*         DISPLAY START UP MESSAGE AND PROMPT FOR USER DATA             *
3610 !*                                                                       *
3620 !*************************************************************************
3630 !
3640 DEG
3650 OUTPUT @Kbd;CHR$(255)&"K";
3660 GINIT
3670 GCLEAR
3680 GRAPHICS ON
3690 LORG 5
3700 CSIZE 5
3710 WINDOW -1,11,-1,11
3720 MOVE 5,9
3730 LABEL "Tank Car Data Acquisition Routine"
3740 MOVE 5,8
3750 LABEL "by"
3760 MOVE 5,7
3770 LABEL "Charles R. Dutcher"
3780 MOVE 5,5
3790 LABEL "Revised July 15, 1985"
3800 CLIP 0,10,4,10
3810 FRAME
3820 CLIP OFF
3830 !
3840 !*************************************************************************
3850 !
3860 INPUT "ENTER UPPER PRESSURE LIMIT   (Psig. )     : ",Upper_pressure
3870 INPUT "ENTER LOWER PRESSURE LIMIT   (Psig. )     : ",Lower_pressure
3880 INPUT "ENTER DESIRED POWER FOR HEATER GROUP # 1 : ",Group_power1
3890 INPUT "ENTER DESIRED POWER FOR HEATER GROUP # 2 : ",Group_power2
3900 INPUT "ENTER DESIRED POWER FOR HEATER GROUP # 3 : ",Group_power3
3910 !
3920 GCLEAR
3930 GRAPHICS ON
3940 WINDOW -1,11,-1,11
3950 MOVE 5,9
3960 LABEL "Check to see that all instruments"
3970 MOVE 5,8
3980 LABEL "are triggered from DACU #2 (C)"
3990 MOVE 5,7
4000 LABEL "before continuing"
4010 MOVE 5,5
4020 LABEL "Press key 'K0' to start scanning"
4030 CLIP 0,10,4,10
4040 FRAME
4050 CLIP OFF
4060 !
4070 !
4080 !
4090 !*************************************************************************
```

```
4100 !
4110 OUTPUT @Scanner2;"DC4,1"          ! CLOSE VALVE FOR POWER ADJUST
4120 !
4130 !*************************************************************************
4140 !
4150 ON KEY 0 GOTO 4170
4160 Loop1:GOTO Loop1
4170 OFF KEY 0
4180 !
4190 !*************************************************************************
4200 !*                                                                       *
4210 !*      INITIALIZE SCANNING VOLTMETER FOR POWER TRANSDUCER INPUTS        *
4220 !*                                                                       *
4230 !*************************************************************************
4240 !
4250 OUTPUT @Scanner2;"S01SD0VR5VT1VD5VA0VF1VN9VS0AF30AL38AE1AC30"
4260 !
4270 !*************************************************************************
4280 !
4290 GINIT
4300 GCLEAR
4310 GRAPHICS ON
4320 WINDOW -2,12,-3,6
4330 CLIP 0,10,0,5
4340 AXES 10,.5,0,0,1,2
4350 FRAME
4360 CLIP OFF
4370 LORG 5
4380 MOVE 5,5.5
4390 LABEL "Heater Power per Group"
4400 LDIR 90
4410 MOVE -1,2.5
4420 LABEL "Kilowatts per Group"
4430 LDIR 0
4440 MOVE 2,-.25
4450 LABEL "Group 1"
4460 MOVE 5,-.25
4470 LABEL "Group 2"
4480 MOVE 8,-.25
4490 LABEL "Group 3"
4500 FOR Index1=0 TO 5
4510     MOVE -.25,Index1
4520     LABEL Index1
4530 NEXT Index1
4540 AREA INTENSITY .1,0,0
4550 MOVE 1,0
4560 RECTANGLE 2,Group_power1/3,FILL,EDGE
4570 AREA INTENSITY .2,0,0
4580 MOVE 4,0
4590 RECTANGLE 2,Group_power2/3,FILL,EDGE
4600 AREA INTENSITY .3,0,0
4610 MOVE 7,0
4620 RECTANGLE 2,Group_power3/3,FILL,EDGE
4630 !
```

```
4640 CLIP ON
4650 !
4660 DISP USING "21X,50A";"*** PRESS ANY KEY TO START SCANNING ***"
4670 ON KBD GOTO 5350
4680 !
4690 Pcf=1/.01375
4700 T0=TIMEDATE
4710 !
4720 Pi1=0
4730 Pi2=0
4740 Pi3=0
4750 Pi4=0
4760 Pi5=0
4770 Pi6=0
4780 Pi7=0
4790 Pi8=0
4800 Pi9=0
4810 !
4820 BEEP 4000,.1
4830 WAIT .9
4840 BEEP 4000,.1
4850 WAIT .9
4860 BEEP 4000,.1
4870 WAIT .9
4880 BEEP 4000,.1
4890 WAIT .9
4900 BEEP 4000,1
4910 !
4920 !*****************************************************************************
4930 !
4940 ENTER @Scanner2;Emf(*)
4950 !
4960 P1=Emf(8)*Pcf
4970 CALL Barplot(1.5,P1,Pi1)
4980 P2=Emf(7)*Pcf
4990 CALL Barplot(2,P2,Pi2)
5000 P3=Emf(6)*Pcf
5010 CALL Barplot(2.5,P3,Pi3)
5020 IF (P1+P2+P3)>Group_power1 THEN BEEP 2000,.1
5030 P4=Emf(5)*Pcf
5040 CALL Barplot(4.5,P4,Pi4)
5050 P5=Emf(4)*Pcf
5060 CALL Barplot(5,P5,Pi5)
5070 P6=Emf(3)*Pcf
5080 CALL Barplot(5.5,P6,Pi6)
5090 IF (P4+P5+P6)>Group_power2 THEN BEEP 4000,.1
5100 P7=Emf(2)*Pcf
5110 CALL Barplot(7.5,P7,Pi3)
5120 P8=Emf(1)*Pcf
5130 CALL Barplot(8,P8,Pi8)
5140 P9=Emf(0)*Pcf
5150 CALL Barplot(8.5,P9,Pi9)
5160 IF (P7+P8+P9)>Group_power3 THEN BEEP 6000,.1
5170 !
```

```
5180 Pi1=P1
5190 Pi2=P2
5200 Pi3=P3
5210 Pi4=P4
5220 Pi5=P5
5230 Pi6=P6
5240 Pi7=P7
5250 Pi8=P8
5260 Pi9=P9
5270 GOTO 4940
5280 !
5290 !*************************************************************************
5300 !*    END OF POWER ADJUST : ENTER REFERENCE TEMPS FOR THERMOCOUPLES   *
5310 !*************************************************************************
5320 !
5330 ! REFERENCE JUNCTION LOCATED ON CHANNEL #19 OF UNIT #2
5340 !
5350 OFF KBD
5360 ABORT @Instr_bus
5370 OUTPUT @Scanner2;"AC19"      ! ENTER REFERENCE TEMPS FOR THERMOCOUPLES
5380 ENTER @Scanner2;Ref_temp
5390 !
5400 !*************************************************************************
5410 !
5420 OUTPUT @Hispeed_scanner;"R3T2F2N650SD.00075S"
5430 OUTPUT @Scanner2;"SO1SD0VR1VT2VD5VA0VF2VN21VS2AF0AL20AE1TE0AC0"
5440 OUTPUT @Scanner1;"AF0AL12AC0AE2"
5450 ENTER @Pressure;Poffset
5460 OUTPUT @Pressure;"S0F1R1T26STG1STN1STIM0Z1D1SO1"&VAL$(Poffset)&"STZ.1STYM?"
5470 LOCAL LOCKOUT @Instr_bus
5480 !
5490 !*************************************************************************
5500 !
5510 GINIT
5520 GRAPHICS OFF
5530 ALPHA ON
5540 CONTROL 1,12;1
5550 CONTROL 1,1;7
5560 OUTPUT @Crt USING "15X,17A";"{   Elapsed Time"
5570 OUTPUT @Crt USING "15X,17A";"{   Tank Pressure"
5580 OUTPUT @Crt USING "15X,17A";"{   Stored Scans"
5590 OUTPUT @Crt USING "15X,17A";"{   Tank Mass"
5600 !
5610 !*************************************************************************
5620 !
5630 DISP USING "21X,50A";"*** PRESS KEY 'K0' TO STOP SCANNING ***"
5640 ON KEY 0 GOTO 6370
5650 !
5660 !
5670 !
5680 !
5690 !
5700 !
5710 !*************************************************************************
```

```
5720 !
5730 Elapsed_time=DROUND((TIMEDATE-T0),4)
5740 Fast_scan_flag=0
5750 Store_counter=0
5760 Store_limit=320
5770 Storage_flag=0
5780 Valve_state$="C"
5790 Mass_factor=2.268E+4
5800 Ref_temp=Ref_temp*10
5810 !
5820 !*************************************************************************
5830 OUTPUT @Scanner2;"TI1"
5840 !*************************************************************************
5850 !
5860 !*************************************************************************
5870 !*                                                                       *
5880 !*          BEGIN COLLECTING SCAN DATA AT ONE SECOND INTERVALS           *
5890 !*                                                                       *
5900 !*************************************************************************
5910 !
5920 Scan_data:ENTER @Hispeed_scanner;Void_info$
5930 ENTER @Pressure;Pressure
5940 !
5950 SELECT Pressure
5960 !
5970 CASE >=Upper_pressure
5980     Fast_scan_flag=1
5990     Valve_state$="O"
6000 CASE <=Lower_pressure
6010     Valve_state$="C"
6020 END SELECT
6030 !
6040 OUTPUT @Scanner2;"VS"
6050 ENTER @Scanner2;Temp_info$
6060 OUTPUT @Scanner2;"D"&Valve_state$&"4,1VS0VS2VT2"
6070 !
6080 IF NOT (Storage_flag=10 OR Fast_scan_flag) THEN 6170
6090 !
6100 Total_time(Store_counter)=Elapsed_time
6110 Tank_pressure(Store_counter)=Pressure
6120 Void_data$(Store_counter)=Void_info$
6130 Temp_data$(Store_counter)=Temp_info$
6140 !
6150 Storage_flag=0
6160 IF Store_counter<Store_limit THEN Store_counter=Store_counter+1
6170 Storage_flag=Storage_flag+1
6180 !
6190 Elapsed_time=Elapsed_time+1
6200 !
6210 Tankmass=FNUnpack(Temp_info$[61,63])*Mass_factor
6220 CONTROL 1,1;7
6230 OUTPUT @Crt USING 6290;Elapsed_time
6240 OUTPUT @Crt USING 6290;Pressure
6250 OUTPUT @Crt USING 6290;Store_counter!
```

```
6260 OUTPUT @Crt USING 6290;Tankmass
6270 GOTO Scan_data
6280 !
6290 IMAGE 5D.DD
6300 !
6310 !*************************************************************************
6320 !*                                                                       *
6330 !*                SCANS COMPLETE : STORE DATA AND QUIT                   *
6340 !*                                                                       *
6350 !*************************************************************************
6360 !
6370 OFF KEY 0
6380 RESET @Instr_bus
6390 BEEP 4000,1
6400 !
6410 !*************************************************************************
6420 !
6430 GRAPHICS OFF
6440 OUTPUT @Kbd;CHR$(255)&"K";
6450 INPUT "ENTER A FILE NAME TO STORE SCAN DATA  : ",File$
6460 OUTPUT @Kbd;CHR$(255)&"K";
6470 CONTROL 1,1;11
6480 OUTPUT @Crt USING "22X,60A";"*** STANDBY : DATA BEING STORED ***"
6490 CREATE ASCII File$&":HP9122,700,1",400
6500 ASSIGN @Testdata TO File$&":HP9122,700,1"
6510 !
6520 ENABLE INTR 8;2
6530 ON INTR 8 GOSUB Pressure_vent
6540 Upper_pressure=5+Poffset
6550 Lower_pressure=2+Poffset
6560 OUTPUT @Pressure;"HSM200T1SO0"&VAL$(Upper_pressure)&"STU"&VAL$(Lower_pressu
re)&"STLM1"
6570 !
6580 !*************************************************************************
6590 !
6600 FOR Index3=0 TO Store_counter
6610 !
6620     FOR Index4=0 TO 12
6630          Void_averages(Index4)=0
6640 !
6650          FOR Index5=1 TO 50
6660               Ofst=LEN(Void_data$(Index3))-2*(12-Index4)-26*(Index5-1)
6670               Void_averages(Index4)=Void_averages(Index4)+FNUnpack37(Void_d
ata$(Index3)[Ofst-1,Ofst])
6680          NEXT Index5
6690 !
6700          Void_averages(Index4)=Void_averages(Index4)/50
6710     NEXT Index4
6720 !
6730 !
6740     OUTPUT @Testdata;Total_time(Index3),Tank_pressure(Index3),Ref_temp,Void
_averages(*),Temp_data$(Index3)
6750     CONTROL 1,1;13
6760     OUTPUT @Crt USING "29X,16A,4D.D";"Stored Scans   : ";Index3
6770 NEXT Index3
6780 ASSIGN @Testdata TO *
6790 !
```

```
6800 !*************************************************************************
6810 !
6820 OUTPUT @Kbd;CHR$(255)&"K";
6830 CONTROL 1,1;11
6840 OUTPUT @Crt USING "22X,60A";"***     DATA TRANSFER COMPLETE    ***"
6850 BEEP 4000,1
6860 STOP
6870 !
6880 !*************************************************************************
6890 !*****                      END OF MAIN PROGRAM                      *****
6900 !*************************************************************************
6910 !
6920 !*************************************************************************
6930 !*                                                                       *
6940 !*                    SHUT-DOWN VENTING SUBROUTINE                       *
6950 !*                                                                       *
6960 !*************************************************************************
6970 !
6980 Pressure_vent:!
6990 Volt_status=SPOLL(@Pressure)
7000 !
7010 ENTER @Pressure;Pressure
7020 SELECT Pressure
7030  !
7040 CASE >Upper_pressure
7050     Valve_state$="O"
7060 CASE <Lower_pressure
7070     Valve_state$="C"
7080 END SELECT
7090 !
7100 OUTPUT @Scanner2;"D"&Valve_state$&"4,1"
7110 ENABLE INTR 8
7120 RETURN
7130  !
7140 END
7150 !
7160 !*************************************************************************
7170 !*                                                                       *
7180 !*               POWER BAR GRAPH PLOTTING SUBROUTINE                     *
7190 !*                                                                       *
7200 !*************************************************************************
7210 !
7220 !      Requires :  Xl    (Position of lower left corner of rectangle)
7230 !                  Final (Final height of rectangle)
7240 !                  Init  (Initial height of rectangle)
7250 !
7260 !      Returns :   Graphics Display
7270 !
7280 SUB Barplot(Xl,Final,Init)
7290     PEN 1
7300     St=.02
7310     IF Final<=Init THEN
7320          PEN -1!
```

```
7330          St=-.02
7340      END IF
7350      FOR J=Init TO Final STEP St
7360           MOVE X1,J
7370           PLOT X1,J
7380           PLOT (X1+.2),J
7390      NEXT J
7400 SUBEND
7410 !
7420 !*************************************************************************
7430 !*                                                                       *
7440 !*              3497A VOLTMETER DATA UNPACKING FUNCTION                  *
7450 !*                                                                       *
7460 !*************************************************************************
7470 !
7480 !       Requires :  3 Character string representing packed 3497 data
7490 !
7500 !       Returns  :  Unpacked real signed number
7510 !
7520 DEF FNUnpack(A$)
7530      O1=NUM(A$[1])
7540      O2=NUM(A$[2])
7550      O3=NUM(A$[3])
7560      P=.1*BINAND(O1,15)+.01*(O2 DIV 16)+1.E-3*BINAND(O2,15)
7570      P=P+1.E-4*(O3 DIV 16)+1.E-5*BINAND(O3,15)
7580      RETURN (P+BIT(O1,4))*(1-2*BIT(O1,5))*10^((O1 DIV 64)-1)
7590 FNEND
7600 !
7610 !*************************************************************************
7620 !*                                                                       *
7630 !*              3437A VOLTMETER DATA UNPACKING FUNCTION                  *
7640 !*                                                                       *
7650 !*************************************************************************
7660 !
7670 DEF FNUnpack37(A$)
7680      O1=NUM(A$[1])
7690      O2=NUM(A$[2])
7700      P=10*BIT(O1,4)+BINAND(O1,15)+.1*(O2 DIV 16)+.01*BINAND(O2,15)
7710      RETURN (2*BIT(O1,5)-1)*10^(-(NOT BIT(O1,7)+BIT(O1,6)))*P
7720 FNEND
```